Fabrication, Characterization and Integration of Carbon Nanotube Cathodes for Field Emission X-Ray Source

By
Xiomara Calderón-Colón

A dissertation submitted to the faculty of the University of North Carolina at Chapel Hill in partial fulfillment of the requirement for the degree of Doctor of Philosophy in the Curriculum in Applied Science and Engineering.

Chapel Hill
2009

Approved by

Advisor: Professor Otto Zhou

Reader: Dr. Jie Liu

Reader: Dr. René López

Reader: Dr. Lu-Chang Qin

Reader: Dr. Sean Washburn

ABSTRACT

XIOMARA CALDERON-COLON: Fabrication, Characterization and Integration of
Carbon Nanotube Cathodes for Field Emission X-Ray Source

(Under the direction of Dr. Otto Zhou)

Carbon nanotube (CNT) field emitters are now being evaluated for a wide range of vacuum electronic applications. Our laboratory pioneer in the development of CNT based field emission X-ray source technology, which has the potential to fundamentally change how X-ray radiation is generated and utilized. Applications of the CNT field emission X-ray source technology in a wide range of applications including biomedical imaging, radiation therapy, and homeland security are being actively pursued. However, problems with the performance of the CNT cathodes for X-ray generation including short lifetime at high current density, instability under high voltage, poor emission uniformity, and cathode-to-cathode inconsistency are still major obstacles for device applications. The goal of this thesis work is the development and optimization of an electrophoretic process to fabricate composite CNT films with controlled nanotube orientation and surface density, and enhanced adhesion.

The CNT cathode fabrication process consist in a combination of photolithography and electrophoretic deposition (EPD) method where parameters such as SU-8 photoresist thickness, deposition time, and deposition voltage were varied to fabricate CNT cathodes with the required properties for X-ray generation. Also the development of CNT alcohol-based suspensions in context of the EPD method requirements with excellent long term stability has been accomplished. The CNT cathodes fabricated by EPD have significantly enhanced *macroscopic* field emission current density and long-term stability under high operating voltages. Also these CNT cathodes compared to others reported previously show significant improved field emission properties with small cathode-to-cathode variation. The integration, characterization, and evaluation of these CNT cathodes into a micro focus field emission X-ray source has been achieved with excellent X-ray source characteristics and performance including X-ray flux and stability at the maximum current and power allowed for a fixed anode. Also, with similar performance afforded in comparison with a conventional thermionic X-ray tube operating at the same focal spot size. The application of this CNT electron source for high-resolution X-ray imaging has been demonstrated.

ACKNOWLEDGEMENTS

TABLE OF CONTENTS

LIST OF TABLES

LIST OF FIGURES

LIST OF EQUATIONS

1 Introduction

Carbon in the solid phase can exist in three allotropic forms: graphite, diamond and bucksminsterfullerene (Figure 1.1) [1]. The crystalline structure of diamond is responsible for the observed hardness, large heat conduction, electrical insulating nature and optical transparency. Graphite is made by layered planar sheets, responsible for softness, slipperiness, opaqueness, and electrically conductive. Fullerene consists of a family of spheroidal or cylindrical molecules. C_{60} is a semiconductor. Carbon nanotubes (CNTs) are a different form of carbon and are part of the fullerenes family. The diversity of properties of CNTs (mechanical, electronic, thermal, and chemical) makes this a unique form of carbon.
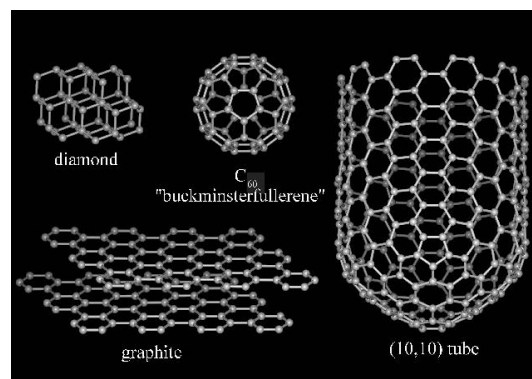
Figure 1.1: Allotropes of Carbon [2].

1.1 Structure, Properties and Applications of Carbon Nanotubes

CNTs were observed the first time in 1991 by Sumio Iijima from by products obtained during the synthesis of fullerenes [3]. At that time Iijima clearly observed multiwalled carbon nanotubes (MWNTs). Two years later in 1993, single-wall carbon nanotubes (SWNTs) were synthesized. A simple explanation of the CNTs structure is a graphite sheet roll-up forming a cylindrical shape with diameter in the nanometer scale as illustrated on Figure 1.2. MWNTs consist of several concentric SWNTs with different diameters.
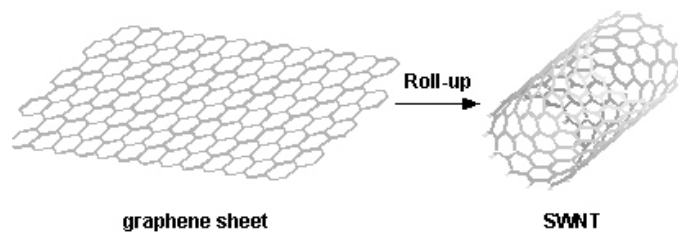
Figure 1.2: Basic Structure of Carbon Nanotubes [4].

The range of MWNTs outer diameter is 2 to 100 nm, while the inner diameter is in the range of 1-3 nm and their length is 1 µm to several millimeters. On the other hand SWNTs diameter varies between 0.4 and 2 nm. Figure 1.3 shows the transmission electron micrographs (TEM) of the first observed MWNTs.
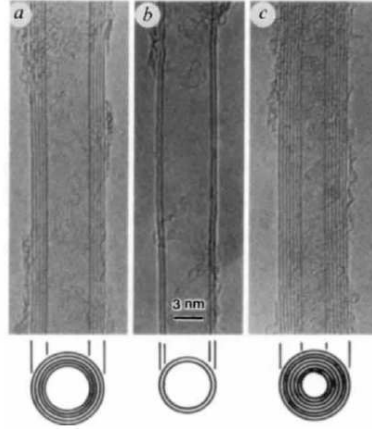
Figure 1.3: Transmission electron micrographs (TEMs) of the first observed MWNTs report by Iijima [3].

CNTs and graphite share the same sp^2 bond structure, which causes the extremely stable covalent bonds. The CNTs bonds are stronger than the sp^3 bonds found in diamond; this difference in bonding gives CNTs their unique strength. SWNTs naturally align themselves into "ropes" held together by Van der Waals forces. The electronic properties of the CNTs depend on their chirality, and so these properties are very sensitive to the geometric structure [5]. The chirality determines if the nanotube is semiconducting or metallic. The chiral vector, C_h, ($C_h = n\, a_1 + m\, a_2$) is related to the way that the graphite sheet is "rolled-up" and is represented by a pair of indices (n and m). Figure 1.4 shows the 2D graphene sheet with the lattice vectors. T denotes the tube axis, and a_1 and a_2 are the unit vectors of graphene in real space. Integers n and m represent the number of carbon atoms around the circumference of the tube and the numbers of atoms down the tube axis, respectively. If m = 0, the nanotubes are called "zigzag". If n = m, the nanotubes are called "armchair". Otherwise, they are called "chiral".
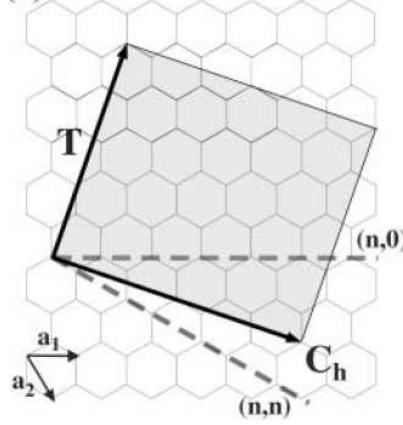
Figure 1.4: 2D graphene sheet illustrating lattice vectors a_1 and a_2, and the roll-up vector $C_h = na_1 + ma_2$. The limiting, achiral cases of (n, 0) zigzag and (n, n) armchair are indicated with dashed lines [4].
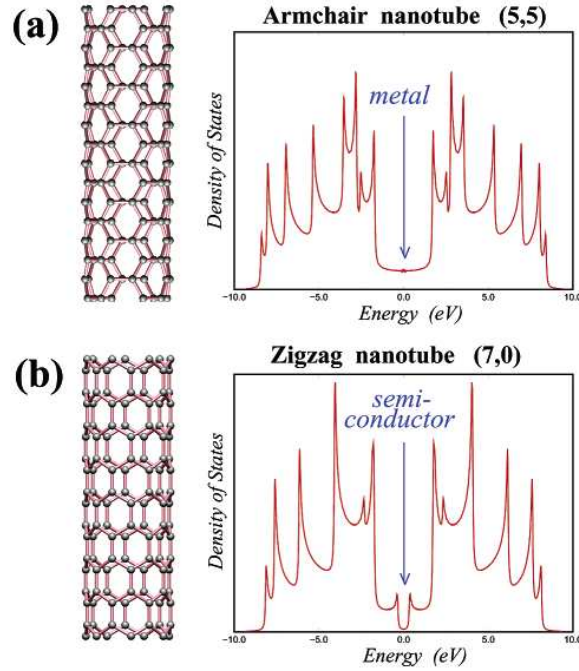
Figure 1.5: Electronic properties of two different carbon nanotubes. (a) The armchair (5, 5) nanotube exhibits a metallic behavior (finite value of charge carriers in the DOS at the Fermi energy, located at zero). (b) The zigzag (7, 0) nanotube is a small gap semiconductor (no charge carriers in the DOS at the Fermi energy). Sharp spikes in the DOS are van Hove singularities (a,b) [6].

The fundamental CNT is a single-wall structure with three basic geometries: (1) armchair, (2) zigzag, and (3) chiral [7]. In Figure 1.5, the electronic properties of two different CNTs are shown. An armchair nanotube exhibits a metallic behavior and a

zigzag nanotube exhibits a semiconductor behavior. As a general rule, if (n-m) is a multiple of 3, then the tube shows a metallic behavior. On the other hand, if (n-m) is not a multiple of 3, then the tube demonstrates a semiconducting behavior. Figure 1.6 shows three typical examples of CNTs; these are (10, 0), (6, 6), and (8, 4) nanotubes.
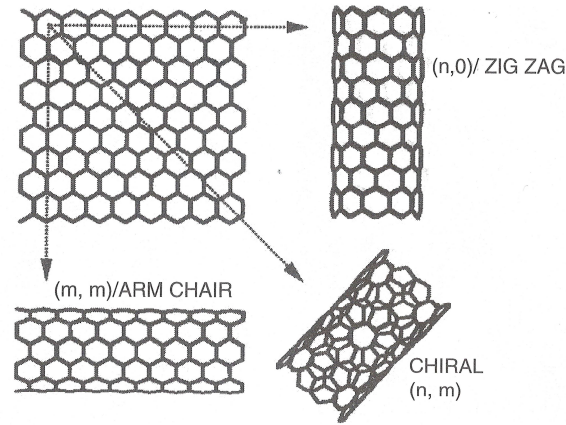
Figure 1.6: By rolling a graphite sheet in different directions, three typical nanotubes can be obtained: zigzag (n, 0), armchair (m, m) and chiral (n, m). In this specific example, they are (10, 0), (6, 6), and (8, 4) nanotubes [8].

Attribute	Comments
Metallic to semiconductor electrical conductivity, depending on microstructure	No other known molecule has this property
Electrical conductivity: 10^8 $\Omega^{-1}m^{-1}$	Comparable to that of copper
Thermal Conductivity: 10^4 $Wm^{-1}K^{-1}$	> that of diamond
Carrier mobility: 10^4 $cm^2V^{-1}s^{-1}$	> that of GaAs
Supports a current density of 10^9 Acm^{-2}	Due to very weak electromigration
Nanoscale heterojunctions	Common defect the can create an on-tube heterojuction
Young's modulus: 1 TPa	Stiffer than any other known material
Tensile strength: 150 GPa	600 times the strength/weight ratio of steel

Table 1.1: Summary of the physical attributes of carbon nanotubes [9].

Since CNTs have such unique properties and versatility, many potential applications have been proposed. Table 1.1 summarizes the physical properties of high

quality SWNTs. MWNTs exhibit comparable properties. The nanoscale diameter with an aspect ratio of ~1000 and a high conductivity make CNTs ideal candidates for field emitters [9]. Potential applications of CNTs in vacuum microelectronics include field emission electron sources for flat panel display, lamps, gas discharge tubes, X-ray, microwave generators, and electron microscope. Many applications depend on the physical attribute of the CNTs such as Young's modulus. Young's modulus is an independent property of the tube chirality, but dependent of the tube diameter [8]. The highest value is from a tube diameter between 1 and 2 nm, about 1 TPa [8]. The stiffness, low density, high aspect ratio and high conductivity make this material ideal for lightweight and conducting composite materials. In terms of mechanical properties (table 1.2), CNTs are useful in a wide range of applications. The material can be used as tip for scanning probe microscopy (SPM), such as atomic force microscopy (AFM) [9].

Material	Young's modulus (GPa)	Tensile Strength (GPa)	Density (g/cm^3)
MWNT	1200	~150	2.6
SWNT	1054	75	1.3
SWNT bundle	563	~150	1.3
Graphite (in-plane)	350	2.5	2.6
Steel	208	0.4	7.8

Table 1.2: Mechanical properties of nanotubes [8].

CNTs are chemically highly inert. The high electrochemical accessible surface area of porous nanotube arrays combined with their high electronic conductivity and useful mechanical properties make this material attractive as electrodes for devices that use electrochemical double-layer charge injection [10]. Electrode material such as graphite has been used for this purpose. Graphite is well known as a stable electrode material because is not reduced or oxidized over a substantial range of potentials. The large

surface area and low resistivity of CNTs make them of great interest for electrochemistry [11].

1.2 Electron Emission Theory

1.2.1 Thermionic Emission

Thermionic cathodes are widely used as an electron source. Thermionic emission is the emission from a material at high temperature (1000 – 3000 ℃) such that the electrons have enough energy to escape from the Fermi-level to the vacuum level of the material as shown in Figure 1.7. The electrons in this mechanism are emitted from heat filaments; this is the most common mechanism to extract them. In this process the electrons have sufficient kinetic energy to surmount the surface barrier.
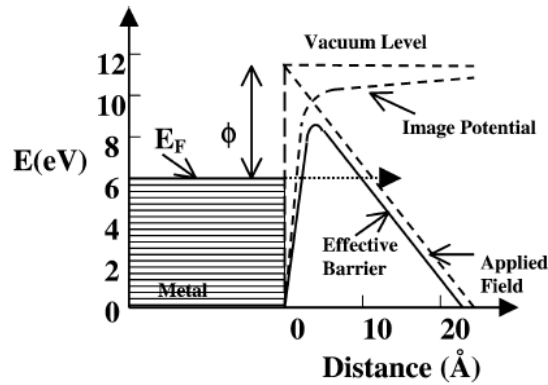
Figure 1.7: Potential-energy diagram illustrating the effect of an external electric field on the energy barrier for electrons at a metal surface [16].

Richardson-Dushman equation describes the thermionic emission phenomena (Equation 1.1) [17], where T is the metal temperature, ϕ is the work function, and k is the Boltzmann constant.

$$J = 120\ T^2\ e^{-\phi/kT}\ [A/cm^2], \text{ where } T \sim 1000\ ℃ \qquad \text{Equation 1.1}$$

During operation, the cathode temperature is raised by resistive or other means of heating and emitted electrons are collected with an electric field [8]. Thermionic source is usually a tungsten filament or a porous tungsten matrix impregnated with a material allowing the reduction of the work function. Figure 1.8 illustrates the principle of the thermionic emitter. Thermionic sources have low energy efficiency due to the high operating temperature that contributes to the energy loss by radiation [8]; this can be considered as a disadvantage. Other disadvantages include the shape of the emitter changing due to the thermal expansion. The outgassing generated for these emitters result in a limited lifetime because of the vacuum degradation. The other disadvantage is that due to the high operating temperature, it is difficult to miniaturize thermionic cathode or pack multiple thermionic cathodes in a small confined space.
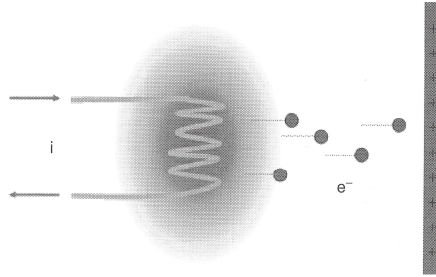
Figure 1.8: Principle of thermionic emitter: a metal is heated high enough to give the free electrons enough energy to overcome the surface potential barrier [8].

1.2.2 Field Emission

High aspect ratio [12, 14 - 15], whisker-like in shape [13 - 14], high electrical and thermal conductivity [13, 16], good chemical and structural stability [16], and a high melting point make an excellent electron emitter. Field emission emitters are use in vacuum microelectronics devices. Vacuum microelectronics devices or field emission devices can operate at higher frequencies and higher power in a wider temperature range

[18]. Flat panel field emission displays (FEDs), miniaturized microwave power amplifier tubes, advanced sensors, and X-ray generators [18] among others applications are included in the vacuum microelectronic technology. Two important events in vacuum microelectronics are microfabrication technology and the use of field emitters as a source of electrons. The most common field emitters are tungsten, molybdenum (in Spindt cathodes), and silicon. New cathode materials such as diamond and CNTs emitters have been used as field emitters.

Field emission is an alternative mechanism to extract electrons [16]. Field emission is a quantum mechanical tunneling phenomenon in which electrons escape from solid surface into vacuum. In contrast to the commonly used thermionic emission from hot filaments, field emission occurs at room temperature from unheated "cold" cathodes under an electric field [18]. In other words, it is the extraction of electrons from a material surface when a voltage is applied. During field emission a high electric field is generated such that the electrons have enough energy to escape from the Fermi-level to the vacuum level (Figure 1.7). The Fowler-Nordheim equation (Equation 1.2) describes the field emission mechanism,

$$I = a\mathrm{V}^2 \exp(-b\phi^{3/2}/\beta\mathrm{V}) \qquad \text{Equation 1.2}$$

where I is the emission current, V is the applied voltage, ϕ is the work function and β is the field enhancement factor [16]. The work function is a basic property of the material that cannot be varied significantly. It determines the emission characteristics of the material. The field enhancement factor is inversely related to the shape of the emitter: as

the radius of the emitter decreases the field enhancement factor increases. Moreover, if the field enhancement factor increases and the effective threshold voltage decreases. When sharp cathodes are used for field emission, the macroscopic electric field required to induce to the point where the macroscopic field of a few V/µm can be sufficient, as seen in Figure 1.9 [8].
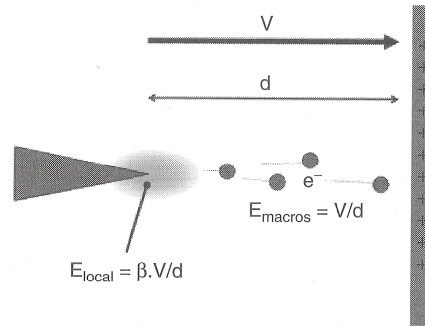
Figure 1.9: Schematic diagram of a field emitter; the electric field around the sharp tip is enhanced to the point where electrons can tunnel through the surface barrier [8].

Field emission is one of the best choices for many applications due to its numerous benefits. This mechanism does not require heat, produces low energy spread of the emitted electrons, has instantaneous response to field variation, is resistance to both temperature fluctuation and radiation and a nonlinear exponential current-voltage relationship in which a small change of voltage can induce a large change of emission current [8,18].

The previous generation of field emission emitters started in the 1950s – 1970s with the etched needles. These needles had many limitations including: the necessity of (1) high voltage and (2) high vacuum were the most problematic. In addition, the limited lifetime resulted in the main disadvantage. Latter, the invention of the Spindt cathodes

consisted of a multilayer structure of Mo gate/SiO$_2$ insulator/ Mo cathode cones on a Si substrate fabricated by thin film vacuum deposition techniques [18]. Basically, the emitter performance relies on the nature of the operating environment and the interaction of the emitter surface. For example, it is clear that environments containing organics are best avoided in any case. The combination of low surface barrier to electron emission in an otherwise robust material has attracted attention to diamond's promise as a high performance cold cathode material [18]. The limitation of the diamond emitters was the emission typically from a set of spots, each of different efficiency. This possibly related to the variations in surface morphologies and adsorbates resulting in a non-uniform distribution of the emission current. The main reason for the failure of the electron field emitters prior CNTs is the adhesion of the emitters to the substrate surface under high voltage. This is the major cause of arching which is detrimental to vacuum electronic devices.

1.2.3 CNTs as Field Emission Emitters

The power of the CNTs as electron field emitters was known since the first articles reported extremely low turn-on fields and high current densities in 1995 [19]. The CNTs can be used as electron sources in two ways: as a single or as a multiple electron beam device. Field emission display (FED) is a good example of a multiple electron beam device. The CNTs have necessary properties to be excellent electron field emission emitters - one reason why this material attracts all the researchers' attention. A key advantage of CNTs is they have a very low turn-on field which is associated with the high aspect ratio ($>10^3$, diameters in nanometers, and lengths in microns) and the atomically sharp tip [12-16, 19]. Because of their geometry the CNTs have an optimal

geometrical field enhancement factor that minimizes the electron emission turn-on field. The field enhancement factor depends mostly on the geometry of the emitter and can be approximated as $\beta = 1/5r$, where r is the radius of the emitter tip [15]. Figure 1.10 shows the classification and ranking of tip-shapes for field enhancement. The best field emission tip is whisker-like, followed by the sharpened pyramid, hemi-spheroidal, and pyramidal shape. CNTs have emission turn-on field of $1 - 2$ V/µm which is significantly lower than other materials shown in Table 1.3 [20].
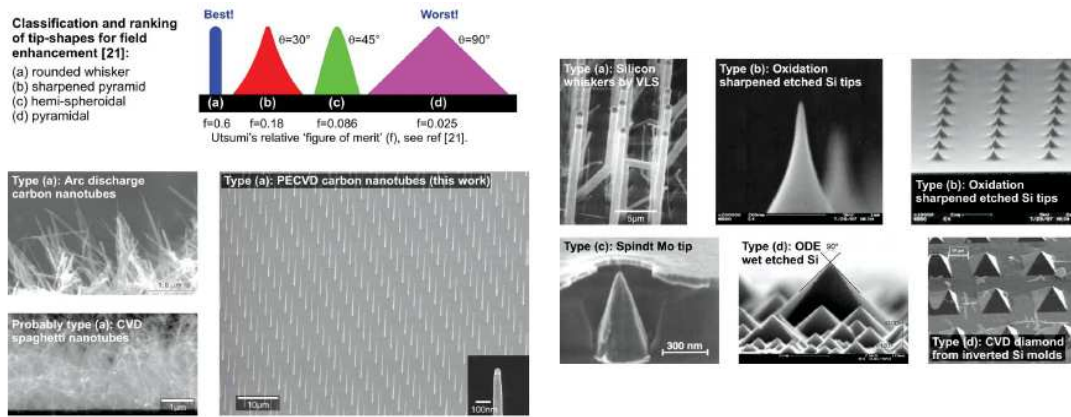
Figure 1.10: Classification and ranking of tip-shapes proposed by Utsumi. From best to worst — (a) rounded whisker which is ideal, (b) sharpened pyramid, (c) hemi-spheroidal, and (d) pyramidal [13].

Cathode Material	Threshold field (V/µm) for a current density of 10 mA/cm^2
Mo tips	50 – 100
Si tips	50 – 100
p-type diamond	160
Defective CVD diamond	30 – 120
amorphous diamond	20 – 40
cesium-coated diamond	20 – 30
graphite powders	10 – 20
nano-diamond	3 – 5 (unstable > 30 mA/cm^2)
carbon nanotubes	2 – 5 (stable > 1 µA/tube)

Table 1.3: Electron Field Emission Characteristics of Typical Emissive Materials [20].

Resistance to temperature fluctuation is another characteristic that has made CNTs attractive as field emission emitters. The material is very stable even at high temperatures [13] because of the strong covalent bonding. They are physically inert to sputtering and chemically inert to poisoning [14]. It has been demonstrated that MWNTs can be heated up to 2000 K in vacuum and remain stable [13]. Figure 1.11 shows a comparison of the field emission properties of nano-tips of amorphous diamond and CNTs at various temperatures. The emission from the CNTs does not change with the increasing temperature.   Metal emitters, however, are different. In metals, the resistance (R) increases with temperature which indicates that more heat (Q) is produced as higher currents (I) are drawn ($Q = I^2R$) [13]. The combination of the high temperature and electric field result in the field-sharpening of the tip by surface diffusion. Overall, metal-based emitters are unstable due to temperature increases, local field, and current and emitter destruction. In contrast, the resistance of a nanotube decreases with temperature which limits I^2R heat generation, and in fact its temperature varies sub-linearly with current [13]. CNTs do not suffer electric field induced sharpening, [14] making them very stable emitters.
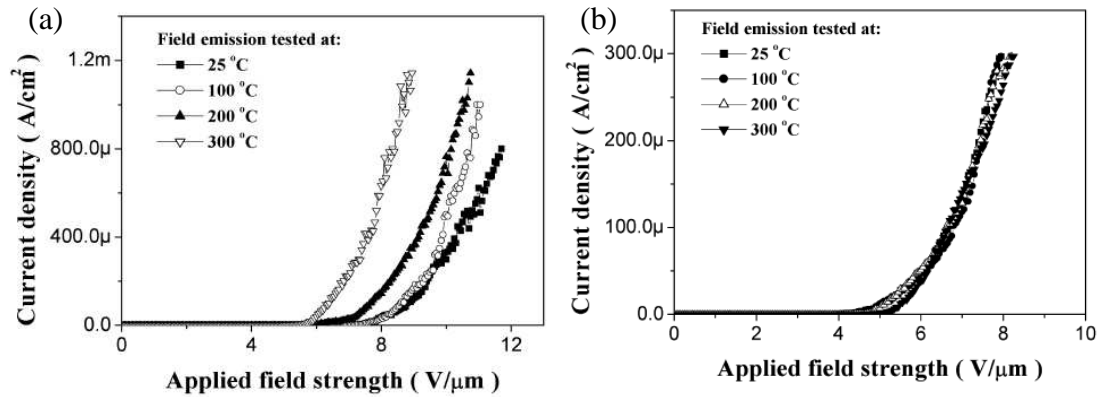
Figure 1.11: (a) Field emission curves for the nano-tips of amorphous diamond at various temperatures. (b) The field emission curves for the aligned CNTs at various temperatures. Note that the emission current remains unchanged with increasing temperatures [21].

CNTs have high electrical conductivity and high thermal conductivity at room temperature as result of the graphene walls parallel to the filament axis [13]. Therefore this material can conduct an electric current and heat, respectively. Their strong covalent bonding allows for good chemical and structural stability. These bonds make this material physically inert to sputtering and chemical inert to poisoning [14]. Since CNTs are chemically inert they only can react at high temperatures with oxygen or hydrogen [12]. As an electron source it is very common for the bombardment of positive ions. One advantage that CNTs offer over silicon or tungsten [14] is the lowest sputter coefficients [12]. Also, the ability of the CNTs to retain a stable tip structure even in moderate vacuum (10^{-8} Torr) makes them excellent electron emitters [10]. CNTs can carry a huge current density (10^9 A/cm^2) before electromigration [14]. Electromigration is a thermally activated process where the flux of electrons through a conductor can push along defects and grain boundaries. During the process, the normal diffusion of defects is given a down-stream bias by scattering with the moving electrons [18]. Field emission currents of 1 µA from a SWNT and current densities as high as 4 A/cm^2 from macroscopic CNT cathode [18] have been observed. CNTs with their particular and unique properties represent the next level of the microelectronic field emission emitters. Also these properties make them attractive "cold" cathode materials for X-ray tubes.

1.3 CNTs as X-Ray Sources

X-ray is a form of electromagnetic radiation with a wavelength in the range of 10 to 0.01 nanometers. X-rays are widely used in different applications such as medical applications (medical imaging, radiotherapy), analytical instruments (crystallography), and in industrial and security inspection. Medical imaging is probably the most common

14

use of the X-ray technology. Examples of medical applications include computed tomography, mammography and radiation therapy. Digital breast tomosynthesis (DBT) is a new experimental technique. DBT which is a three dimensional imaging technique. It a limited angle tomography technique that provides reconstruction planes in the breast using projection images from a limited angular range. On the other hand, radiation therapy is a curative medical intervention that employs higher energies of radiation. The large increase in interest in micro-CT over the last decade reflects the need for a non-destructively method to visualize the internal three-dimensional structure of an object [22]. Computer tomography is used to generate 3D image of the inside of an object by collecting a large series of 2D images. The benefit of computed tomography is that it is available for a wide range of nominal resolutions, which allows the imaging of whole bodies down to the tissue level [22]. Figure 1.12 shows computed tomography-generated images, including high resolution CT, micro- CT and nano-CT.
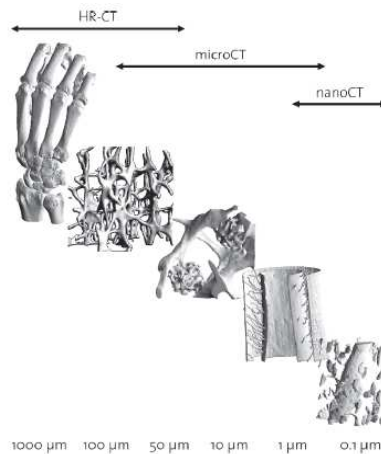
Figure 1.12: Hierarchical imaging using computed tomography (CT). The technique can be used on a large scale with different resolutions while always using the same physical principles. In high resolution CT (HR-CT) domain, normal x-ray tubes can be used as a source whereas for micro-CT special micro focus x-ray tubes are required. The lower range of micro-CT as well as the nano-CT domain is currently best assessed using synchrotron radiation (SR). The images show from left to right, the human hand, trabecular bone structure, microcallus, murine cortical bone surface of a femur with internal vasculature, and a capillary in bone surrounded by osteocyte lacunae [22].

15

1.3.1 Conventional X-Ray Source Technology vs. CNT X-Ray Source Technology

X-ray tubes are devices that allow controlled emission of X-rays [8]. Typical X-ray tubes consists of an electron source, a vacuum region, and an anode where the electrons are collected and continues to flow. The principle of X-ray generation in tube involves the bombardment of a target with high energy electrons. For applications where small emitting spots are required, such as X-ray imaging of any application requiring X-ray optics, the tube is fitted with electron optics to concentrate the electron beam on a small area on a small target [8]. X-ray tubes require high current density in the order of $10^2 - 10^3$ mA/cm^2 and high acceleration voltage ranging from 30 KV for mammography to over 180 KV for airport baggage inspection. Table 1.4 shows some practical requirements for X-ray tubes. Basically, the requirements depend strongly on the applications. For example, security inspection does not require a focal spot size in the micron domain versus small animal imaging that requires very high resolution.

Parameters	Conditions
High anode voltage	160-180kV for airport security inspection 30-140kV for medical imaging
High tube current	0.5-1.0A at 1x1mm focal spot for clinical CT ~1mA at ~50um focal spot for micro-focus tube
Non-ideal vacuum	Ion bombardment, arcing
Lifetime	Over 3 years

Table 1.4: Some practical requirements for X-ray tubes
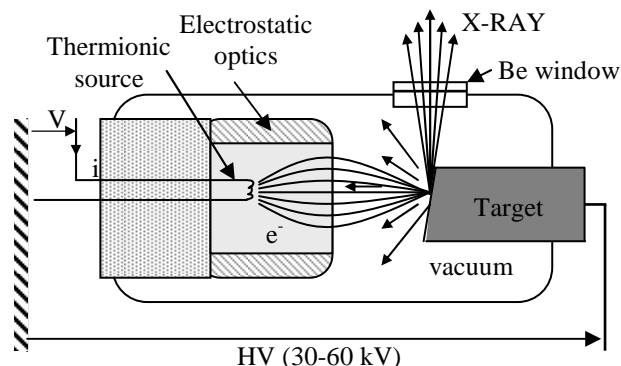
Figure 1.13: **Schematic structure of an X-ray tube based on thermionic source [8].**

Conventional X-ray source technology uses thermionic sources. Figure 1.13 shows a schematic structure of an X-ray tube based on a thermionic source. In terms of practicality, miniature X-ray tubes are limited by the most critical component: the electron source [8]. Conventional thermionic sources do not have the appropriate efficiency with low power X-ray tubes because of the heat produce during operation from the filament. CNT X-ray source technology has many advantages over the conventional technology because CNT technology is more energy efficient and less outgases species that would deteriorate the vacuum and contaminate the target. Other disadvantages related with the high operating temperature are the additional power dissipation (heat or radiation) and time delays in starting the operation of the device. The large size of the device is another disadvantage in term of practicality. The thermionic source undergoes thermal expansion which changes the shape of the emitters. In addition, this non-high vacuum contributes to the increases in the number of gaseous molecules. These hot cathodes react with the residual water and oxygen to produce oxides. These oxides contribute to the filament thinning over time and eventually filament failure affecting the emission current. Conventional thermionic sources also suffer from low temporal resolution (this determines how fast the source can be turn-on and off), limited

17

programmability, and are only available in single source. All of these disadvantages limit the performance of the commercial micro-CT scanners. The poor performance makes gated imaging of moving objects very difficult because the motion blur significantly decreases the image quality.

CNT X-ray source technology offers the solution to the conventional thermionic X-ray source technology. CNT technology advantages include high temporal resolution, high spatial resolution (this determines when two objects can be distinguishable), programmability, and has the potential to reduce the size of the device. Also this technology is available in multi-pixel, with different pixel resolutions (different focal points on the X-ray anode) or same pixel resolution in the same tube and multiplexing which will reduce the scanning time. Multiplexing is a collection of multiple images at the same time. In order to ascertain the high performance of the CNT X-ray electron sources, the CNT cathode must have the required properties for X-ray generation which include low turn-on field, high emission current, uniformity, reproducibility, and stability under high emission current density and high anode voltage.

1.3.2 *Applications of CNT X-Ray Sources*

CNT X-ray source technology enables the fabrication of single pixel X-ray sources and spatially distributed X-ray sources with multiple independently controlled X-ray beams. Figure 1.14 illustrated the spatially distributed X-ray sources in different configurations. These X-ray sources are used in applications from digital breast tomosynthesis to security screening. Some of these multi-beam field emission X-ray (MBFEX) sources are commercially available as CNT X-ray tubes. Other application that

18

this technology allows includes CNT X-ray tubes for micro-CT which is widely used for small animal imaging and other studies for which high resolution are required.
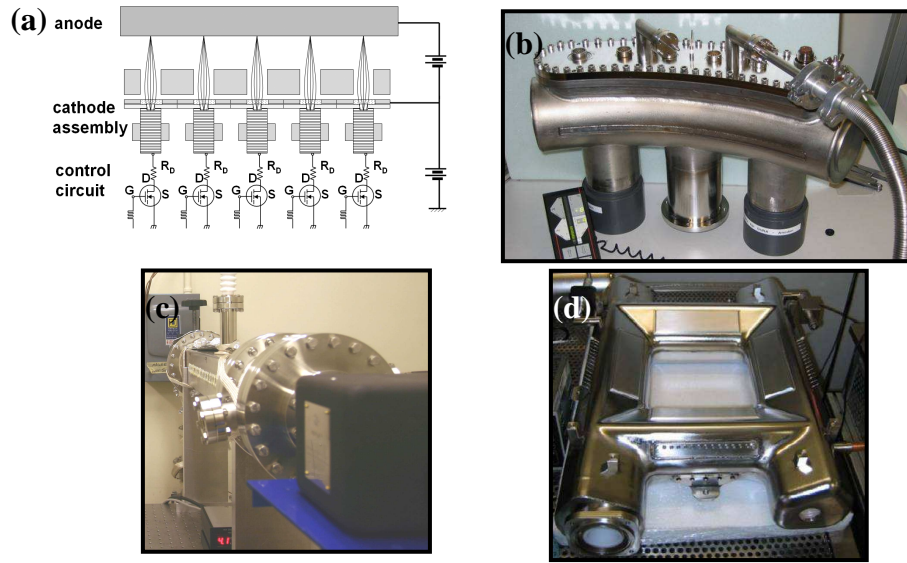
Figure 1.14: (a) A schematic illustration of a distributed multi-beam field emission X-ray (MBFEX) source with 5 independently controllable X-ray pixels, (b and d) images of MBFEX tubes with different configurations manufactured by XinRay Systems LLC, and (c) images of linear array of 25 individual X-ray beam for digital breast tomosynthesis.

Micro-CT scanners developed at UNC-Chapel Hill are single or multi-beam X-ray source systems. The single X-ray source system consists in a rotating source and detector pair and a stationary sample. On the other hand, the multi-beam X-ray source system consists in a linear CNT field emission source array, a 3-axis rotary table as the object stage, and an X-ray detector. All these applications employ CNT cathodes as X-ray source; these CNT cathodes are the main and the most important part of these X-ray tubes.
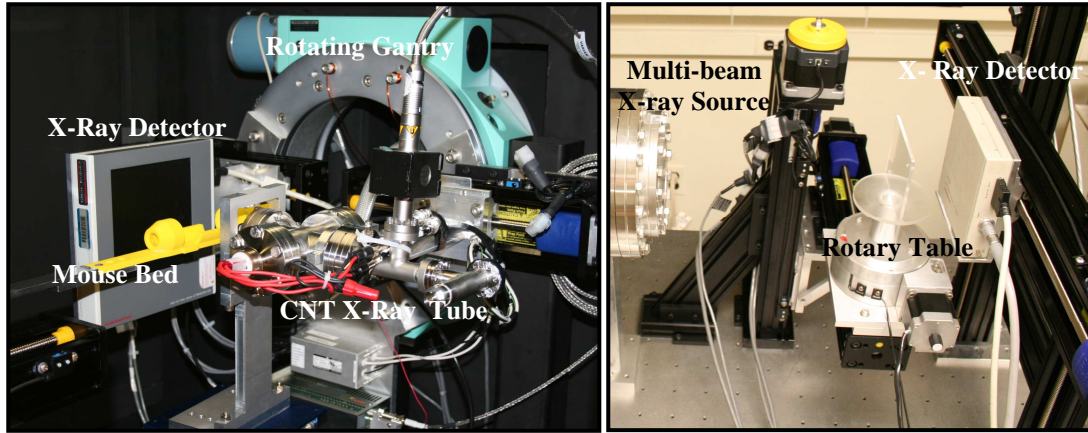
Figure 1.15: Images of single and multi-beam X-ray source micro- CT scanners.

1.4 CNT Cathode Fabrication Methods

CNT cathodes production is necessary and essential for field emission applications such as field emission displays (FED), CNT X-ray electron sources and vacuum microelectronics in general. The most commonly used methods to fabricate CNT cathodes are chemical vapor deposition (CVD), screen printing, and electrophoretic deposition (EPD). These fabrication methods must be capable of producing CNT alignment or patterns with uniform structures to meet device requirements.

1.4.1 Chemical Vapor Deposition and Screen Printing Methods

A wide range of CNTs applications such as nanoelectronic, sensors, and field emitters require a reliable method capable of producing high quality CNT cathodes. The CVD process encompasses a wide range of synthesis techniques, from the gram-quantity bulk formation of nanotube material to the formation of individually aligned SWNTs on SiO_2 substrates for use in electronics [23]. CVD is gas phase technique that uses the decomposition of a carbon source at a certain temperature. This technique uses different hydrocarbons or carbon sources, catalysts, catalyst particles-size, and growth temperatures to vary the size, morphology and quality of the CNTs. Figure 1.14 shows a

20

simple schematic of a CVD furnace that consist of a gas carbon feedstock. The CNTs are

produced when the feedstock is flowed over the transition metal nanoparticles at medium

to high temperature and reacts with the nanoparticles [23]. Some of the advantages of

chemical vapor deposition are no purification steps, growth directly on the substrate,

random and vertical aligned fabrication [24]. On the other hand, the disadvantages of this

method include: (1) expensive compared with others methods, (2) difficult to control

density and CNTs length, (3) not reliable to large-area depositions, (4) complicated

vacuum process, and (5) high growth temperature especially for large area FED [25].
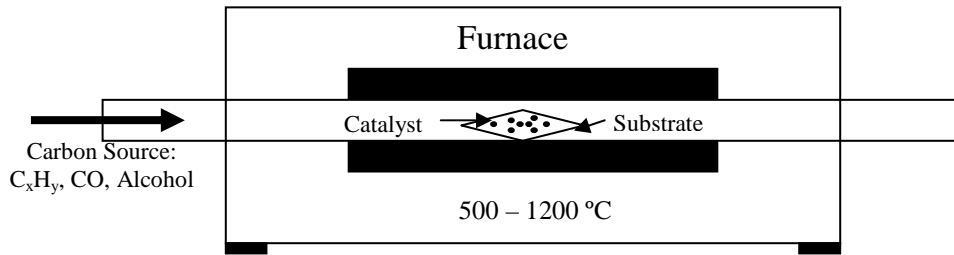
Figure 1.16: Schematic of CVD furnace.

In 2006, Samsung designed 4.75 in. diagonal field emitter arrays, as illustrated in

Figure 1.15, with a double-gated structure where the CNTs were synthesized by CVD

[26]. The nanotubes were grown directly inside the gate hole and used as an emitter.
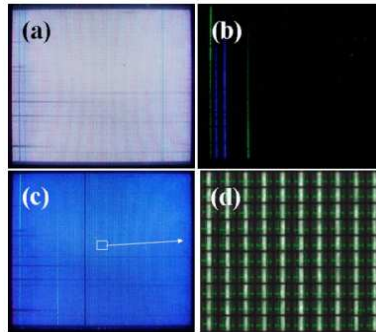
Figure 1.17: Emission image obtained from the green-blue-red patterned phosphor. (a) The image of all pixels being turned on. (b) Dark image resulting from applying *Vc*=40 V. (c) Blue image resulting from applying *Vc*=40 V to green and red pixel lines. (d) The image of 100 blue pixels selected for the evaluation of PU [26].

Besides CVD, the screenprinting method can also be used to the fabrication of CNT cathodes. Moreover, the method has several advantages such as the ability to use large are cold cathode because of low costs, simplicity in design, a uniform emission site, and mass production [24]. The screen printing method uses CNT paste that it is composed of CNT powder, organic vehicle and inorganic binders. The paste is ultimately transferred to a substrate. Unfortunately this simple method has several disadvantages including contamination from the organic paste [25], it is inconvenient to integrate to gate electrode [25], weak adhesion of CNT to substrate [24], non-uniformity of electron emission [24], etc. Samsung used this method to make a 4.5 inch shown in Figure 1.16, and a nine-inch CNT field emission display [27] with very good results. In 2003, Samsung showed significant improvement in large area 38" prototype FED with very few point defects using screen printing method.

Figure 1.18: 4.5 in. CNT field emission display made using screen printing [27].

These methods are widely used to make CNT cathodes for different applications. After careful analysis of the advantages, disadvantages, effectiveness and capabilities of these methods and taking in consideration the requirements for the CNT cathode for X-ray generation, these methods are not the best alternative. A contamination free environment is essential and these methods do not meet such an important requirement for X-ray generation applications. As results of the analysis of the CVD and screen

22

printing method as a fabrication method, Zhou's research group uses EPD for the CNT cathode production for X-ray generation.

1.4.1.1 Field Emission Properties of CNT Cathodes Fabricated by CVD and Screen Printing

As previously mentioned, CNTs are now being investigated as "cold cathodes" for a wide range of applications. Most published CNT field emission research so far has focused on FED where the field emission properties requirements are different from CNT X-ray source technology. The field emission properties for CNT cathodes fabricated by CVD and screen printing for different applications will be present in this section. Park et al. reported the use of screen printing method to fabricated CNT cathodes of 2 x 2 cm^2, the emission current density at an applied field of 7.95 V/µm is 265 µA/cm^2 [28]. Also in this method is commonly investigate different activation process to improve the performance of the CNT cathodes; this include laser irradiation, ion irradiation, adhesive tape method, firing the sample at high temperature, and aging treatment.
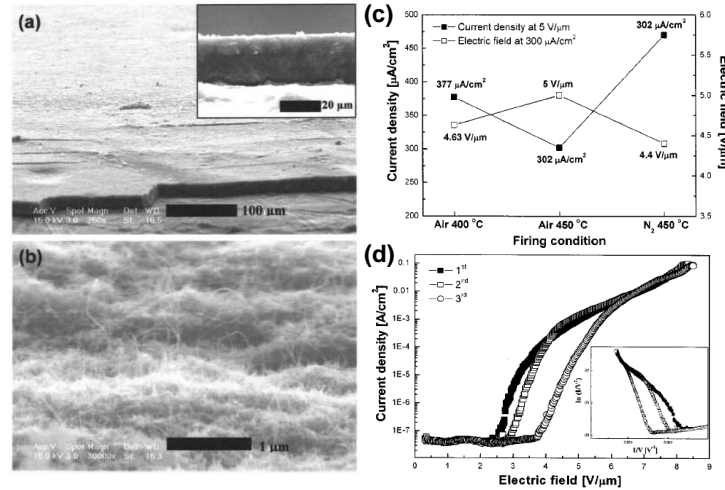
Figure 1.19: SEM images of acryl-based CNT paste with SOG printed on a Ni plate: (a) cross sectional and (b) tilt view of CNT paste after firing at 450 °C in N$_2$. Inset of sad shows the thickness of the CNT paste. (c) The emission characteristics of acryl-based CNT paste with SOG depending on different firing conditions. (d) Cycled *J–E* plot from acryl-based CNT paste with SOG printed onto a Ni plate fired at 450 °C in N$_2$. Inset indicates the F-N plot [28].

23

Figure 1.19 shows the SEM images for a CNT paste printed on a Ni plate, the field emission properties of this CNT paste are also shown. The firing temperature does make the difference in the field emission properties of the CNT paste, similar to other activation methods. Figure 1.19d shows the emission properties for a 1 x 1 cm^2 CNT paste film printed on the Ni plate. For 1 x 1 cm^2 cathode fabricated by screen printing method the emission current of about 100 mA at an electric field of 8.35 V/µm, which represent 100 mA/cm^2 [28].

In 2007, Mu et al. used CVD for grown and fabricated random oriented CNTs on silicon substrate [29]. The field emission properties in diode mode showed emission current of 13 mA which corresponding to a density of 414 mA/cm^2 under an electric field of 23 V/µm after an aging process. Other geometry approaches have been investigated to fabricate cathodes using CVD.
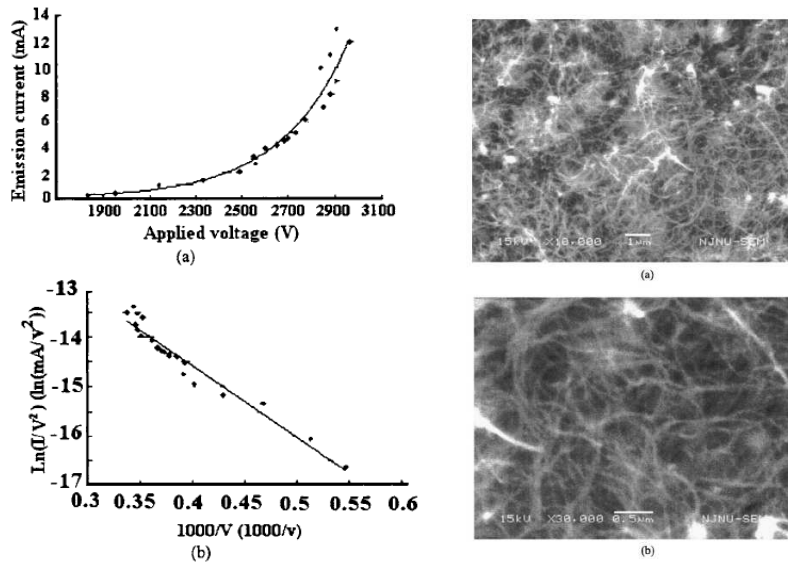
Figure 1.20: *I-V* **curve and Fowler-Nordheim plot of CNT emitters. SEM images of CNT emitters with different resolutions after the field-emission test [29].**

CVD has been use to fabricate CNT arrays on gated substrate [30-32]. The arrays contained 7670 cells occupying 0.1 mm^2 area [30]. Figure 1.21a-b shows scanning electron micrographs showing randomly oriented CNTs with small diameters and vertically aligned CNTs with larger diameters grown on top of gated silicon posts by dc plasma-enhanced CVD. Figure 1.21c shows the field emission properties of a 7670-cell. A table with the summary of maximum anode current density values corresponding to the current-voltage data from emitter arrays is shown in Figure 1.21d. The table showed the field emission properties from nine different arrays exhibiting current densities greater than 100 mA/cm^2 after similar conditioning of successively higher voltage intervals. It is interesting to note the large variation of the field emission properties for samples made under the same conditions.

Array	Area (mm^2)	Gate V (V)	Anode I (mA)	Current density (A/cm^2)	Transconductance (mS/cm^2)
a	0.1	75	1.37	1.37	174
b	0.1	60	1.19	1.19	168
c	0.1	71	1.07	1.07	143
d	0.1	67	0.71	0.71	89
e	0.1	76	0.56	0.56	58
f	0.1	65	0.50	0.50	83
g	0.1	70	0.26	0.26	25
h	0.05	50	0.12	0.24	38
i	0.1	70	0.12	0.12	29
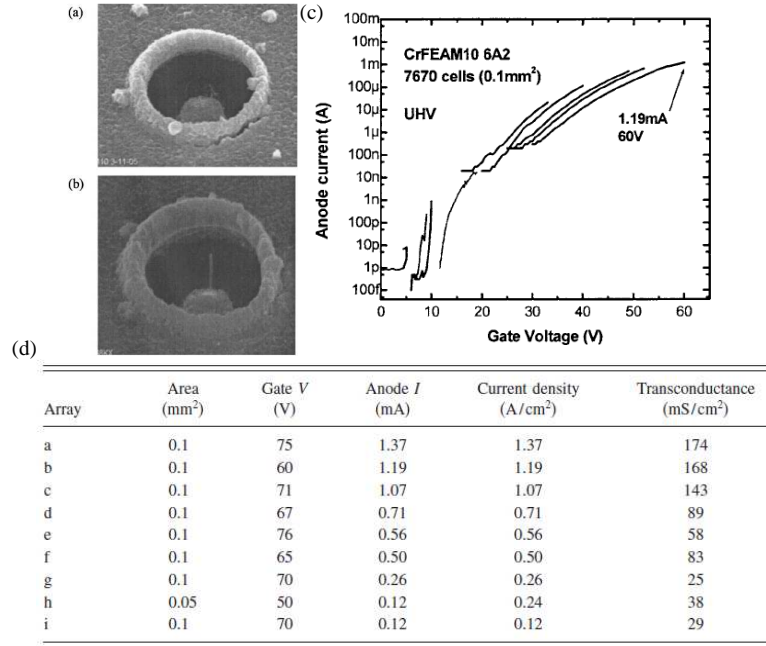
Figure 1.21: Scanning electron micrographs showing (a) randomly oriented CNTs with small diameters (<10 nm) and (b) vertically aligned CNTs with larger diameters (<50 nm) grown on top of gated silicon posts by using dc plasma-enhanced CVD. Anode current-gate voltage characteristics of a 7670-cell array of CNT on silicon post field emitters corresponding to a, obtained during the conditioning process of ramping up in successively higher voltage ranges. (d) Table with the summary of maximum anode current density and corresponding transconductance values corresponding to the current-voltage data from emitter arrays [30].

CNT pillar arrays (CPA) have been explore as an alternative to improve the field emission properties of the CNT cathodes made by CVD. Niemann et al. worked on the integration of a gate electrode with array of CNT emitters suggesting applications where gated cathode structures with high emission current density are required such as X-ray tubes, traveling wave tubes, and ion propulsion systems [31]. One of the limiting factors in the progress of gated cathode structure is the inability to fabricate arrays of individual CNTs in a highly controllable and reproducible manner. Figure 1.22 shows SEM image of a typical CPA and a side view SEM image of a highly ordered and vertically aligned bundle of CNTs. The plot of current density as a function of applied field for a 15 µm pitch CPA composed of 10 µm diameter pillars revealed current density of 60 mA/cm^2 in diode geometry [31].
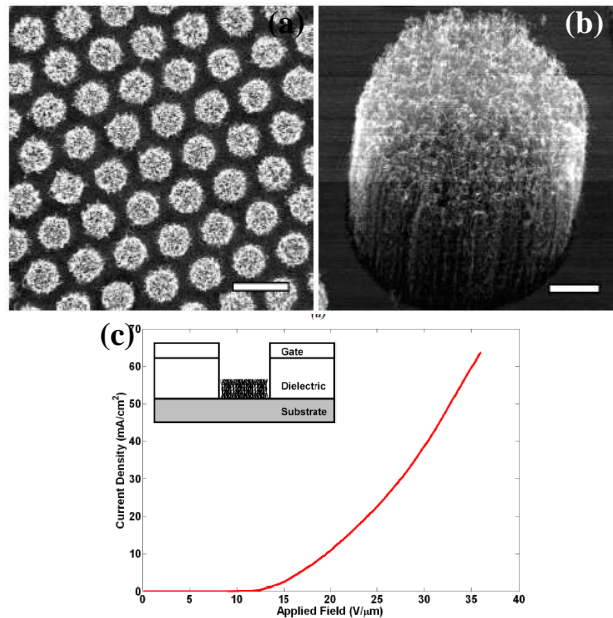
Figure 1.22: (a) A top down SEM image of a typical CPA (scale bar is 20 µm) and (b) A side view SEM image of a highly ordered and vertically aligned bundle of CNTs (scale bar is 2 μm). A plot of current density as a function of applied field for a 15 µm pitch CPA composed of 10 um diameter pillars. Measurements were conducted in a diode configuration with an anode cathode separation of 100 µm. (inset) A schematic representation of the cross-section for a gated CNT cathode incorporating a single CNT pillar. A patterned Molybdenum layer acts as the extracting gate electrode. The dielectric stack is comprised of Polyimide and Oxide and the substrate acts as the Cathode in this system. This structure may be repeated to produce large arrays of emitters [31].

26

Recently, well aligned CNT arrays were fabricated using the resist-assited patterning (RAP) process [32]. The use of these CNT arrays for high resolution X-ray generation was demonstrated. Figure 1.23a shows the schematic of X-ray generator and measurement system. The system consists of a CNT cathode, gate, anode, and Mo windows used to filter the X-rays. The quality of the X-ray generation depends on the emitters arrays geometry, especially the dot size as shown in Figure 1.23b. The whole CNT area of 0.5 x 0.5 mm^2 was used to optimize the resolution of X-rays (Figure 1.23c). RAP process allows the growing of CNTs on metal substrate in different pattern and shapes as shown in Figure 1.23d.
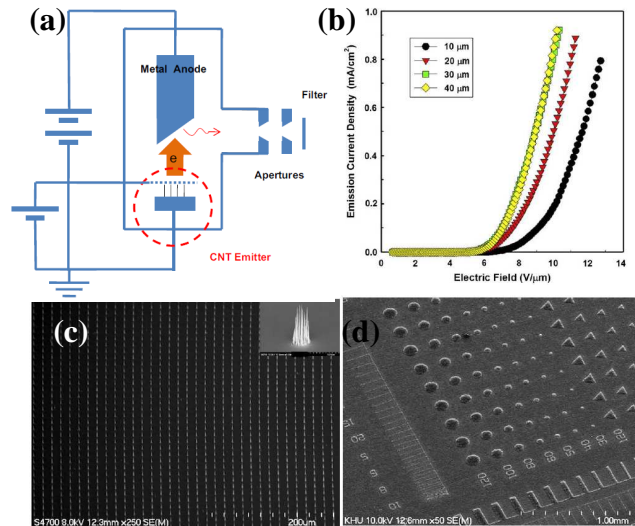
Figure 1.23: (a) Schematic diagram of the X-ray generator and measurement system. (b) Electron emission properties of CNT-FEAs as a function of pitch. (c) Carbon nanotube arrays grown with the resist-assisted patterning (RAP) process. (d) CNT emitters grown on metal substrates [32].

The use of these CNT cathodes for X-ray generation has been demonstrated. Figure 1.24 shows the X-ray image of printed circuit board, during the image acquisition the anode current was 300 µA with an exposure time of 3 seconds. The anode voltage was 30 KVp which correspond to a total power of 10 W.

27
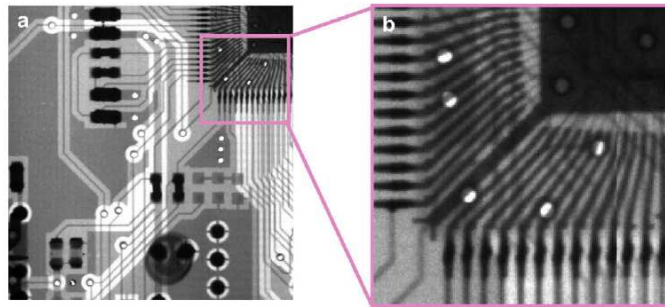
Figure 1.24: X-ray image of printed circuit board produced by CNT electron emitters [32].

CNT cathodes for different applications have been fabricated using CVD and screen printing methods. The field emission properties revealed current densities that agree with the FED requirements. On the other hand, for X-ray applications the field emission properties did not correspond to the requirement of this technology. The emission currents are a limiting factor of the CNT cathode fabricated by CVD and screen printing for some applications.

1.4.2 *Electrophoretic Deposition (EPD)*

EPD method is a high throughput, room temperature liquid phase process, easy to scale up, low investment, high flexibility, and capable in the deposition of uniform thickness thin film. This is a two-step process. In the first step, particles suspended in a liquid are forced to move forward on an electrode by applying an electric field to the suspension (electrophoresis) [33-34]. In the second step, the particles collect at one of the electrode and form a coherent deposit on it [33-34]. Only charged particles in the suspensions will move only in response to electric field [33]. The process and the schematic of EPD set-up which have been used for the CNT cathode fabrication in

Zhou's research group are shown in Figure 1.17 [35-37]. The deposition occurs when a dc field causes the charged particles move toward the oppositely charged electrode.
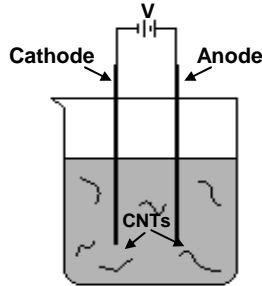
Figure 1.25: Schematic of electrophorethic deposition set-up [35-37].

The method can be applied to any solid that is available in the form of fine powder, less than 30 µm, or in a colloidal suspension. EPD, a versatile method that can be applied to almost any material including metals, polymers, carbides, oxides, nitrides, and glasses [33]. This method has been use in different applications such as general industrial coating (automotive, appliances), phosphor coating in the manufacture of screens for cathode ray tubes, deposition of insulating glass for electronic applications [33], thin film, layered material, and laminates.

EPD requires a conductive substrate such as indium tin oxide (ITO) coated glass, stainless steel, aluminium, titanium, silicon wafers, nickel, etc. In addition, the optimization of this method requires the control of voltage, deposition time, electrodes distance. The thickness, uniformity and density is controlled by voltage, deposition time and electrodes distance. One important requirement of this method is the utilization of a stable suspension. The suspension is an essential part of EPD and must meet certain requirements.

1.4.2.1 Suspensions for EPD

The suspensions for EPD need to meet certain requirements to achieve the desire results. The first requirement is that particles in suspension must have a high zeta potential. Zeta potential is a physical property that is characteristic of any particle in suspension [38] indicating the magnitude of the interaction of the colloidal particles and help to predict long-term stability. In some colloidal systems, the particles in dispersion may collide and agregate making the system unstable and with poor particle dispersion. In order to create a stable colloidal system, a necessary balance between the repulsive and attractive forces, as suggested by the DVLO (Deryaguin and Landau and Verwey and Overbeek) theory. DVLO theory combines the van der Waals attration with the double-layer repulsion which created a energy-distance curve to describe the conditions of stability/instability [39]. The theory, developed in the 1940s is represented by Equation 1.3 which describes the stability of particles in solution,

$$V_T = V_A + V_R + V_s \qquad \text{Equation 1.3}$$

where V_T is the total potential energy function, V_A is the van der Waals attractive forces, V_R is the electrical double layer repulsive forces and V_S is the potential due to the solvent [39]. The potential due to the solvent ussually makes a marginal contribution to the total energy. This physical property is determined via two ways: (1) from measuring the mobility of charged particles in dispersion under an electric field or (2) the electrophorethic mobility of the charged particles. The Henry equation depicts the relationship between the electrophorethic mobility and the zeta potential:

$$U_e = \frac{2\varepsilon\zeta f(\kappa a)}{3\eta}$$

Equation 1.4

In Equation 1.4, Ue is the electrophoretic mobility, ε is the dielectric constant of the sample, ζ is the zeta potential, $f(ka)$ is the Henry's Function (most often used are the Huckel and Smoluchowski approximations of 1 and 1.5, respectively) and η is the viscosity of the solvent.

Likewise, it is important keep the ion conductivity of the suspension low [33], which is achivieved when certain measures are taken. IUPAC Compendium of Chemical Terminology define ion conductivity as an ionic species B by

$$\lambda = |z_B| F u_B$$

Equation 1.5

where z_B is the charge number of the ionic species B, F is the Faraday constant, and u_B is the electric mobility of species B [40]. One important requirement is that the particles in suspension must carry a charge [33] to be able to move under an electric field. This method depends directly on how charged particles respond to an electric field. The dielectric constant of the solvent is an important property for these suspensions [33]. The dielectric constant expresses the dissociation power of the solvent, or their polarity. In general, organics solvent have lower dielectric constant; this is a disadvantage because the lower constant limits the charge on the particle. But at the same time organic solvents

are preferred over water because the electrolysis of water occurs at low voltage (~5V). An empirical study of EPD deposition of beta-alumina revealed that a dielectric constant in the range 12 to 25 was required for EPD [33]. The last requirement is the suspension has to be stable, where the particles are dispersed homogeneously in a solvent. These requirements are necessary for a successful EPD deposition.

In general the CNT suspensions for EPD include CNT powder (SWNTs or MWNTs), charger salts, and solvent. The solvents include water, mixture of organic solvents (acetone and ethanol), pure organic solvents (tetrahydrofuran (THF), ethanol, isopropyl alcohol (IPA), methanol, dimethylformamide (DMF)) and mixture of water and organic solvents (water and pyrrole) [41]. The most commonly used charger salts are quaternary ammonium salts: $Mg(NO_3)_2$, $MgCl_2$, NaOH [41].

1.4.2.2 *Field Emission Properties of CNT Cathodes Fabricated by EPD*

Similar to CVD and screen printing method, EDP have been use to fabricated CNT cathodes for different applications. As previously mentioned, Zhou's research group have been using this method for the fabrication of CNT cathodes for X-ray application where high current densities and stability at high anode voltage are required. In 2001, the use of EPD in Zhou's research laboratories reported current densities as high as 67 mA/cm^2 for a 6 mm^2 CNT cathode [35]. Figure 1.26 shows the field emission current as a function of applied voltage and the emission stability of a 6 mm^2 area electrophoretically deposited SWNT film.

32
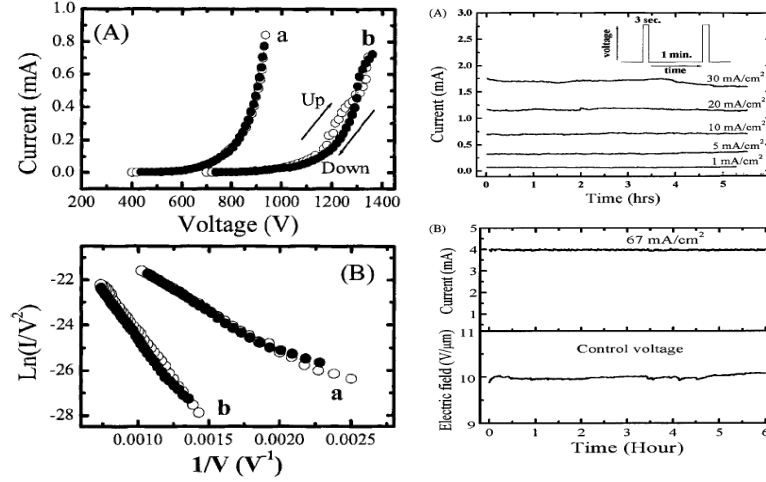
Figure 1.26: (A) The total electron field emission current versus applied voltage. Samples a and b are SWNT films prepared using methanol and DMF, respectively. In both cases, the emission was from a 6 mm² area. The cathode-anode distance was 160 μm. The base pressure was 2 x 10⁻⁷ Torr. (B) The same data as for (A) plotted as ln(I/V²) versus 1/V. (A) Emission stability of a 6 mm² area electrophoretically deposited SWNT film measured using a pulsed electrical field with a constant pulsed height (3 s duration pulse, 1 min repetition rate). (B) Total emission current from a 6 mm² area SWNT film obtained using a feedback loop (top) and the electrical field (bottom). The applied electrical field was adjusted automatically to maintain the 4 mA emission current [35].

The field emission performance of a CNT X-ray source [42] is shown in Figure 1.27. Figure 1.27b shows the field emission properties in triode geometry at an anode potential of 40 KV. A current density of 100 mA/cm² was obtained at a gate electric field of 12 V/μm. Also the electron source was tested in the pulsed as shown in Figure 1.27c, the conditions used were 100 Hz and 2 % duty cycle. The emission stability was tested and peak emission current of 0.3 mA was obtained with negligible degradation during 15 hours as shown in Figure 1.27d.
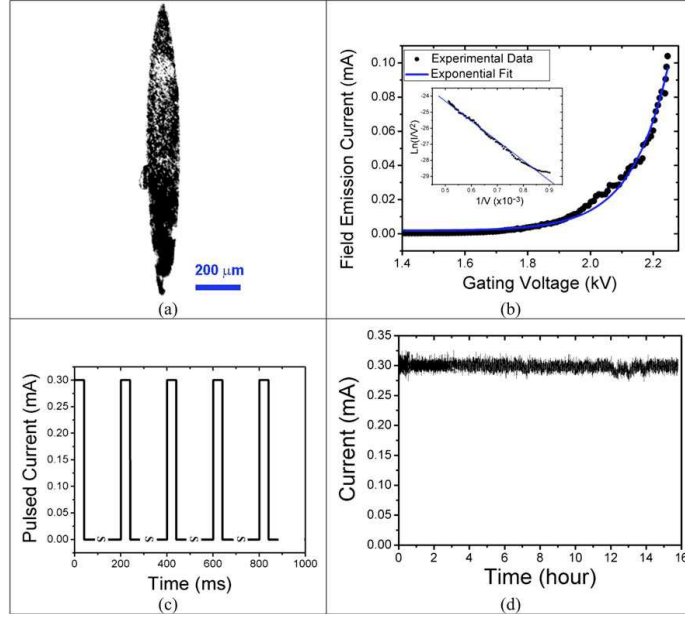
Figure 1.27: Field emission characteristics of an elliptical carbon nanotube based cathode measured in triode geometry. (a) An optical image of the elliptical cathode formed by combined lithography and electrophoresis deposition techniques. (b) The field emission current-voltage curve of the elliptical cathode in (a). (c) The field emission current operated in the pulsed mode with the frequency and duty cycle of 100 Hz and 2%, respectively. (d) The stability of the field emission current in pulsed mode with the same frequency and duty cycle as those in (c) [42].

The improvement of the field emission properties of the CNT cathode fabricated by EPD is essential for high current density applications. In addition, the improvement of the emission stability at high anode voltage is fundamental for X-ray application where the anode voltage operation range is from 30 KV to over 180 KV depending on the application.

1.5 Summary and Dissertation Motivation

CNTs with their diverse properties (mechanical, electronic, thermal, and chemical) have been demonstrated be excellent field emission emitters. Likewise, the application of CNTs as X-ray sources offers solutions to the problems which conventional thermionic X-ray sources have been unable to solve. The motivations of this dissertation involve the

understanding of the relation between the structure and morphology of the macroscopic CNT cathodes and their field emission properties. The development of a process to fabricate CNT cathodes with high current densities and high voltage stability is essential for X-ray applications. The most important part is the integration and the evaluation of the CNT cathodes performance in an X-ray tube.

The major problem at this moment is the performance of the CNT cathodes; these cathodes cannot generate enough current for X-ray generation and this is reflected on the X-ray imaging performance. Beside this general problem with the CNT cathodes, making cathodes with small dimensions have not been possible. Moreover, to improve the resolution of the micro-CT scanner, CNT cathodes must be made with smaller dimensions. The high current density and high voltage stability with long term stability in non-ideal vacuum environment are, however, a big challenge in CNT X-ray source technology. These are the main challenges in developing the CNT X-ray electron source technology. The experimental approaches on this dissertation includes: (1) the improvement of the CNT-alcohol based suspensions, (2) the optimization of the CNT cathode fabrication process, (3) the characterization of the structure, morphology and field emission properties for CNT cathodes with different sizes, and (4) the characterization and evaluation of the micro focus X-ray tube.

References

1. O'Connell, M. J. (2006). Carbon Nanotubes: Properties and Applications. Boca Raton: CRC Press; Taylor & Francis.

2. http://cohesion.rice.edu/naturalsciences/smalley/smalley.cfm?doc_id=4866

3. Nature 1991; **8,** 354-356. Helical microtubes of graphitic carbon.

4. Topics Appl. Phys.; 2001, **80**, 173. Scanning Probe Microscopy Studies of Carbon Nanotubes.

5. A. Loiseau et al. (2006). Understanding Carbon Nanotubes: From Basics to Application. Springer, Berlin Heidelberg.

6. Acc. Chem. Res.; 2002**, 35**, 1063-1069. Defects in Carbon Nanotubes.

7. Annu. Rev. Mater. Sci.; 1997, **27**:1-34. Future Directions in Carbon Science.

8. Meyyappan, M. (2005). Carbon Nanotubes: Science and Applications. Boca Raton: CRC Press.

9. Journal of Materials Science: Materials in Electronics; 2003, **14**, 657-659. The physics and applications of carbon nanotubes.

10. Science; 2002, **297**, 787-792. Carbon Nanotubes: the Route Toward Applications.

11. Materialstoday: Applications Features; 2004, **7**, issue 10, 46-52. Realistic applications of CNTs.

12. Phil. Trans. R. Soc. Lond. A; 2004, **362**, 2239-2266. Carbon nanotube electron sources and application.

13. J. Mater. Chem., 2004, **14**, 933-943. Carbon nanotubes as field emission source.

14. phys. Stat. sol. (a); 2006, **203**, No. 6, 1058-1063. Carbon nanotubes as electron sources.

15. Topics. Appl. Phys.; 2001, **80**, 391-425. Applications of Carbon Nanotubes.

16. C.R. Physique 4, 2003, 1021-1033. Electron field emission from carbon nanotubes.

17. Owen W. Richardson, Thermionic phenomena and the laws which govern them Nobel Lecture, December 12, 1929.

18. Zhu W. (2001). Vacuum Microelectronics. New York: John Wiley & Sons, Inc.

19. Solid-State Electronics; 2001, **45**, 893-914. Field emission from carbon nanotubes: the first five years.

20. Acc. Chem. Res.; 2002, **35**, 1045-1053. Materials Science of Carbon Nanotubes: Fabrication, Integration, and Properties of Macroscopic Structure of Carbon Nnaotubes.

21. Carbon; 2003, **41**, 2839–2845. Thermionic emission of amorphous diamond and field emission of carbon nanotubes.

22. Methods in Molecular Biology, Vol. 455: Osteoporosis: Methods and Protocols. Micro-Computed Tomography: A Method for the Non-Destructive Evaluation of the Three-Dimensional Structure of Biological Specimens.

23. O'Connell, M. J. (2006). Carbon Nanotubes: Properties and Applications. Boca Raton: CRC Press; Taylor & Francis.

24. Diamond & Related Materials 14 (2005) 1463-1468. Effect of binders and organic vehicles on the emission properties of carbon nanotubes paste.

25. Materials Chemistry and Physics, 2005, **93**, 473-477. Large-area carbon nanotubes film synthesized for field emission display by special CVD equipment and the field emission properties.

26. Appl. Phys. Lett. **88**, 263504 (2006). Double-gated field emitter array with carbon nanotubes grown by chemical vapor deposition.

27. Diamond and Related Materials 10 (2001) 265-270. Application of carbon nanotubes to field emission display.

28. J. Vac. Sci. Technol. B 23 (2), (2005). Stable and high emission current from carbon nanotube paste with spin on glass.

29. J. Vac. Sci. Technol. B 25 (2), (2007). High-current-density field emission from multiwalled carbon naotubes by chemical-vapor deposition with effective aging treatment.

30. J. Vac. Sci. Technol. B 24 (2), (2006). 1 A/cm^2 current density from microgated carbon naotubes field-emitter arrays grown by dc plasma chemical-vapor deposition.

31. IEEE 2008. Carbon Nanotubes Field Emission Devices with Integrated Gate for High Current Applications.

32. Vacuum (2009) article in press. X-ray image resolution of carbon nanotube emitters grown with resist-assisted patterning process.

33. Annu. Rev. Mater. Sci. 1999. 29: 327-52. Electrophoretic deposition of materials.

34. J. Am. Ceram. Soc., 79 [8] 1987-2002 (2006). Electrophoretic Deposition (EPD): Mechanisms, Kinetics, and Application to Ceramics.

35. Adv. Mater. 2001, 13, No. 23, December 3. Fabrication and Electron Field Emission Properties of Carbon Nanotube Films by Electrophoretic Deposition

36. Acc. Chem. Res. **2002,** 35, 1045-1053 Materials Science of Carbon Nanotubes: Fabrication, Integration, and Properties of Macroscopic Structures of Carbon Nanotubes.

37. Appl. Phys. Lett. **87** (19), 3738 (2004). Liquid-phase fabrication of patterned carbon nanotube field emission cathodes

38. www.malvern.co.uk Zetasizer Nano series technical notes.

39. Tadros T.F. (2007). Colloid Stability The Role of Surface Forces - Part I. Weinheim: Wiley-VCH; Verlag GmbH & Co. KGaA.

40. IUPAC Compedium of Chemical Terminology, 2nd Edition (1997), 1974, 37, 512.

41. Carbon 44 (2006) 3149–3160. Electrophoretic deposition of carbon nanotubes.

42. Appl. Phys. Lett. **89**, 103111 (2006). Carbon nanotube based microfocus field emission x-ray source for microcomputed tomography.

2 CNT Alcohol-Based Suspension

Since the discovery of CNTs, one of the biggest challenges has been the pre

paration of stable CNT suspensions for a given application. The CNT suspension is the

essential part of different applications such as CNTs reinforcing composite materials,

bioapplications, and the incorporation into a variety of water-based chemical

environments. In the following sections CNT suspensions problems and approaches will

be discussed. Furthermore, the studies and developments of CNT alcohol-based

suspensions will be explained.

2.1.1 Problems and Approaches

One of the main challenges in CNT research is the manipulating the material for

use in diverse applications. CNTs dispersion technology is still under development and

different approaches have been made in order to manipulate them based on the potential

applications. The main problem with CNT suspensions in any media is after a short time

the CNTs collide and aggregate due to the strong attractive interactions. The difficulty to

disrupt these ropes or bundles makes the dispersion of CNTs very difficult. In order to

understand the difficulty to disperse CNTs in suspension, it is necessary to study their

structure. Graphite and CNTs share the same sp^2 hybridization, the p_z orbital is

responsible for van der Waals interactions. The free electrons in the p_z are delocalized,

moving within this cloud and are no longer restricted to a single atom [15]; this explains why these materials can conduct electricity. Also, the delocalized π-electrons of CNTs can be use to promote adsorption with different varieties of molecules through π- π interactions.

The nano-scale dimensions of CNTs results in an increases in both the surface area of the particle and the attractive forces between the aggregates. High aspect ratios combined with high flexibilities increase the possibility of nanotube entanglement and close packing [15]. Figure 2.1 shows SEM and TEM images of a SWNT bundle. The bundles or ropes contain hundreds of closely packed CNTs tightly bound by Van der Waals attraction energy of 500 eV/µm of tube-tube contact [15].
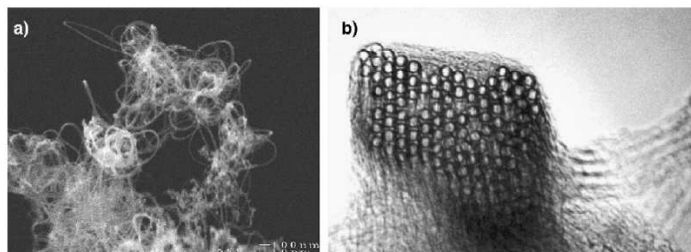
Figure 2.1: (a) SEM image of a SWN bundle. (b) TEM Image of the cross section of a SWNT bundle [15].

There are two main approaches to dispersing CNTs: mechanical dispersion and chemical methods. Mechanical dispersion methods include ultrasonication and high shear mixing [15]; these methods separate the nanotubes from each other. The use of ultrasound, however, has been shown to damage the nanotubes [16]. The general disadvantage of the mechanical dispersion method is the fragmentation of the nanotubes, which decrease the aspect ratio. The second approach to dispersing CNTs is altering the

surface chemistry of the CNTs side wall. Chemical methods include a covalent process (fuctionalization) and non-covalent process (adsorption).

2.1.1.1 Chemical Dispersion Method

2.1.1.1.1 Covalent Process

Covalent process (or surface funtionalization) of CNTs improves the chemical compatibility with the dispersion media and reduce the aggregation of the CNTs in suspension. The chemical oxidation of the CNTs surfaces is an example of functionalization and can dramatically increase the suspension stability. The oxidation of nanotubes induces a negatively charged surface, particularly through the ionization of acidic surface groups. The oxidation introduces oxygen-containing functional groups onto the surface and as a result electrostatic repulsion leads to a dramatic increase in the stability of the CNT dispersion. Figure 2.2 shows different oxygen-containing surface groups on carbon: a) carboxy groups, b)carboxyic anhydride groups, c)lactone groups, d)phenol groups, e)c arbonyl groups, f) quinone groups, g) xanthene or ether groups [17]. Also the oxidation of CNTs is the initial step for other reaction such as esterification or amidation.
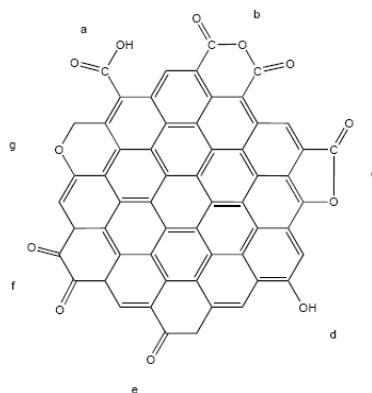
Figure 2.2: Different oxygen-containing surface groups on carbon: a) carboxyl groups, b)carboxyic anhydride groups, c)lactone groups, d)phenol groups, e)c arbonyl groups, f) quinone groups, g) xanthene or ether groups [17].

Amidation of oxidized CNTs is a common and versatile reaction where CNTs can react with long-chain alkylamines or directly condensate with amines. Figure 2.3 illustrates the reaction of oxidized CNTs with amines through thionyl chloride-activated carboxyl functional groups. The solubility of functionalized CNTs is about 0.5 mg/mL in tetrahydrofuran (THF) or dichlorobenzene. The esterification or amidation of CNTs results in a soluble functionalized material. The native electronic properties stays the same with functionalized CNTs remain intact whereas the length of CNTs is shortened [18]. However, aggressive chemical functionalization, such the use of neat acids at high temperatures, might introduce structural defects resulting in inferior properties for the CNTs [15].
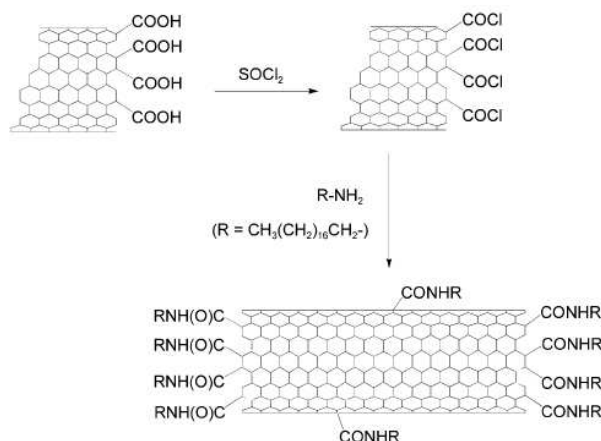
Figure 2.3: Schematic of amidization process of oxidized CNTs [18].

Mickelson [19] studied the side wall functionalization of SWNTs (Figure 2.4) by reacting them with elemental fluorine and note the high degree of solvation of fluorinated SWNTs in variety of alcohol solvents. Basically the solvation of fluorinated SWNTs in alcohol occurs because the F^- ion acts as one of the hydrogen bond acceptors. The solvation of fluorinated SWNT is 10 % wt in alcohol solvents. Sonicating the fluorotubes in alcohol solvents produces metastable solutions. These solutions were stable for a couple of days to over 1 week, depending on the concentration and solvent used. Alcohol solvents used included methanol, ethanol, 2,2,2-trifluoroethanol, 2-propanol, 2-butanol, *n*-pentanol, *n*-hexanol, cyclohexanol, and *n*-heptanol [19]. Other covalent approaches include reacting CNTs with chlorinated polypropylene, substitution by alkyl groups, and addition of nitrenes, carbenes or radicals [15].
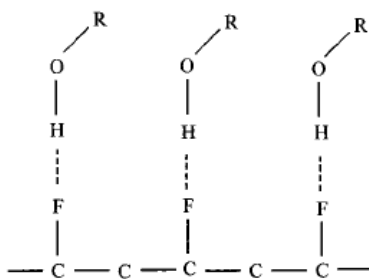
Figure 2.4: Fluorinated SWNTs [19].

2.1.1.1.2 Non-covalent process

Non-covalent process (or adsorption) is very attractive alternative to dispersing CNTs in suspension. The main advantage of this process is the possibility of different groups adsorbing and/or attaching to the CNTs surface without disturbing the π system. Research has shown that CNTs can be dispersed in water in the presence of surfactants. A surfactant (a contraction of the term surface-active agent) is a substance that, when present at low concentration in a system, has the property of being adsorbed by the surfaces or interfaces of the system and of altering their free energies to a marked degree [20]. Surfactants adsorption at the solid-liquid interface is a major event in which the surfactant molecules can interact with the solid surface [21]. The use of surfactant aid to disperse CNTs and has been demonstrated in applications such as CNTs reinforce composite materials, bioapplications, and to incorporate into a variety of water-based chemical environment [22-25]. A surfactant is an amphiphilic molecule, i.e. it has polar and apolar groups and acts to reduce the surface tension of two immiscible phases. The distinct surfactant structure consist of a hydrophilic (or polar head group) region and a hydrophobic (apolar tail group) region and are classified according to the charge of the head group, thus cationic, anionic, non-ionic, and zwitterionic.

The selection of surfactants usually depends on the chemical characteristic of particles, the nature of surfactant molecule, and the solvent. Furthermore, equally important is the concentration and the type of interaction with the particles of interest as well with the CNTs. A mechanism of nanotube isolation from a bundle has been proposed [15] where the use of a surfactant combined with the assistance of ultrasonication. Figure 2.5 describes the mechanism of nanotube isolation from the bundle (i), and how the role of the ultrasonic treatment is likely to provide high local shear, particularly to the nanotube bundle end (ii). Once spaces or gaps at the bundle ends are formed, they are propagated by surfactant adsorption (iii), ultimately separating the individual nanotubes from the bundle (iv) [15].
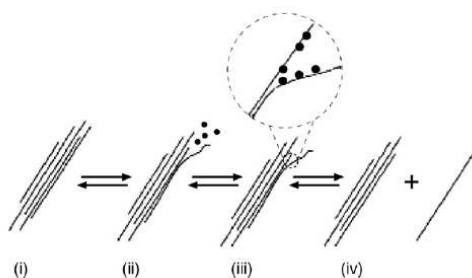
Figure 2.5 Mechanism of nanotube isolation from bundle obtained by ultrasonication and surfactant stabilization [15].

Non-covalent solubilization using aromatic molecules on SWNTs side wall has been achieved [18]. In Figure 2.6 a molecule containing a planar pyrene group (1-Pyrenebutanoic Acid, Succinimidyl Ester) is adsorbed to the CNT surface wall through strong π-π stacking interactions.
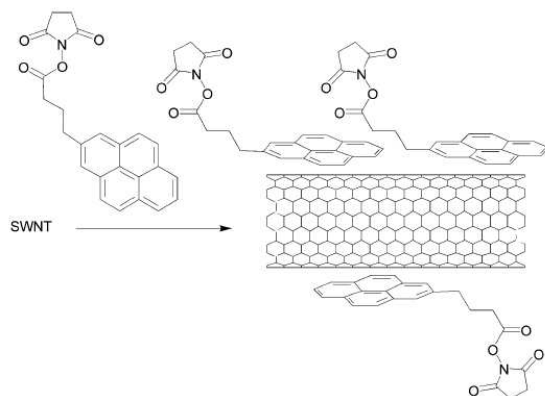
Figure 2.6: Schematic of molecule containing a planar pyrene group adsorb to the CNT surface wall through strong π-π stacking interactions [18].

In a water-based environment sodium dodecyl sulfate (SDS) and dodecylbenzenesulfonic sodium (DBSS) are the most common surfactants to disperse CNTs in water. Figure 2.7 shows the molecular structure of SDS and DBSS. The surface charge of the CNTs is essential to understanding the interaction of these in any media. Studies such as zeta potential have been demonstrated that MWNTs are negatively charged in water and this is important to understand the adsorption mechanism of ionic surfactants. The effect of the surfactant head-group charge (cationic or anionic) on dispersing the CNTs in water is unclear because different research groups have reported different results. One group has successfully performed CNTs dispersion in water using SDS, whereas others reported the insufficient debundling power of the anionic surfactant, SDS.
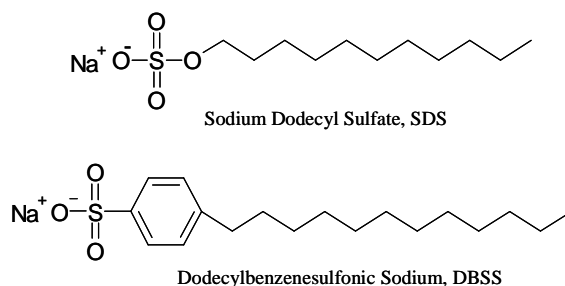
Figure 2.7: The most common surfactants to disperse CNTs in water.

Yurekli [26] reported the study of the mechanism by which surfactants help disperse SWNTs. Previously research has revealed that SWNTs form a core of cylindrical micelles of surfactant (Figure 2.8a) or are coated by adsorbed hemimicellar surfactant (Figure 2.8b). Hemimicellar adsorption on the high-curvature surfaces of SWNTs is sterically and energetically unfavorable [26]. In this study they reported that a structureless random adsorption with no preferential arrangement of the head and tail of the surfactant is responsible for the stabilization of the dispersions (Figure 2.8c) using SDS.
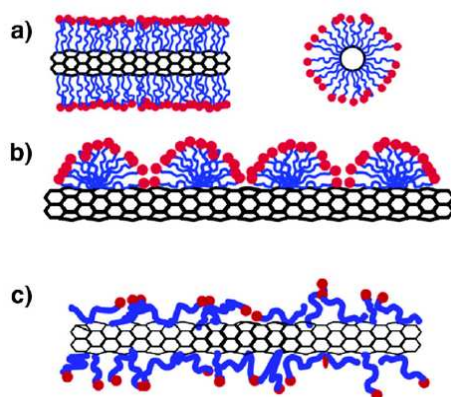
Figure 2.8: Schematic representations of the mechanism by which surfactants help to disperse SWNT. (a) SWNTencapsulated in a cylindrical surfactant micelle (both cross section and side-view); (b) hemimicellar adsorption of surfactant molecules on a SWNT; (c) random adsorption of surfactant molecules on a SWNT [26].

The production of aqueous dispersions of CNTs using SDS [27] has been demonstrated. One of the advantages of water-based suspension is the control of the pH. Figure 2.9 I shows the behavior of the CNT suspension in water without and with SDS and it is clear that SDS help to increases the dispersion of CNTs with only 15 % of CNT concentration falling at 500 hours. The behavior of the water-based suspensions as function of pH is illustrated in Figure 2.9 II. Zeta potential of CNT suspension using SDS exhibits an increase as the pH of the suspension increases, indicating an increase in CNT suspension stability.
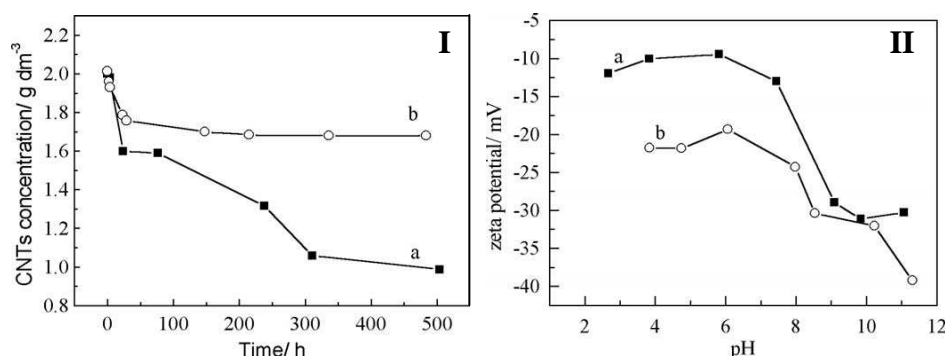
Figure 2.9: (I) CNT concentrations vs. time for 0.2 wt% CNT suspensions (a) without SDS and (b) with 0.1 wt% SDS at pH 9. (II) Zeta potential of CNT suspension vs. pH (a) without SDS and (b) with 0.005 wt% SDS [27].

The concentration of surfactant plays an important and crucial role in the behavior of the colloidal suspension. Figure 2.10a shows the zeta potential distribution of SDS-wrapped SWNTs under different SDS concentration. Increasing amounts of SDS result in more SDS molecules adsorbed onto the nanotube side walls. Therefore, the nanotubes become more negative until a value of about -80.3 mV is reached at 1.5 % SDS concentration [28]. Increasing the surfactant concentration helps to increase the stability of the CNT suspension but only to a certain point. This limit is defined by the critical

micelle concentration (CMC). CMC is defined as the concentration of surfactant above which micelles are spontaneously formed. In other words when the adsorption of the surfactant molecules on the particles is established, the self organization of the surfactant into micelles is expected to occur above a CMC [15]. Figure 2.10b shows the conductivity of the CNT suspension as a function of SDS concentration. The conductivity increases with the surfactant concentration because of the increase of ionic species [28]. Suspensions for EPD require a low conductivity, emphasizing the need to keep the concentration of surfactant as low as possible in order to meet this requirement. In the case of ionic surfactant, it is more important to keep the surfactant concentration low because the presence of ionic species contributes to the suspension conductivity.
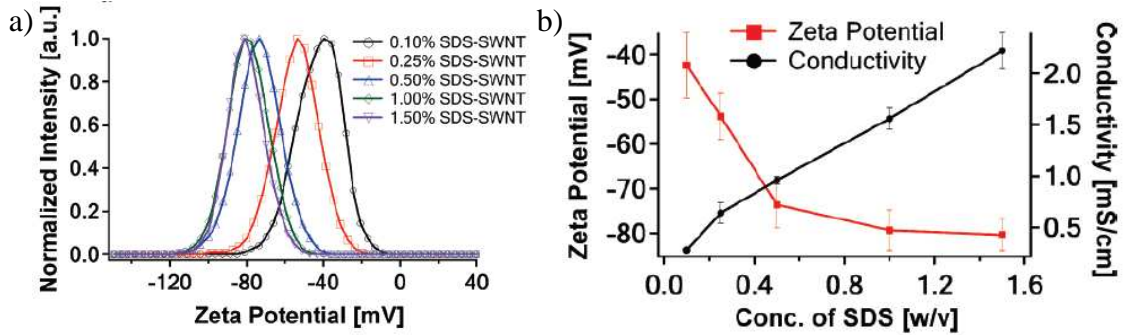
Figure 2.10: (a) The ζ-potential distribution of SDS-wrapped SWNTs for different SDS concentrations. (b) Plot of the peak maximum of the ζ-potential distribution and the conductivity of the surfactant-wrapped SWNT solutions versus the SDS concentration [28].

2.2 CNT Alcohol-Based Suspension

Surfactants are commonly used in water-based environments. In general, ionic surfactants are preferable for CNT-water suspension and non-ionic surfactants are preferred when organic solvents have to be used [15]. The main challenge in dispersing CNTs in alcohol for EPD is the need of a charger salt in the suspension. EPD method requires the presence of the charger salt to improve the adhesion of CNTs to substrate

and help to increase the deposition rate [6]. The ions from the charger salts, however, destabilize the suspension but their are fundamental and essential. The addition of ions destabilizes the suspension in accordance with an expected reduction in the Debye screening length [16]. Also EPD method is controlled by the surface charge (negatively for oxidized CNTs) and the charger salts determines the direction (anode or cathode) of the CNTs during the deposition process.
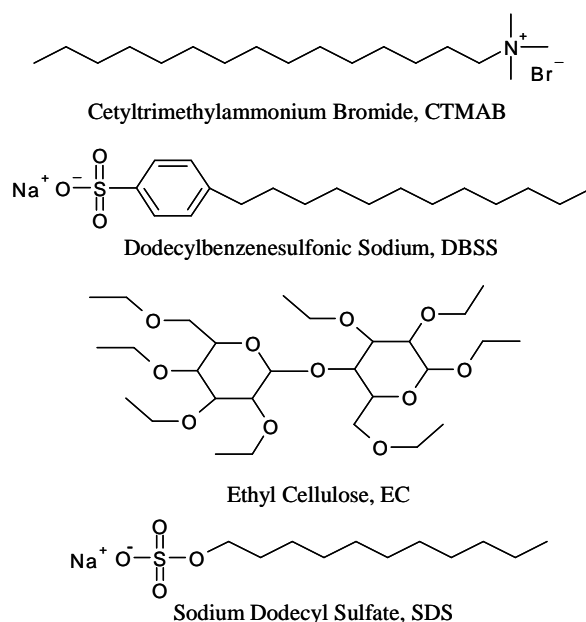
Figure 2.11: Surfactants/Dispersant used in CNT alcohol-based suspension. (Top to bottom) Cetyltrimethylammonium Bromide, CTMAB, cationic; Dodecylbenzenesulfonic Sodium, DBSS, anionic; Ethyl Cellulose, EC, dispersant; Sodium Dodecyl Sulfate, SDS, anionic.

The surfactants selected for CNT alcohol-based suspension are Cetyltrimethylammonium Bromide, CTMAB, cationic; Dodecylbenzenesulfonic Sodium, DBSS, anionic; Ethyl Cellulose, EC, dispersant; Sodium Dodecyl Sulfate, SDS, anionic. The selection of surfactants and dispersant for CNT alcohol-based suspension was made based on their structural characteristics. CTMAB was selected due to the simple cationic structure; this simple structure can increase the electrostatic repulsion more than steric

repulsion. On the other hand, DBSS and SDS were selected based on the difference that these two present, a benzene ring. Also these surfactants are able to disperse CNTs in high concentrations in aqueous suspension. SDS is a common surfactant used in many applications such as emulsions, electroplating industry, whipping agent, cleaning agent in personal care products, etc. Finally, ethyl cellulose or EC was selected based on its particular structure can increase the steric or repulsion effect between the nanotubes. This is defined as a dispersant and is used in the pharmaceutical and food industry.

In the following sections the study of CNT alcohol-based suspension will be discussed. The study of the effects of surfactant concentration, alcohol solvents and solvent ratio, charger salts, and charger salts concentration will be examined. In addition, the study of different cellulose and long term stability of CNT alcohol-based suspension will be reviewed. The field emission properties of random CNT films were also studied.

2.2.1 Effect of Surfactant Concentration

The determination of the effective surfactant concentration is the first and the most important step in developing CNT alcohol-based suspensions. A series of CNT suspensions were prepared to determine the effective surfactant concentration. The suspensions contained a CNT (oxidized CNTs) concentration of 0.010 mg/mL (1.0 % wt), 5.0 % vol of water and three different surfactant concentrations were used, 0.010 mg/mL (1.0 % wt), 0.030 mg/mL (3.0 % wt) and 0.050 mg/mL (5.0 % wt) in ethanol as suspension media. These suspensions were ultrasonicated for an hour to disperse the nanotubes. Figure 2.12 shows suspensions without charger salts 3 hours after sonication. In general CNT alcohol-based suspensions without charger salts are stable. Furthermore,

suspensions with 1.0 and 3.0 % wt of surfactant are stable for longer times in comparison with suspensions with a surfactant concentration of 5 % wt.
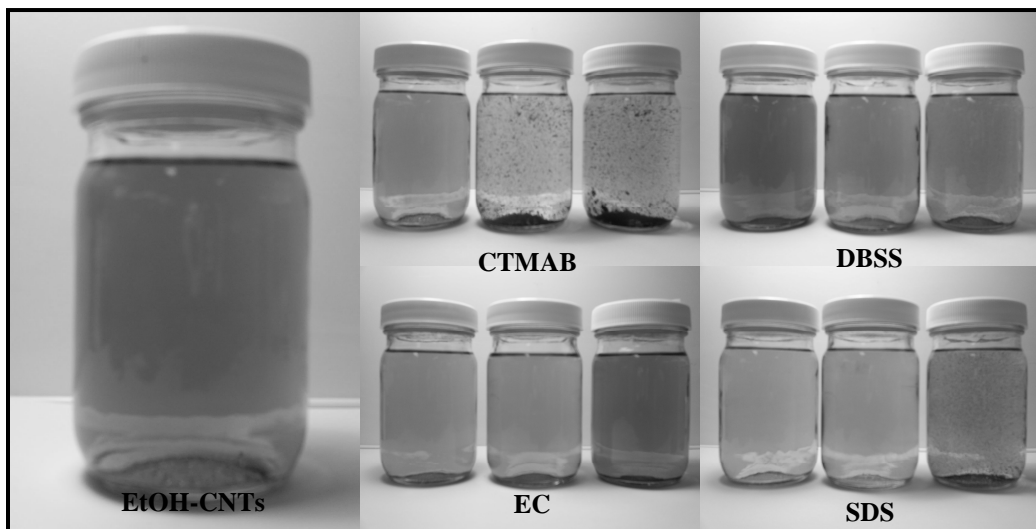
Figure 2.12: Suspensions without charger salt at 3 hours after sonication (left to right 1.0, 3.0 and 5.0 % wt/vol surfactant).

The stability of these suspensions is due to three factors: (1) surfactant/dispersant used, (2) surfactant concentration, and (3) oxidized CNTs. The use of purified CNTs does not show the quality of dispersion. The behavior of the purified nanotubes is similar with and without surfactant. The oxidized CNTs were made under mild conditions. A 50 % nitric acid solution (HNO_3) and 50 % sulfuric acid solution (H_2SO_4) mixture (1:1) was placed in a conical flask with purified CNTs and ultrasonicated for one hour. After the reaction, the oxidized CNTs were filtered out and rinsed with water until a neutral pH was achieved. The IR spectrums for CNTs before and after oxidation are shown in Figure 2.13. The IR spectra for the oxidized CNTs showed peaks that correspond to carboxyl and hydroxyl groups indicating the oxidation.
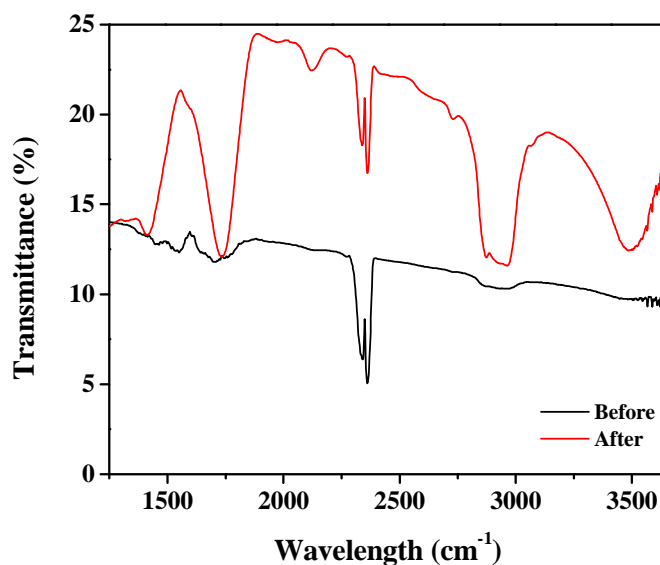
Figure 2.13: IR spectrums of CNTs before and after oxidation.

The effective CNT to surfactant ratio is 1 to 1 for CNT alcohol-based suspensions. The effective ratio was determined using the zeta potential results of the CNT alcohol-based suspensions with charger salt. These suspensions are for EPD and the charger salt is needed. The zeta potential was measured using a ZETA SIZER Nano Series. The zeta potential is measured by applying an electric field across the dispersion. Particles within the dispersion with a zeta potential will migrate toward the electrode of opposite charge with a velocity proportional to the magnitude of the zeta potential. This velocity is measured using the laser Doppler anemometry technique. The frequency shift or phase shift of an incident laser beam caused by these moving particles is measured as the particle mobility, and this mobility is then converted to the zeta potential by inputting the dispersant viscosity, and applying of the Smoluchowski or Huckel theories.

The suspensions used for the zeta potential measurements contained a CNT concentration of 0.010 mg/mL (1.0 % wt), 0.020 mg/mL (2.0 % wt) of charger salt

(NaOH, sodium hydroxide), 5.0 % by volume water, and three different surfactant concentrations were used, 1.0, 3.0 and 5.0 % wt in ethanol. Zeta potentials for CMTAB suspensions are shown in Table 2.1. Figure 2.12 show that the zeta potential of these suspensions has an inverse relationship with the CMTAB concentration, as the latter increases the zeta potential decreases making the suspension unstable. The behavior of these suspensions can be explained as the high CMTAB concentration reaching the CMC limit.

Surfactant Concentration (%)	Zeta Potential (mV)
CMTAB 1.0	- 28.00
CMTAB 3.0	- 26.05
CMTAB 5.0	- 24.00

Table 2.1: Zeta Potential for CNT alcohol-based suspensions with different CMTAB concentration and NaOH as charger salt in ethanol.

The summary of zeta potentials for CNT-alcohol based suspensions with different surfactants and varying surfactant concentrations is shown in Table 2.2. The results of the zeta potential show a higher zeta potential for suspensions with lower surfactant concentration. These results are expected due to the increasing ionic strength destabilizing the suspensions.

Surfactant	Surfactant Concentration (%)	Zeta Potential (mV)
DBSS	1.0	- 32.25
DBSS	5.0	- 27.50
EC	1.0	- 6.40
EC	5.0	-4.61
SDS	1.0	- 26.80
SDS	5.0	-26.15

Table 2.2: Zeta Potential for CNT alcohol-based suspensions with different surfactants, different surfactant concentration and NaOH as the charger salt in ethanol.

The effective CNT to surfactant concentration was determined using ethanol as the suspension media, but after analysis with Equation 1.4, it is evident the zeta potential increases if the dielectric constant decreases and the viscosity increases. The dielectric constant and viscosity for ethanol is 25.3 and 1.074 cp, respectively. On the other hand the dielectric constant and viscosity for isopropanol and propanol is 20.18 and 2.038 cp and 20.8 and 1.945 cp, respectively. Section 2.2.2 will be focused on studying of the effects of solvent in CNT alcohol-based suspensions.

2.2.2 Effect of Alcohol Solvents and Different Solvents Ratio

The alcohol solvent or the mixture of solvents used as a suspension media can make a difference in the stability of the CNT alcohol-based suspensions. The viscosity of the suspension media is an important property in developing suspensions. Viscosity is a measure of a liquid's resistance to flow [29]. Other properties such as dielectric constant, zeta potential and the behavior of the suspensions over time are also important in the study of CNT suspensions. Zeta potential and UV-Vis spectroscopy were used to characterize CNT alcohol-based suspensions. UV-Vis spectroscopy was used to measure the dispersion stability of different solvents and different solvent ratio CNT suspensions. This technique was used to measure the CNT concentration as function of sediment time. The suspensions used for the zeta potential and UV-Vis spectroscopic measurements contained a CNT concentration of 0.010 mg/mL (1 % wt), 0.020 mg/mL (2.0 % wt) of charger salt (NaOH, sodium hydroxide) and a surfactant concentration of 0.010 mg/mL (1.0 % wt).

The zeta potential of CNT suspensions using EC is shown in Table 2.3. The zeta potential increases when a mixture of 95:5 IPA:H_2O is used as a suspension media as expected because of the viscosity of isopropanol. The viscosity of isopropanol is almost the double of the ethanol. The zeta potential is used as a magnitude of the electrostatic interaction between colloidal particles. Particles with zeta potential between –15 and 15 mV can still be stable if they are sterically stable [28]. EC stabilize CNT suspensions through the steric repulsion, which explains the low magnitude of the zeta potential for these suspensions. In general, the zeta potential results showed higher or similar magnitude for suspensions with 95:5 IPA:H_2O as the suspension media in comparison with 95:5 EtOH:H_2O.

Suspension	Zeta Potential (mV) Isopropanol	Zeta Potential (mV) Ethanol
1 % EC	- 12.75	- 6.40
3% EC	- 11.55	- 3.34
5% EC	- 10.29	- 4.61

Table 2.3: Zeta Potential for CNT alcohol-based suspensions with EC as the dispersant and NaOH as charger salt in isopropanol and ethanol.

Water is the most common solvent used as expected with the advantage of being able to control of pH when developing colloidal suspensions. An easy way to increase the zeta potential of CNT suspensions is to increase the amount of water used in the ethanol mixture. In order to proof this statement, a series of CNT suspensions were prepared using 90:10, 80:20, 75:25 and 60:40 EtOH:H_2O. The zeta potential results for these suspensions are shown in Table 2.4. As expected, the zeta potential and water concentration have a positive relationship. In general these results are only excellent in developing a stable CNT suspension. For EPD, however, it is inconvenient because water undergoes electrolysis at low voltage (~ 5V).

Suspension	Zeta Potential (mV)
90:10	- 8.05
80:20	- 10.10
75:25	- 10.74
60:40	- 12.70

Table 2.4: Zeta Potential for CNT suspensions with EC (1.0 % wt) as the dispersant and NaOH (2.0 % wt) as charger salt in different EtOH:H$_2$O ratio.

As previously mentioned, zeta potential is a good indicator of the suspension stability but the use of UV-Vis spectroscopy as a characterization technique is more effective in monitoring the suspension behavior over time. The determination of the CNT absorbance in 95:5 EtOH:H$_2$O was the first step in this technique. The maximum absorbance of CNT in this mixture is at 259.9 nm and Figure 2.14 shows the UV-Vis spectra for a 95:5 EtOH:H$_2$O mixture as the blank and 1.0 % wt CNT as the standard. The wavelength with the maximum CNT absorbance was used for the determination of the CNT concentration. The same determination was made for all the suspension media of the CNT alcohol-based suspensions analyzed.
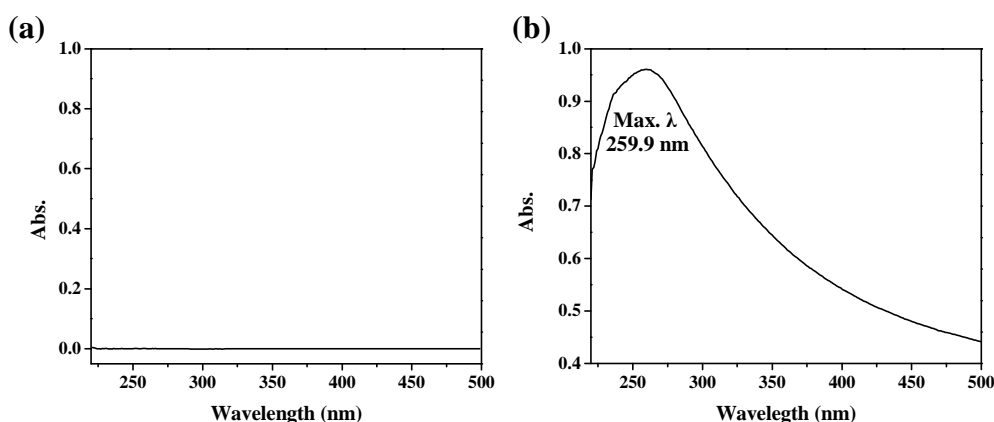
Figure 2.14: (a) UV-Vis spectrum for 95:5 EtOH:H$_2$O mixture (blank). (b) UV-Vis spectrum for 1.0 % wt CNT (Std).

A calibration curve was constructed at each specific wavelength depending on the suspension media. The wavelength is defined where the absorbance of the CNTs is

maximum. The CNT standards were prepared in a range of 0.10 – 1.00 wt % of CNTs. Figure 2.15 shows a calibration curve for CNT suspensions in 95:5 EtOH:H$_2$O at 259.9 nm. The suspensions were characterized using a UV-Vis spectrophotometer, Varian Cary 50 Scan.
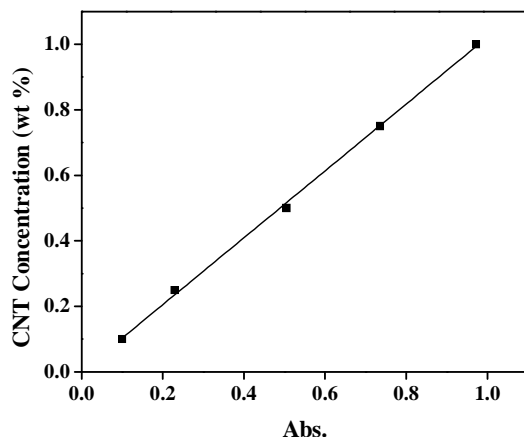
Figure 2.15: Calibration curve of CNT suspensions in 95:5 EtOH:H$_2$O at 259.9 nm.

A collection of UV-Vis spectras, collected every 30 minutes, for 1.0 wt % of SDS, 1.0 wt % of CNT and 2.0 wt % of NaOH in 95:5 EtOH:H$_2$O are shown in Figure 2.16. The concentration of CNT was determined by fitting the absorbance to the calibration curve similar to the one showed in Figure 2.15. Figure 2.17 show the behavior of the CNT alcohol-based suspensions with 95:5 EtOH:H$_2$O and 95:5 IPA:H$_2$O as a function of sediment time. Evidently the suspension media made a significant difference in the CNTs dispersion and stability over time.
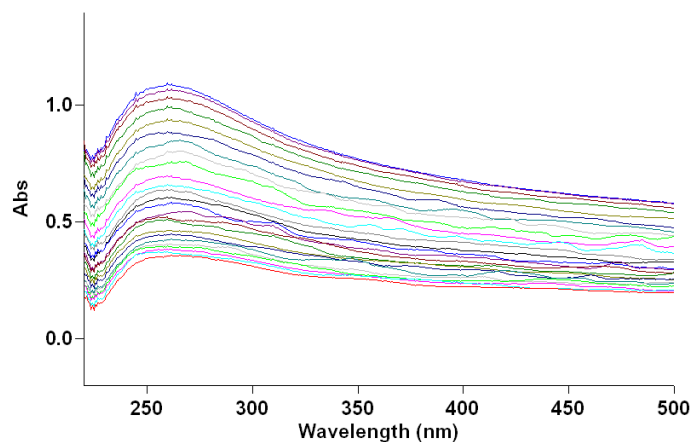
Figure 2.16: UV-Vis spectrum for CNT suspension using 1.0 % wt of SDS in 95:5 EtOH:H₂O.

95:5 IPA:H_2O as the suspension media change the behavior of the CNTs in suspension. The stability of the CNT alcohol-based suspensions with and without surfactants has been improved. The exception is CNT alcohol-based suspension with EC, which shows the same behavior in both mixtures. The stabilization of the CNT suspensions (with the exception of the suspensions with EC) is from the electrostatic repulsion, but the use of a charger salt makes the suspension harder to stabilize due to the increasing of the ionic species. The use of different solvents can help to stabilize CNT alcohol-based suspensions without change the concentration of the ionic species that are needed for the EPD process. The use of solvents with higher viscosities can also increase the stability of the CNTs in suspension. These solvents with extremely high viscosities, however, are not recommended in the EPD process because the particles have to be able to move. In this scenario, the EPD process would not work. Table 2.5 summarizes the percent of CNT concentration drop for the CNT alcohol-based suspensions analyzed in Figure 2.17. The quantitative analysis clearly shows the significant improvement of the stability for CNT alcohol-based suspensions using a 95:5 IPA:H_2O mixture.
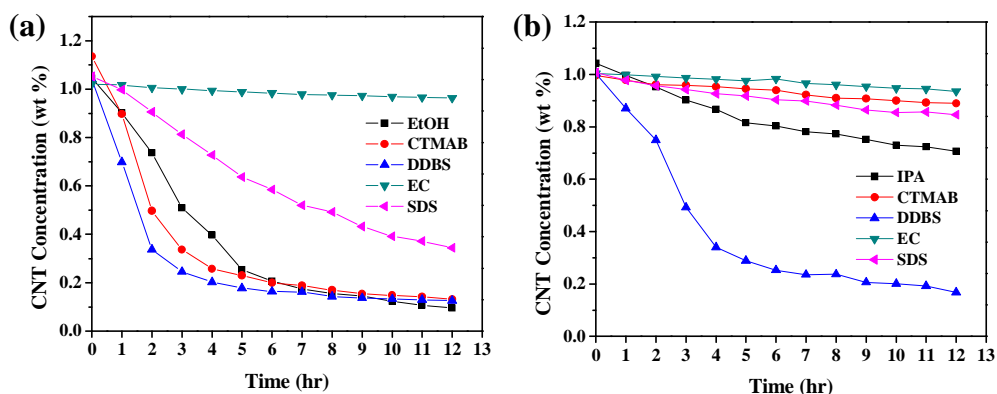
Figure 2.17: CNT concentration as function of sediment time for (a) 95:5 EtOH:H$_2$O and (b) 95:5 IPA:H$_2$O, respectively, during 12 hours.

Suspension	CNT Concentration Drop (%) 95:5 EtOH:H$_2$O	CNT Concentration Drop (%) 95:5 IPA:H$_2$O
Without Surfactant	90.85	32.24
CTMAB	88.46	10.65
DDBS	87.91	83.25
EC	5.69	6.80
SDS	67.33	15.93

Table 2.5 CNT concentration drop for suspensions using 95:5 EtOH:H$_2$O and 95:5 IPA:H$_2$O, respectively, after 12 hours.

EC as a dispersant has been shown to stabilize the CNT alcohol-based suspensions more effectively than other surfactants previously analyzed. In order to study clearly the effects of different solvent mixtures, EC was used as a dispersant for the CNT alcohol-based suspensions in the following studies. 95:5 PROP:H$_2$O (1-propanol:water) as a suspension media was analyzed and studied, revealing a good stability of the CNT alcohol-based suspensions. Propanol is an excellent alternative as suspension media and is efficient during the EPD process. The CNT concentration that drops over time depends strongly on the solvent or mixture used. The percent of CNT concentration drop for different alcohol-based suspensions were analyzed and the results are shown in Table 2.6. The percent of CNT concentration drop is negligible for these three solvent mixtures.

These suspensions are the most stable CNT alcohol-based suspensions in comparison with the suspensions previously analyzed. Figure 2.18 shows the CNT concentration as function of sediment time for three different 95:5 mixtures during 24 hours. Obviously these suspensions can be stable at least for 2 days with a small change in CNT concentration. The main difference in these solvent mixtures is the viscosity of the alcohol solvents used.

The kinematic viscosity of these alcohol-water mixtures was determined to characterize these mixtures. The kinematic viscosity is the ratio of absolute or dynamic viscosity to density (a quantity in which no force is involved). To determine the kinematic viscosity, the efflux time of these mixtures were collected and averaged. The kinematic viscosity was calculated by first the subtracting of the kinetic energy correction (which is related with the efflux time) from the average efflux time for each mixture to obtain the corrected flow time. Then the corrected flow time was multiplied by the viscometer constants to give the kinematic viscosity in mm^2/s. The kinematic viscosity for 95:5 $EtOH:H_2O$, 95:5 $IPA:H_2O$ and 95:5 $PROP:H_2O$ is 1.70, 2.68 and 2.70 mm^2/s, respectively.

Suspension	CNT Concentration Drop (%)
95:5 $EtOH:H_2O$	4.91
95:5 $IPA:H_2O$	9.05
95:5 $PROP:H_2O$	2.94

Table 2.6: CNT concentration drop for suspensions using 95:5 $EtOH:H_2O$, 95:5 $IPA:H_2O$ and 95:5 $PROP:H_2O$ after 24 hours. The CNT suspensions contained 1.0 wt% CNTs, 1.0 wt% EC and 4.0 wt % NaOH.
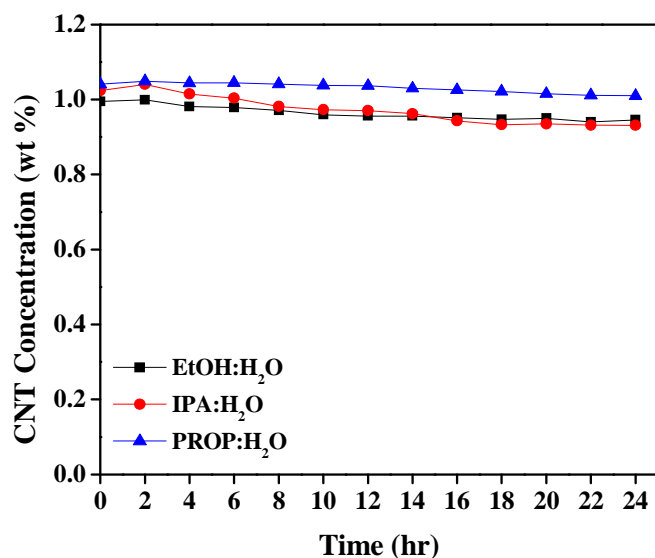
Figure 2.18: CNT concentration as function of sediment time for 95:5 EtOH:H₂O, 95:5 IPA:H₂O and 95:5 PROP:H₂O suspensions. The CNT suspensions contained 1.0 wt% CNTs, 1.0 wt% EC and 4.0 wt % NaOH.

The behavior of CNT suspensions contrasted significantly between, EtOH:IPA and IPA:EtOH; when IPA is in higher concentration the stability of the suspension decreases significantly as shown in Figure 2.19b.
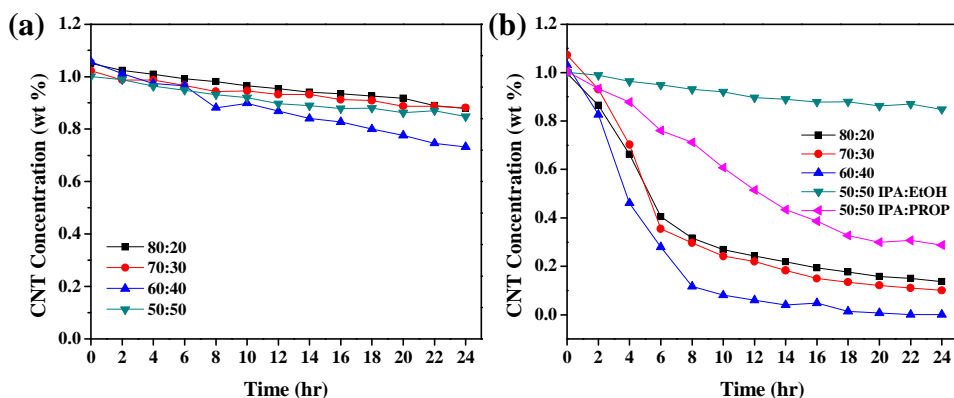
Figure 2.19: CNT concentration as function of sediment time for (a) EtOH:IPA and (b) IPA:EtOH, respectively during 24 hours. The CNT suspensions contained 1.0 wt% CNTs, 1.0 wt% EC and 4.0 wt % NaOH.

Suspension	Solvent Ratio	CNT Concentration Drop (%)
	80:20	16.44
EtOH:IPA	70:30	13.78
	60:40	30.71
	50:50	15.27
	80:20	86.29
IPA:EtOH	70:30	90.63
	60:40	99.92
IPA:PROP	50:50	71.33

Table 2.7: CNT concentration drop for suspensions using different solvent ratios of EtOH:IPA, IPA:EtOH and IPA:PROP after 24 hours. The CNT suspensions contained 1.0 wt% CNTs, 1.0 wt% EC and 4.0 wt % NaOH.

CNT alcohol-based suspensions with 95:5 solvent ratio showed good stability and good CNTs dispersion independently of the alcohol solvent used as shown in Table 2.8. Figure 2.20 show CNT concentration as a function of sediment time for 95:5 ratios for different solvents after 24 hours. CNT alcohol-based suspensions in Table 2.6 and 2.8 show comparable drops in the CNT concentration at 24 hours. The effective solvent ratio is 95:5 for the CNT alcohol-based suspensions when EC is the dispersant and used at a 1 to 1 ratio with CNTs.

Suspension	CNT Concentration Drop (%)
EtOH:PROP	13.16
EtOH:IPA	4.14
PROP:EtOH	3.29
PROP:IPA	10.32
IPA:PROP	5.96
IPA:EtOH	8.39

Table 2.8: CNT concentration drop for suspensions using different solvents mixtures at 95:5 solvents ratio after 24 hours. The CNT suspensions contained 1.0 wt% CNTs, 1.0 wt% EC and 4.0 wt % NaOH.
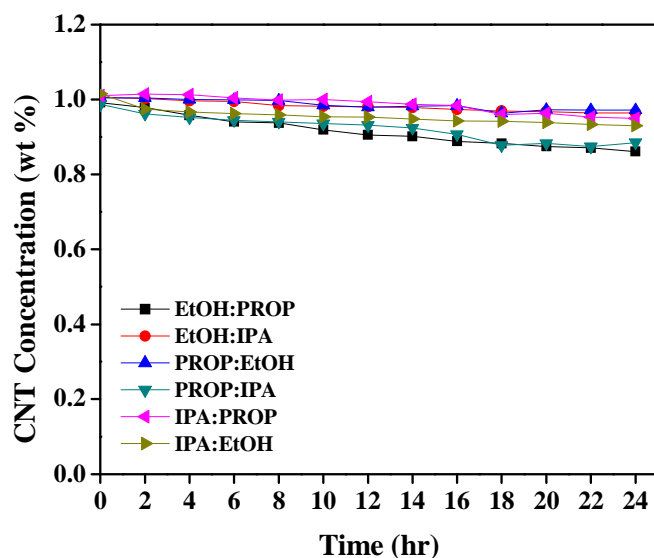
Figure 2.20: CNT concentration as function of sediment time for 95:5 ratios for different solvents suspensions. The CNT suspensions contained 1.0 wt% CNTs, 1.0 wt% EC and 4.0 wt % NaOH.

Water as a suspension media offers advantages and disadvantages in developing CNT suspensions for EPD. One advantage is that increasing the water concentration in CNT alcohol-based suspensions results in an increase in the zeta potential of the suspension. On the other hand, the increase of the water concentration in the CNT alcohol-based suspension will result in a failure of the EPD process. Isopropanol as a suspension media result in an increase in the zeta potential of the CNT alcohol-based suspensions and consequently the stability of the suspensions improves. Also, the study of different solvent ratios showed that the 95:5 ratio is the most effective ratio independent of the solvent used. The developed CNT alcohol-based suspensions were used for EPD. EPD, in this case, was used as a characterization method.

2.2.3 *Effect of Charger Salts and Varying Charger Salt Concentration*

The charger salt plays an important role in the EPD process. During the process the charger salt determines the deposition direction and the deposition rate of the CNTs.

64

This provides the electrical charge to the CNTs in suspension and makes the CNTs respond to the electrical field. The presence of the charger salt also improves the adhesion of CNTs to the substrate. Unfortunately, this destabilizes the stability of the CNT suspension making the development of the CNT alcohol-based suspension a challenge. Furthermore, the charger salt selection needs to meet the EPD process requirements. These requirements include the presence of the charger salt, a minimum concentration for the process completion, and minimally affect the CNT suspension stability. In this section the effects of the different charger salt, including their effect on the stability of CNT alcohol-based suspensions, will be discussed.

The CNT alcohol-based suspensions used to study the effect of different charger salt were prepared with a CNT concentration of 0.010 mg/mL (1 % wt), 0.020 mg/mL (2.0 % wt) of charger salt (NaOH, sodium hydroxide and $MgCl_2$, magnesium chloride) and 0.010 mg/mL (1.0 % wt) EC. UV-Vis spectroscopy was used to study the CNT concentration as a function of sediment time of these CNT alcohol-based suspensions. The solvent mixtures used were 95:5 EtOH:H_2O and 95:5 IPA:H_2O. The standards and blank suspensions and/or solutions preparations were performed as described in the previous section. Figure 2.21 shows the behavior of the CNT concentration as function of sediment time in two different solvent mixtures and with two different charger salts. CNT alcohol-based suspensions with NaOH as the charger salt are more stable independently of the solvent mixture used. This is expected since the NaOH is a monovalent electrolyte in comparison with $MgCl_2$ that is a multivalent electrolyte. In general, multivalent

electrolytes (divalent electrolyte in this case) destroy easier the colloidal suspensions than monovalent electrolyte.
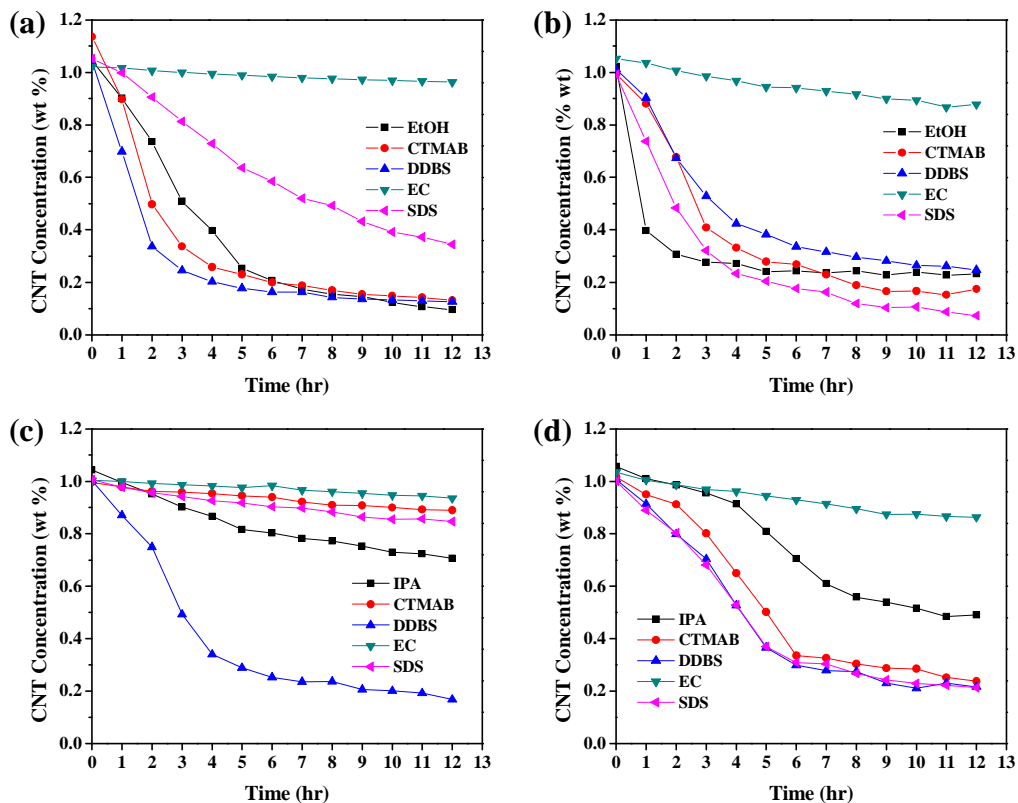
Figure 2.21: CNT concentration as function of sediment time for (a) 95:5 EtOH:H$_2$O with NaOH, (b) 95:5 EtOH:H$_2$O with MgCl$_2$, (c) 95:5 IPA:H$_2$O with NaOH and (d) IPA:H$_2$O with MgCl$_2$, respectively during 12 hours.

As previously noted, changing the suspension media can cause a significant difference in the stability of the CNT alcohol-based suspension. However, when the suspension contain divalent electrolytes the improvement is not as significant in comparison with the same suspensions that have monovalent electrolytes (NaOH) as is shown in Table 2.9. The quantitative analysis clearly shows that 95:5 IPA:H$_2$O does not make any difference in suspensions with MgCl$_2$, with the exception of the CNT alcohol-based suspension without surfactants.

Suspension	CNT Conc. Drop (%) 95:5 EtOH:H$_2$O	CNT Conc. Drop (%) 95:5 IPA:H$_2$O	CNT Conc. Drop (%) 95:5 EtOH:H$_2$O	CNT Conc. Drop (%) 95:5 IPA:H$_2$O
	NaOH		MgCl$_2$	
Without Surfactant	90.85	32.24	77.29	53.57
CTMAB	88.46	10.64	82.43	76.64
DDBS	87.90	83.25	75.54	78.51
EC	5.69	6.80	16.54	16.57
SDS	67.33	15.93	92.66	78.68

Table 2.9: CNT concentration drop for suspensions using 95:5 EtOH:H$_2$O and 95:5 IPA:H$_2$O mixtures and NaOH and MgCl$_2$ as charger salts after 12 hours.

Moreover, the zeta potential results in Table 2.10 confirm that CNT alcohol-based suspensions with NaOH as the charger salt are more stable than those with MgCl$_2$. The improvement can be quantified from 3 to 6 orders of magnitude for CNT alcohol-based suspension without surfactant and with CTMAB, respectively. The results revealed that NaOH is an effective charger salt for the EPD process. Also, the CNT alcohol-based suspensions are more stable in comparison with the same suspensions with MgCl$_2$ as a charger salt.

Suspension	Zeta Potential (mV) NaOH	Zeta Potential (mV) MgCl$_2$
Without Surfactant	-31.20	9.57
CTMAB	- 28.00	4.70
DDBS	-32.25	7.09
EC	-6.40	1.51
SDS	-26.80	6.16

Table 2.10: Zeta Potential for CNT alcohol-based suspensions with different charger salts, NaOH and MgCl$_2$, respectively in 95:5 EtOH:H$_2$O.

The study of charger salt concentration is important because it plays an important role in the stability of the CNT alcohol-based suspensions. The determination of the minimum and effective charger salt concentration for the EPD process is important for creating stable CNT alcohol-based suspensions. The minimum charger salt concentration can be defined as the smallest concentration where the EPD process is successful. The

effective charger salt concentration is the concentration where the CNT alcohol-based suspension is more stable. The CNT alcohol-based suspensions used in this study were prepared with a CNT concentration of 0.010 mg/mL (1 % wt), 0.010 mg/mL (1.0 % wt) of surfactants/dispersant and 0.020, 0.030 and 0.040 mg/mL (2.0, 3.0 and 4.0 % wt) of charger salt (NaOH, sodium hydroxide and $MgCl_2$, Magnesium Chloride) in 95:5 EtOH:H_2O. The CNT suspensions were analyzed using UV-Vis spectroscopy to monitor the CNT concentration as a function of sediment time.

Figure 2.22 shows the effect of the charger salt concentration on the CNT alcohol-based suspensions stability. The stability of the CNT alcohol-based suspension is affected when the charger salt concentration increases, regardless, if the charger salt is monovalent or multivalent. Basically, CNT alcohol-based suspensions using $MgCl_2$ exhibit the same behavior no matter the concentration used. The exceptions include SDS and EC.
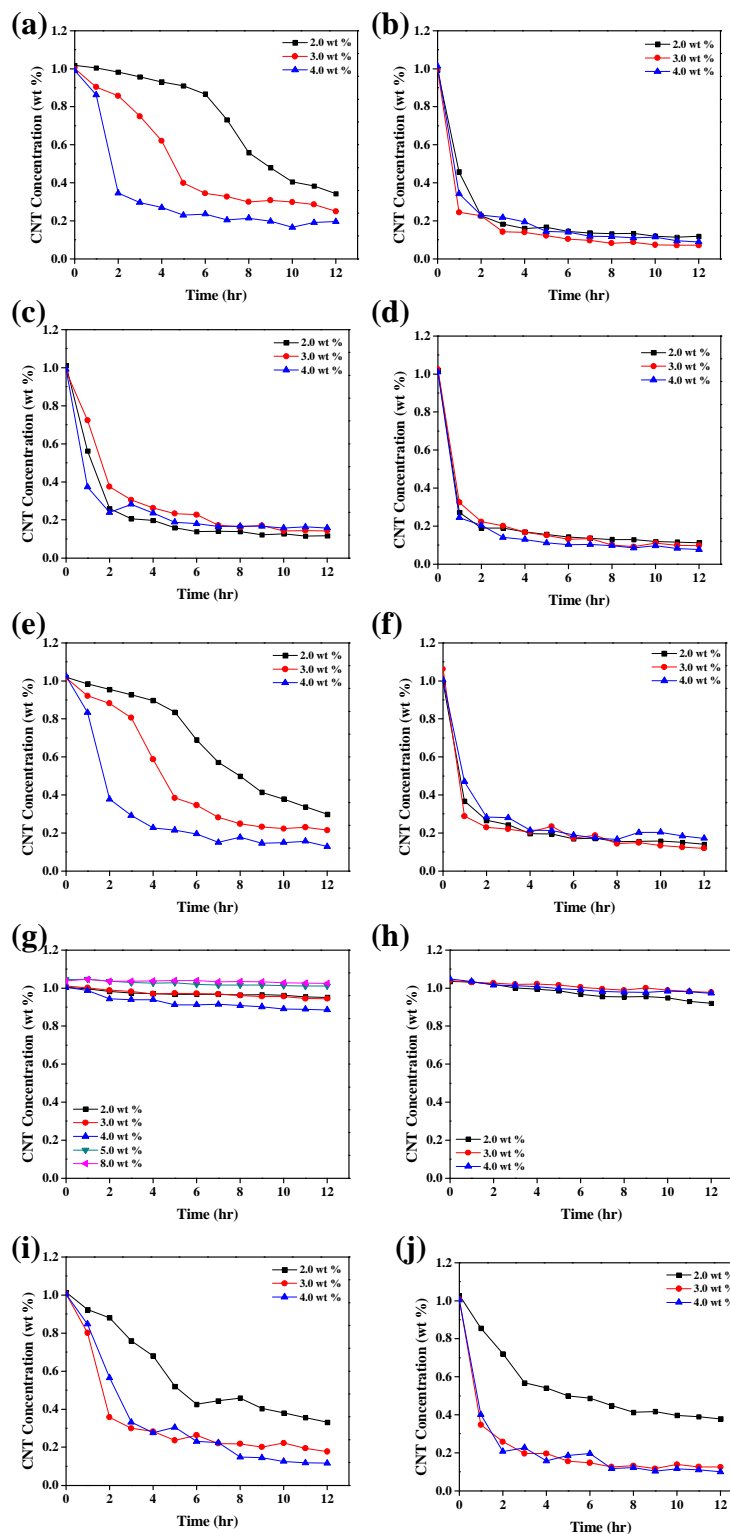
Figure 2.22: Effect of charger salt concentration on the CNT concentration as a function of time for CNT suspensions using 95:5 EtOH:H₂O, (a) without surfactant-NaOH, (b) without surfactant-MgCl₂, (c) CTMAB-NaOH, (d) CTMAB-MgCl₂, (e) DDBS-NaOH, (f) DDBS-MgCl₂, (g) EC-NaOH, (h) EC-MgCl₂, (i) SDS-NaOH, (j) SDS-MgCl₂, during 12 hours.

CNT alcohol-based suspensions with SDS are more stable at lower concentrations of charger salts as shown in Figure 2.26j. When EC is used as a dispersant, the stability of the suspensions is independent of the charger salt concentration. CNT alcohol-based suspensions with NaOH as the charger salt are more stable at lower charger salt concentrations with the exception of CMTAB that show the same unstable behavior. EC is able to disperse the CNTs in suspension more effectively when NaOH and $MgCl_2$ are used as shown in Figure 2.26 g and h, respectively. Moreover, the stability of the CNT alcohol-based suspension is not affected by the charger salt concentration when EC is used. The highest NaOH concentration used was 8.0 wt %, which represents an EC to NaOH ratio of 1 to 8 without affecting the stability. This is attributed to the minimum interactions of EC with the ionic species in suspension.

2.2.4 Study of Different Celluloses

Ethyl cellulose has been show to be an excellent dispersant for CNT alcohol-based suspensions. The different celluloses are studied to determine the effects of ionic cellulose and how different substituents affect the suspension stability. The CNT alcohol-based suspensions used for this study were prepared using 1.0 wt % (0.010 mg/mL) CNTs, 1.0 wt % (0.010 mg/mL) cellulose, and 4.0 wt % (0.040 mg/mL) NaOH in 95:5 EtOH:H_2O and IPA:H_2O. The celluloses used in this study include: carboxymethyl cellulose sodium salt (CMC), ionic cellulose, ethyl cellulose (EC), hydroxypropyl cellulose (HPC), and hydroxypropylmethyl cellulose phthalate (HPMC). Figure 2.23 shows the chemical structure of the celluloses used in this study. CMC is used in food science as food additive. HPC is used in food science and pharmaceuticals applications

and similarly HPMC is used as dispersant in pharmaceuticals applications. The main difference of these celluloses is the substituents and the presence of an ionic charge.
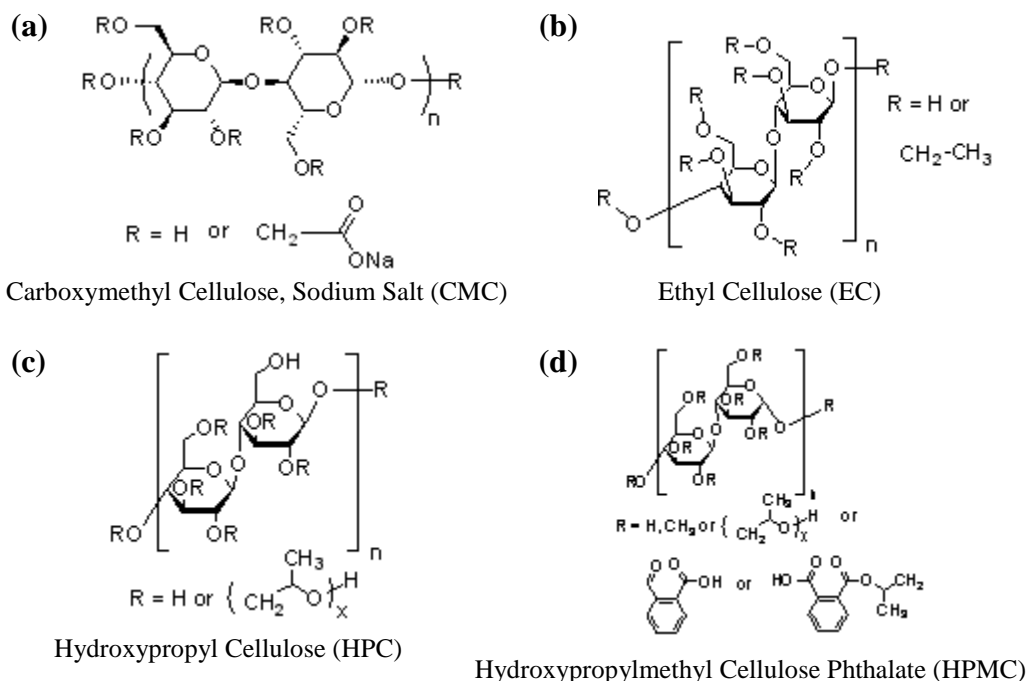
Figure 2.23: Celluloses used in CNT alcohol-based suspensions as dispersant; (a) carboxymethyl cellulose,sodium salt (CMC), ionic cellulose,(b) ethyl cellulose (EC), (c) hydroxypropyl cellulose (HPC) and (d) hydroxypropylmethyl cellulose phthalate (HPMC).

The results of the analysis of the CNT alcohol-based suspensions with different cellulose are shown in Figure 2.28 and Table 2.11. The different celluloses did not affect the stability of the CNT alcohol-based suspensions with the exception CNT alcohol-based suspensions with CMC. Also, the ionic cellulose did not have the capability to stabilize CNTs in alcohol mixture. The different substituents in these celluloses did not make a significant difference in the CNT alcohol-based suspensions stability. These celluloses are able to disperse CNTs in suspension with excellent stability. Besides, the

use of any of these CNT alcohol-based suspensions for EPD results in a good and easy CNTs deposition.
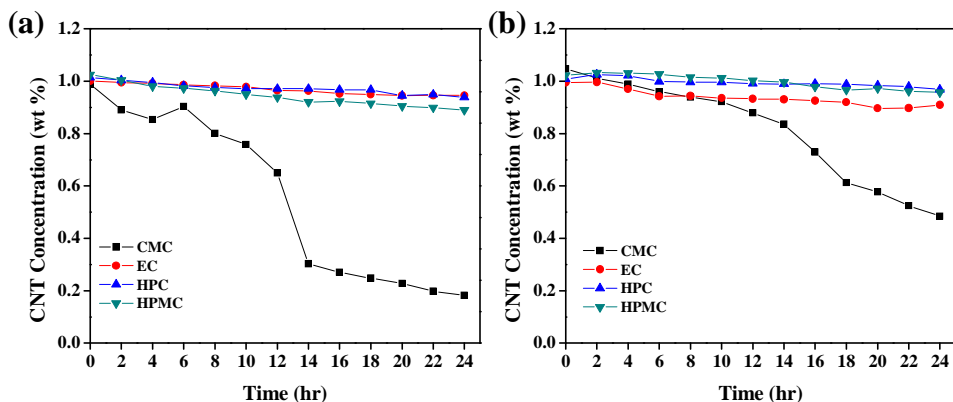
Figure 2.24: CNT concentration as a function of time for suspension using different cellulose (a) 95:5 EtOH:H$_2$O and (b) 95:5 IPA:H$_2$O, respectively during 24 hours.

Suspension	CNT Concentratration Drop (%) 95:5 EtOH:H$_2$O	CNT Concentratration Drop (%) 95:5 IPA:H$_2$O
CMC	81.51	53.75
EC	5.51	8.60
HPC	7.54	3.96
HPMC	13.20	6.35

Table 2.11: CNT concentration drop for suspensions using different celluloses and different solvent mixtures after 24 hours.

As mentioned previously, the EPD method was used as a characterization technique to test the capabilities of the CNT alcohol-based suspensions. Figure 2.25 shows the CNT film for the CNT alcohol-based suspensions using 95:5 EtOH:H$_2$O. The substrate used to deposit the CNTs was indium tin oxide (ITO) glass, the EPD conditions were 1.0 cm electrodes distance, 5.0 min deposition time and an applied voltage of 300V. The initial current range for these suspensions during deposition is 3.40 – 4.50 mA. The main difference of these CNT films is the amount of CNTs deposit on the ITO-glass. Evidently, CNT alcohol-based suspensions with HPC and HPMC as dispersant showed denser films. These suspensions show an initial current of 4.50 and 4.00 mA for HPC and

HPMC, respectively. However, higher CNTs density on the film does not represent better CNT alcohol-based suspension or better field emission properties. For each CNT alcohol-based suspension the optimal EPD conditions are unique.
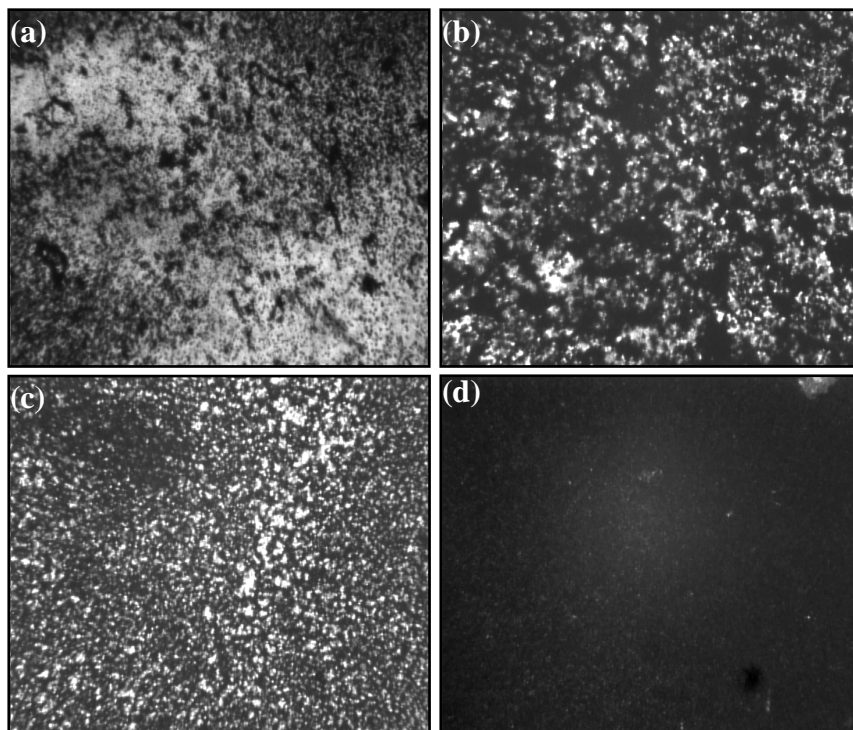
Figure 2.25: CNT films made using EPD method; (a) CMC, (b) EC, (c) HPC, and (d) HPMC.

Non-ionic celluloses have been demonstrated to be more effective in dispersing CNTs in suspension. This is can be attributed to the ionic species in suspensions are less because these came from the charger salts. In contrast, when an ionic cellulose is used the source of ionic species is from the cellulose it self and the charger salt. An increase in the amount of the ionic species in the suspension makes the suspension unstable due to the lower dissociation power of the organic solvents. For example, water as a suspension media can stabilize the ionic species reducing this problem. On the other hand, the cellulose substituents did not affects the stability of the CNT alcohol-based suspensions

because of the small difference of these. The EPD method as a characterization technique has been shown to be an effective way to qualitatively analyze the CNT alcohol-based suspensions. Importantly, varying CNT alcohol-based suspensions behave differently under the same EPD conditions, for example, the deposition rate of the CNTs.

2.2.5 *Study of Different CNT Concentrations and Long Term Stability of CNT Alcohol-based Suspensions*

The CNT concentration in suspension controls the CNTs protruding density, which is important because it allows control over the field emission properties of the CNT cathodes. The field emission properties are directly related with the CNT to CNT spacing, with the ideal geometry being 2 to 1 thereby reducing the screening effect. On the other hand, the long term stability of the CNT alcohol-based suspensions is very important because less sonication time will be required to disperse the CNT prior the EPD process. Reducing the sonication time is an advantage because the quality of the CNT will be not affected by this process.

The suspensions used for this study were prepared using a CNT concentration of 2.0 wt % (0.020 mg/mL), 2.0 wt % (0.020 mg/mL) of EC and 1.0 wt % (0.010 mg/mL) of charger salt in 95:5 EtOH:H_2O. The charger salts used were magnesium chloride ($MgCl_2$), potassium chloride (KCl), and sodium hydroxide (NaOH). KCl is a monovalent alternative to replace $MgCl_2$. The CNT concentration that drops after 48 hours is 12.49, 8.61 and 9.45 % for $MgCl_2$, KCl, and NaOH respectively. Figure 2.26 shows CNT concentration as a function of sediment time for CNT alcohol-based suspension using different charger salts over a period of 48 hours. These CNT alcohol-based suspensions

74

with higher CNT concentrations have the same stability as those with 1.0 wt % CNT. These results reveal that CNT alcohol-based suspensions with 1.0 and 2.0 wt % CNT concentrations are equally stable.
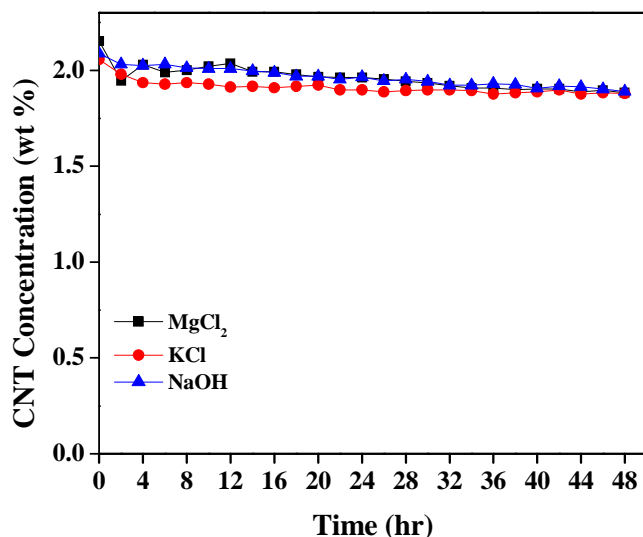
Figure 2.26: CNT concentration as a function of time for suspension using different charger salts and a CNT concentration of 2.0 wt% in 95:5 EtOH:H$_2$O over a period of 48 hours.

The increase in the CNT concentration did not affect the stability of the CNT alcohol-based suspensions. This is important because increasing the CNT concentration can alternatively be used to control the CNT density on the film. The study of the long term stability of CNT alcohol-based suspensions was made using suspensions with a CNT concentration of 1.0 wt % (0.010 mg/mL), 1.0 wt % (0.020 mg/mL) of EC and 1.0 wt % (0.010 mg/mL) of NaOH in different solvent mixtures.
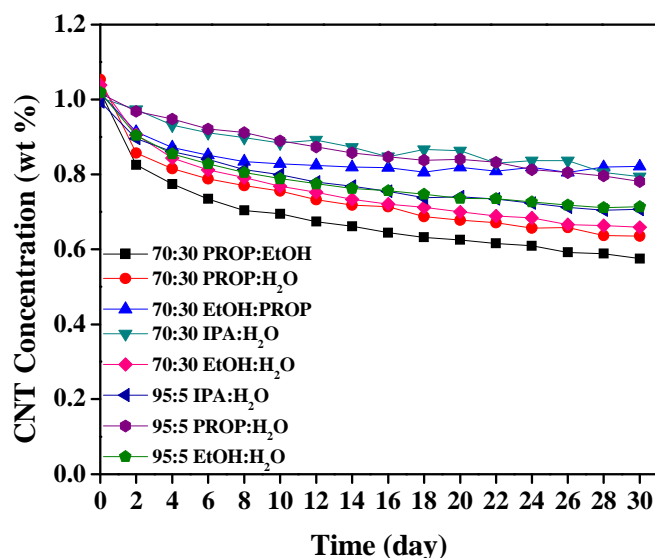
Figure 2.27: Long term stability study for CNT alcohol-based suspensions in a period of 30 days.

The long term stability analysis of the CNT alcohol-based suspensions after 30 days is shown in Figure 2.27 and Table 2.12. The long term study shows that depending on the solvent mixture, the range of the CNT concentration can drop 20 to 40 %. The results of the long term stability of CNT alcohol-based suspensions at this CNT concentration level are promising in comparison with the results published in the literature.

Suspension	Ratio	CNT Concentration Drop (wt %)
PROP:EtOH		43.70
PROP:H$_2$O		39.65
EtOH:PROP	70:30	19.33
IPA:H$_2$O		20.91
EtOH:H$_2$O		36.57
IPA:H$_2$O		28.86
PROP:H$_2$O	95:5	23.14
EtOH:H$_2$O		30.02

Table 2.12: Summary of CNT concentration drops in CNT alcohol-based suspensions in different solvent mixtures after 30 days.

CNT alcohol-based suspensions with high CNT concentration were successfully prepared with similar stability as low CNT concentration suspensions. The increase in CNT concentration did not compromise stability which is important for EPD. Moreover, the stability of the CNT alcohol-based suspensions for a period of 30 days is very satisfactory. The main goal in developing CNT alcohol-based suspensions is to use them as part of the EPD method. As noted earlier, one requirement for this method is to use a stable colloidal suspension and the development of CNT alcohol-based suspensions has successfully been completed. In the following section, the EPD method was used to deposit CNTs onto ITO glass and the film morphology and field emission properties were studied.

2.2.6   Field Emission of Random CNT Films

The CNT alcohol-based suspensions were used to deposit CNT film onto ITO glass. The CNT films made on this section are random films; these films do not represent the best geometry for field emission applications (discussed in Chapter 3). The EPD conditions used varies from constant current to constant voltage to study the effect of these two parameters. The suspensions used to deposit CNTs on ITO glass contained a CNT concentration of 0.010 mg/mL (1 % wt), 0.020 mg/mL (2.0 % wt) of charger salt (NaOH and $MgCl_2$) and a surfactants/dispersant concentration of 0.010 mg/mL (1.0 % wt) in 95:5 $EtOH:H_2O$.

The EPD conditions used were a constant current of 1.0 mA, an electrode distance of 1.0 cm was used and 5 minutes deposition time. The size of the cathode is 5 mm (0.196 cm^2 cathode area) for all the cathodes made in this section. High voltage power

supply (Model PS350/5000V-25W; Standford Research System, INC.) was used in the EPD process. Figure 2.28 shows high magnification SEM images of the CNT film made using the CNT alcohol-based suspensions previously described. The scanning electron microscope (SEM; FEI XL30 SEM-FEG) was used to characterize the CNT films on the ITO-glass. The high magnification SEM image did not show a significant difference in these CNT films. The conditions used for the CNTs deposition will work for all the suspensions prepared. The EPD conditions used might not represent the optimal conditions for these CNT alcohol-based suspensions. The used of a constant current condition resulted in the increase of the applied voltage over deposition time; this is to keep the current level. Hence, the electric field applied varies as the applied voltage change. The best alternative to keep the same electric field during the deposition process is to use a constant voltage condition.
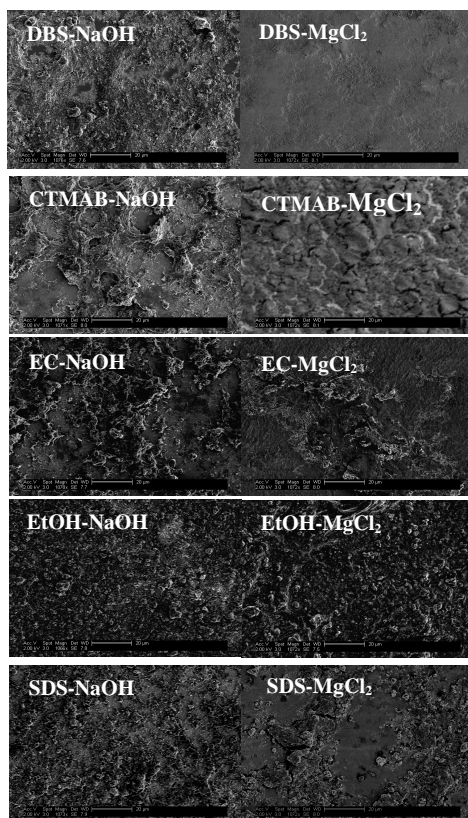
Figure 2.28: High magnification SEM images for CNT alcohol-based suspensions with 1.0 wt % CNT, 1.0 wt % charger salt and 1.0 wt % surfactant/dispersant. The scale bar is 20 μm.

Figure 2.29 shows optical and SEM images of the CNT film made using (a) EtOH-NaOH, (b) EtOH-EC-NaOH, (c) EtOH-MgCl$_2$ and (d) EtOH-EC-MgCl$_2$. The CNT film morphology reveals information about the EPD process, which includes film uniformity and CNTs density. The optical and low magnification SEM images show uniform film deposition. In addition, CNT films made from suspensions without dispersant (EtOH-NaOH and EtOH-MgCl2) seem to have a smooth surface in comparison with CNT films made with EC as the dispersant (EtOH-EC-NaOH and EtOH-EC-MgCl$_2$), which seem to be rough. High magnification SEM images do not show a significant difference as well for CNT films as seen in Figure 2.29.
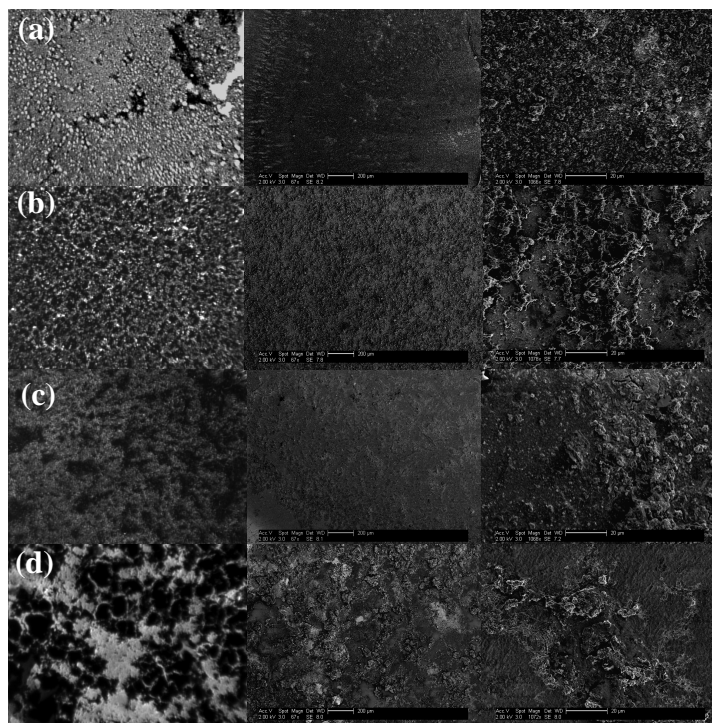
Figure 2.29: Optical images (5X, left) and SEM images (low magnification (scale bar 200 μm), center and high magnification (scale bar 20 μm), right) for cathodes made using a ethanol/water mixture; (a) EtOH-NaOH, (b) EtOH-EC-NaOH, (c) EtOH-MgCl₂, (d) EtOH-EC-MgCl₂.

The CNT density can be controlled in through (1) CNT concentration in suspension, (2) deposition time during EPD process and (3) applied voltage used during EPD process. Figure 2.30 shows the optical images at different deposition time for CNT films made using EtOH-EC-NaOH suspension. The EPD conditions used were an applied voltage of 40 V, an electrode distance of 1.0 cm, and a charger concentration of 2.0 wt % NaOH in the CNT suspensions. The deposition time plays an important role in control the CNT density on the film. As the deposition time increases the CNT film became darker as more CNTs were deposited as seen in Figure 2.30 (a) and (e). Higher CNT surface density does not always translate to a better emission property because of the electrical screening effect. Figure 2.31 shows the optical images of CNT film made using the same EPD conditions with the exception of the applied voltage. The EPD conditions used were an electrode distance of 1.0 cm, 3 minutes deposition time, and EtOH-EC-

80

NaOH CNT suspensions. The applied voltage was 40 V (Figure 2.31a) and 80 V (Figure 2.31b). The images clearly show the difference on the CNT films i.e. the CNT density increased as the applied voltage increased because the deposition rate is higher.
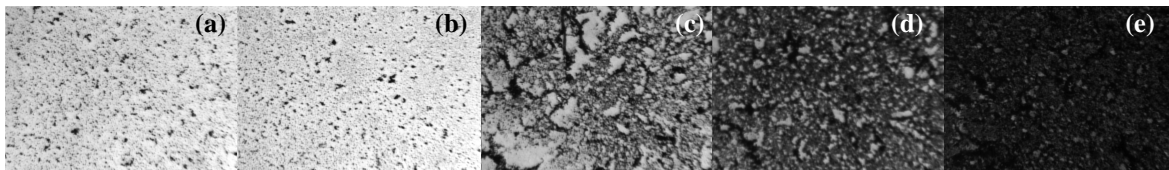
Figure 2.30: Optical images for CNT film made using the same EPD conditions but at different deposition times (a) 1 min, (b) 2 min, (c) 3 min, (d) 4 min and (e) 5 min.
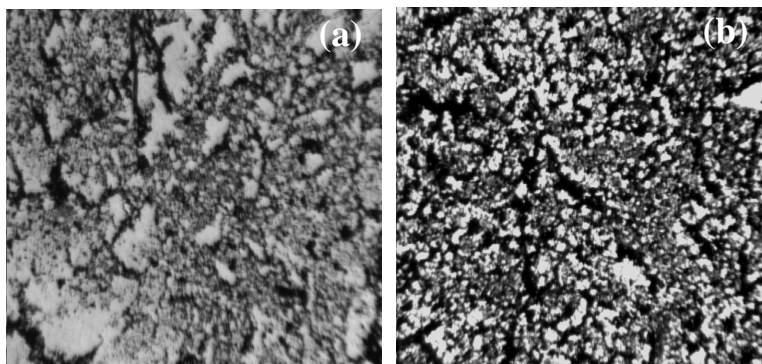
Figure 2.31: Optical images for CNT film made using the same EPD conditions but using different applied voltages (a) 40 Volts and (b) 80 Volts.

The field emission properties of the random CNT films made by EPD were measured. The field emission measurements were performed at high vacuum (10^{-7} Torr) with a gap distance of 200 μm, the anode was phosphor screen, 100 Kohm external resistance. Prior to the measurements the CNTs cathodes were annealed at 500°C for 1 hour. Figure 2.32 shows the phosphor screen images for a CNT cathode made using different CNT alcohol-based suspensions developed in the previous sections (a) EtOH-CTMA-NaOH, (b) EtOH-CTMA-MgCl$_2$, (c) EtOH-EC-NaOH, (d) EtOH-EC-MgCl2 and (e) EtOH-MgCl$_2$. The duty cycle used to take the phosphor coated ITO glass images was

0.1 %. The images show the circular geometry at different electric fields with good emission uniformity for these cathodes without activation. The random film morphology means that some tubes are aligned with the substrate whereas others are standing up and/or orientated differently with respect to the substrate and other tubes. The activation process simply removes the loose material that can cause arching and aligns the tubes vertically to the substrate.
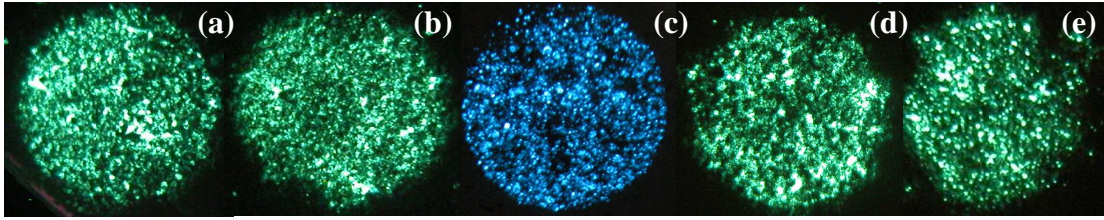
Figure 2.32: Phosphor screen images for CNT films on ITO glass. The cathode size is 5 mm in diameter (0.196 cm^2). The measurement was performed under high vacuum, with a distance of 200 μm between the anode and CNT cathode, duty cycle was 0.1 % and an external resistance of 100 KΩ was used. (a) 1000 V (5.0 V/μm) EtOH-CTMA-NaOH, (b) 1800 V (9.0 V/μm) EtOH-CTMA-MgCl$_2$, (c) 600 V (3.0 V/μm) EtOH-EC-NaOH, (d) 1200 V (6.0 V/μm) EtOH-EC-MgCl$_2$ and (e) 1900 V (9.5 V/μm) EtOH-MgCl$_2$.

The plots of current density as a function of the electric field for CNT alcohol-based suspensions with EC as a dispersant are shown in Figure 2.33. The measurements were performed at high vacuum with gap distance of 200 μm and 10 % duty cycle. The field emission properties of random CNT films, fabricated using the CNT alcohol-based suspensions with EC, were better than the field emission properties of those without EC. The turn-on field for these CNT film is ~ 3 V/μm for both CNT suspensions with NaOH and MgCl$_2$ as charger salts. On the other hand, the turn-on field for suspensions without EC is ~ 4.5 and ~ 6 V/μm for CNT suspension with NaOH and MgCl$_2$, respectively. For cathodes with randomly oriented CNTs, the emitters come from two sources. One source is the small fraction of CNTs that point to the current collector due to simple statistical

distribution. The second group comes from field induced alignment. Several experiments have shown the CNTs can be easily bent and aligned to the electrical field direction under a moderate electrical field.
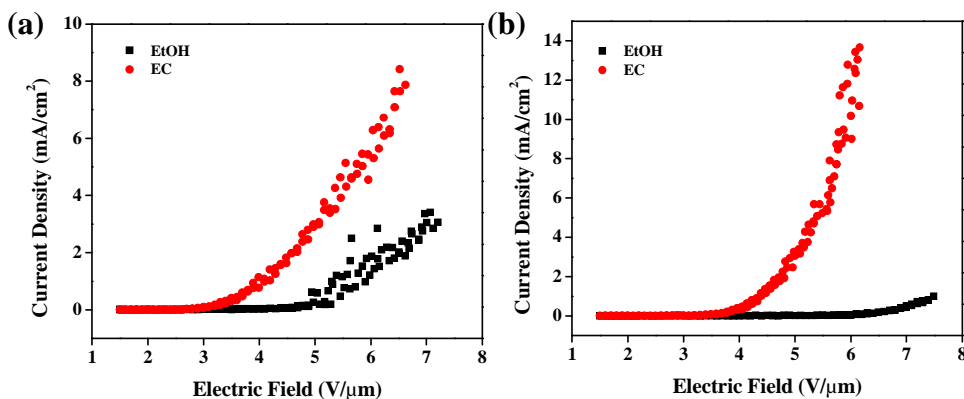
Figure 2.33: Current density as a function of electric field of random CNT film on ITO-glass, (a) CNT alcohol-based suspensions with NaOH as the charger salt and (b) CNT alcohol-based suspensions with MgCl$_2$ as the charger salt.

The current densities for these CNT cathodes are low for a field emission electron source since these films were not activated. However, the main purpose of these films is to characterize the CNT alcohol-based suspensions and determine if the field emission properties were comparable with the CNT suspensions without dispersant/surfactant. The results revealed that at the EPD conditions used to make these CNT cathodes, CNT cathodes made using a CNT suspension with EC had better performance.

2.3 Summary and Conclusions

The development of CNT alcohol-based suspensions has been a successful accomplish with the use of different dispersants. These suspensions were developed in based on the EPD method requirements. The effective CNT to surfactant ratio is 1 to 1 for CNT alcohol-based suspensions; this result is comparable with CNT suspension in the

literature. When DDBS and SDS are used as surfactants, they only stabilize the CNT alcohol-based suspensions better when the charger salt is not present. These suspensions are very stable and can be use in different applications that involves a stable CNT suspension. The study of different solvent ratios has shown that the 95:5 ratio is the most effective ratio independent of the solvent used. Solvents such as ethanol and propanol have been demonstrated to be excellent suspension media for the EPD method. The charger salt concentration plays important roles in the stability of the CNT alcohol-based suspensions and in the EPD process. The studies have shown that an effective range of the charger concentration for EPD is 1-2 wt %. On the other hand, CNT suspensions with EC did not show any change in the stability as the charger concentration increases.

Different celluloses have been analyzed and the use of non-ionic celluloses has been demonstrated to be more effective in dispersing CNTs in alcohol suspension media. CNT alcohol-based suspensions with high CNT concentration were successfully prepared with stability similar to low CNT concentration suspensions. The increase in CNT concentration did not compromise stability, which is important for EPD. The 30 days analysis of the stability of the CNT alcohol-based suspensions produced very satisfactory results with the range of the CNT concentration can drop from 20 to 40 % depending on the solvent mixture. As part of the characterization of the CNT alcohol-based suspensions, EPD was used to make CNT cathodes. The field emission properties of these CNT films without, any activation process, show equal or greater performance for the same suspensions without surfactant. Also, these cathodes have good film uniformity, which is important for the CNT cathode to act as a field emission electron source.

References

1. O'Connell, M. J. (2006). Carbon Nanotubes: Properties and Applications. Boca Raton: CRC Press; Taylor & Francis.

2. Diamond & Related Materials 14 (2005) 1463-1468. Effect of binders and organic vehicles on the emission properties of carbon nanotubes paste.

3. Materials Chemistry and Physics, 2005, **93**, 473-477. Large-area carbon nanotubes film synthesized for field emission display by special CVD equipment and the field emission properties.

4. Appl. Phys. Lett. **88**, 263504 (2006). Double-gated field emitter array with carbon nanotubes grown by chemical vapor deposition.

5. Diamond and Related Materials 10 (2001) 265-270. Application of carbon nanotubes to field emission display.

6. Annu. Rev. Mater. Sci. 1999. 29: 327-52. Electrophoretic deposition of materials.

7. J. Am. Ceram. Soc., 79 [8] 1987-2002 (2006). Electrophoretic Deposition (EPD): Mechanisms, Kinetics, and Application to Ceramics.

8. Adv. Mater. 2001, 13, No. 23, December 3. Fabrication and Electron Field Emission Properties of Carbon Nanotube Films by Electrophoretic Deposition.

9. Acc. Chem. Res. **2002,** 35, 1045-1053 Materials Science of Carbon Nanotubes: Fabrication, Integration, and Properties of Macroscopic Structures of Carbon Nanotubes.

10. Appl. Phys. Lett. **87** (19), 3738 (2004). Liquid-phase fabrication of patterned carbon nanotube field emission cathodes.

11. www.malvern.co.uk Zetasizer Nano series technical notes.

12. Tadros T.F. (2007). Colloid Stability The Role of Surface Forces - Part I. Weinheim: Wiley-VCH; Verlag GmbH & Co. KGaA.

13. IUPAC Compedium of Chemical Terminology, 2nd Edition (1997), 1974, 37, 512.

14. Carbon 44 (2006) 3149–3160. Electrophoretic deposition of carbon nanotubes.

15. Advances in Colloid and Interface Science 128–130 (2006) 37–46. The role of surfactants in dispersion of carbon nanotubes.

16. Carbon Vol. 36, No. 11, pp. 1603-1612, 1998. Dispersion and packing of carbon nanotubes.

17. Chem. Eur. J. 2002, 8, No. 5. Surface Oxidation of Carbon Nanofibres.

18. Chem. Eur. J. 2003, 9, 4000 – 4008. Soluble Carbon Nanotubes.

19. *J. Phys. Chem. B* **1999**, 103, 4318-4322. Solvatation of Fluorinated Single-Wall Carbon Nanotubes in Alcohol Solvents.

20. Rosen M.J. (2004). Surfactants and Interfacial Phenomena. Hoboken, New Jersey: John Wiley & Sons, Inc.

21. Journal of Colloid and Interface Science **241**, 1-17 (2001). Interactions between Surfactants and Particles: Dispersion, Surface Modification, and Adsolubilization.

22. *J. Mater. Chem.*, 2001, **11**, 1722-1725. Carbon nanotubes reinforced ceramic.

23. *J. Mater. Chem.*, 2004, **14**, 527-541. Advances toward bioaaplications of carbon nanotubes.

24. Nano Lett., Vol. 3, No. 10, **2003**. Individually Suspended Single-Walled Carbon Nanotubes in Various Surfactants.

25. Journal of Colloid and Interface Science 260 (2003) 89-94. Production of aqueous colloidal dispersions of carbon nanotubes.

26. J. Am. Chem. Soc. 2004, 126, 9902-9903. Small-Angle Neutron Scattering from Surfactant-Assisted Aqueous Dispersions of Carbon Nanotubes.

27. Journal of Colloid and Interface Science 260 (2003) 89–94. Production of aqueous colloidal dispersions of carbon nanotubes.

28. J. Phys. Chem. C, Vol. 111, No. 37, 2007. Zeta-Potential Measurements of Surfactant-Wrapped Individual Single-Walled Carbon Nanotubes.

29. Zumdahl, S.S. (1995).Chemical Principles. Lexington, MA: D.C. Heath and Company.

3 *Fabrication of CNT Cathode for X-ray Generation by Electrophoretic Deposition*

Fabrication of CNT cathodes is essential for developing applications such as field emission display (FED), CNT X-ray electron source and vacuum microelectronics. However, problems including short lifetime at high current density, instability under high voltage, poor emission uniformity, and cathode to cathode inconsistency are still major obstacles for many device applications. The most commonly used methods to fabricate CNT cathodes are CVD, screen printing and EPD. These fabrication methods were described in the Chapter 1. The challenge for CNT X-ray sources is the performance of these sources under high emission current density and high anode voltage. The anode voltage in X-ray source applications can vary from 40 KV for small animal imaging to 140 KV for clinical applications [1]. Most CNT field emission research has been focused on FEDs which are operated at much lower anode voltage (~ 10 KV) and low emission current density [2] but require up to millions of addressable pixels to perform consistently over a long period of time under poor vacuum conditions [3]. In this chapter, the main focus will be the study of CNT cathodes fabricated by EPD. The studies of parameters that affect the structure and morphology of the macroscopic CNT cathodes and their

emission properties will be discussed. In addition, the development of a process to fabricate CNT cathodes with high current and high voltage stability will be explained.

3.1   CNT Cathode Fabrication Process

The behavior of the macroscopic CNT cathodes under high emission current and high voltage has not been adequately investigated, aside from a few published studies with less than satisfactory results either from local measurement, without or with very short lifetime [4, 5, 6]. Although an individual CNT can emit over 1μA [7-9], obtaining high current from a macroscopic cathode is a difficult [4], complicated and challenging materials science problem. Several factors influence the performance of the macroscopic CNT cathodes such as (1) CNT density, (2) CNT-substrate adhesion, (3) CNT surface orientation among others factors. Limited by the emitter non-uniformity and electrical screening affect the density of active emitters is typically low which is directly related with the CNTs density at the film surface. This results in a high current from each active emitter even under a moderate extraction current density, which leads to failure of the nanotubes within a relatively short time. This is evidenced by the low emission current densities achieved in prior published studies, typically in the order of mA/cm^2. Adhesion of the CNTs to the substrate surface also plays a significant role in the emission stability, especially under high voltage. Removal of the CNTs under high potential is a common cause of arcing, which is detrimental to vacuum electronic devices. Moreover, this is attributed to the failure of previous generation of electron field emitters [2].

The CNT cathode fabrication for field emission X-ray sources consists of a combination of photolithography to pattern the deposition area and electrophoretic

88

deposition method to deposit the CNT composite film (Figure 3.1) [10-11]. The starting material used for the cathode fabrication was multi-wall CNTs with outer-shell diameters of 3 - 8 nm synthesized by the thermal CVD process, which were found to have enhanced emission properties [12]. Multi-wall CNTs were first purified, and then dispersed in alcohol with $MgCl_2$ as charger. The charger salt and the charger salt concentration used will determine the deposition direction and the deposition rate of the CNTs during the EPD process. The CNT suspensions used contained 1.0 % wt of CNT and 0.4 % wt of $MgCl_2$. To improve the adhesion, glass frits as binders were added to the EPD suspension [13]. The glass suspensions used contained 2.0 g of SCB-13 a commercial glass powder in a liter of alcohol. In addition, the glass suspensions contained 8.0 % wt of $MgCl_2$ and 60 % wt of Fe to increase the electrical conductivity of the CNT composite film. In order to evaluate the feasibility of fabricating high performance CNT cathodes on glass substrates, a glass substrate with printed silver contact lines were used (Figure 3.1b). The glass substrate consists of a 4 mm wide silver line with a 1 mm wide glass space; the silver lines are approximately 5.5 µm (Figure 3.1c). The use of this substrate provides low-cost and scalability to the CNT cathode fabrication process.
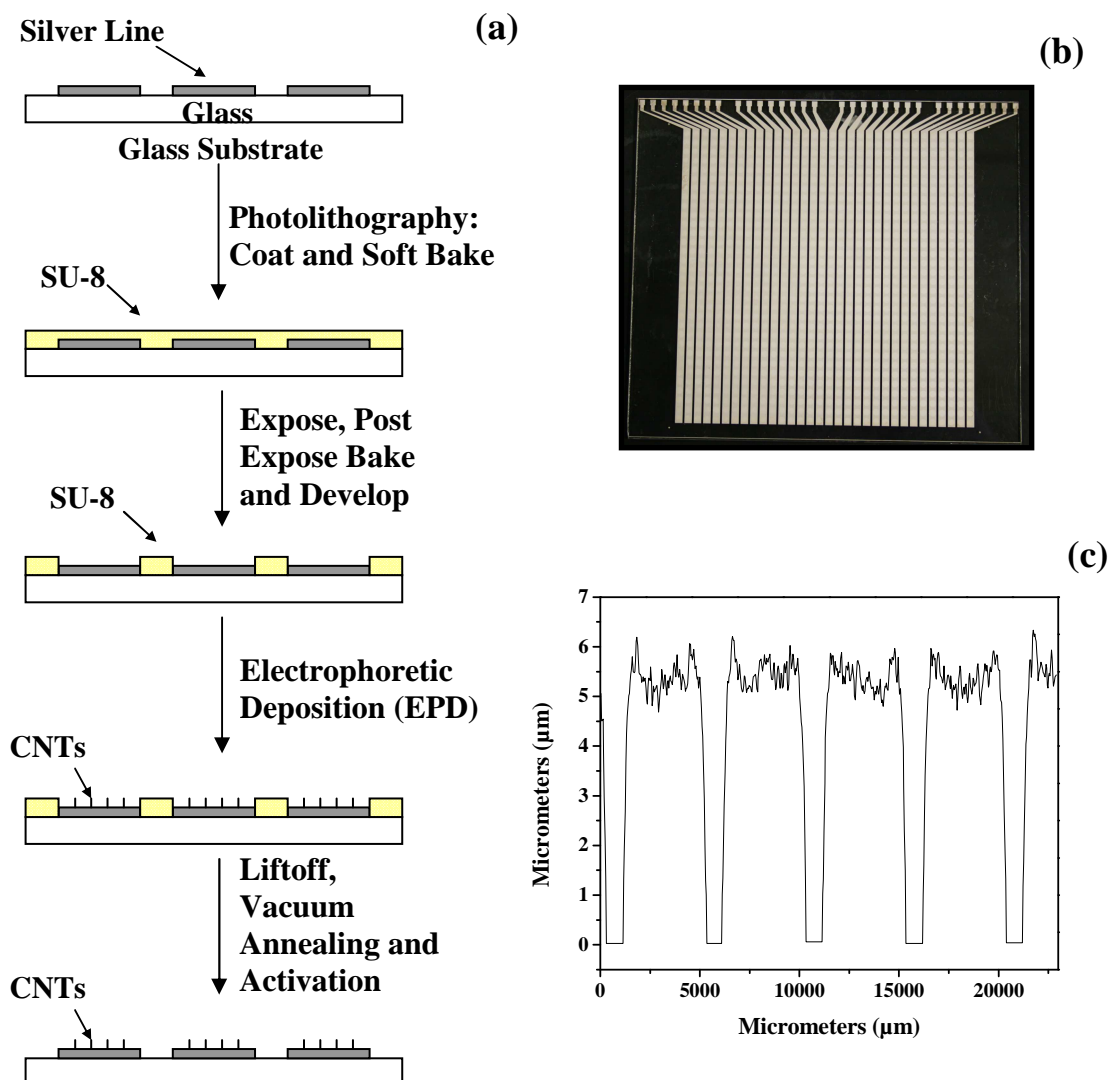
Figure 3.1: (a) A scheme showing the procedure used to patterned deposition of CNT cathode by EPD, (b) glass plate provided by TECO Nanotech Co. and (c) height profile across glass substrate.

The first step in the photolithography process was spin-coating the glass substrate with OmniCoat[TM] (MicroChem, Inc.). Following a layer of SU-8 (MicroChem, Inc.) was deposited. SU-8 is an epoxy based negative photoresist. Before the UV exposure a soft bake of the substrate was performed. Then the UV exposure patterned the photoresist to define the deposition area. After the exposure, a post expose bake was performed and the unexposed area was developed using SU-8 developer and MF-319 to remove SU-8 and OmniCoat, respectively. Figure 3.2a shows the substrate after the photolithography

process with the intended elliptical geometry and the user-specified dimensions. It should be noted that the boundaries of these features are well defined. The conditions, including the time of each photolithography step, depend on the SU-8 used and the desire SU-8 thickness. The variation in the SU-8 thickness used is from $10 - 100 \, \mu$m.

The CNTs and the binders were co-deposited onto the exposed silver surface by applying a DC electrical field between the substrate and the counter electrode submerged in the EPD suspension. The electrically charged CNTs and binders were driven to and deposited onto the substrate exposed area to form a composite film composed of the CNTs dispersed inside the binder matrix. The CNT composite film thickness is controlled by the applied voltage and the deposition time. The EPD deposition time typically used to fabricate CNT cathodes are $20 - 60$ seconds, depending on the cathode size. Figure 3.2b shows an optical image after CNT deposition. Importantly, the sample uniformity is consistent throughout the sample thickness; this was observed in all samples produced. After deposition, the photoresist was removed by immersion in N-Methyl-2-Pyrrolidone (NMP). To remove the residual NMP, the sample was rinsed with water and the bonding between CNT composite film and the substrate was strong enough that most of the CNTs remained on the substrate surface. After removal of the photoresist the CNT cathode was vacuum annealed at 500 ˚C for one hour. The CNT cathode after vacuum annealing has been shown in Figure 3.2c. This figure indicates that the CNT cathode has a well defined dimensions and geometry. The vacuum annealing process sinter the CNTs and the binders into a composite film adhered to the Ag contact line. The CNTs are randomly oriented on the top surface of the composite film both before and after annealing.
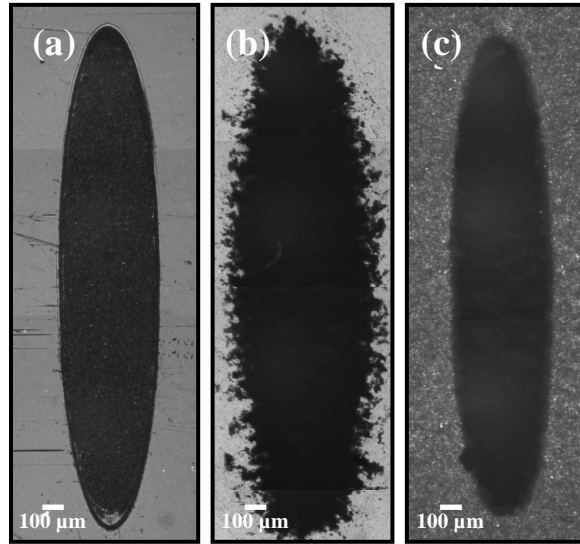
Figure 3.2: Optical microscope images of a 2.35 x 0.50 mm size cathode after (a) Photolithography, (b) CNT deposition, and (c) Lift-off with NMP and vacuum annealing.

In the final step or the activation process, the CNTs are vertically aligned, each CNT having one ends embedded inside the matrix and the other ends protruding from the surface. The activation process consists of mechanically removing a top surface layer of the composite film through tape activation and the strong adhesion of the CNTs to the substrate lies in the fact that one ends are inside the matrix. Also these films are composite rather than bare CNTs. Figure 3.3 shows SEM images of the top surface of the composite CNT film both (a) before and (b) after activation process. After annealing, the composite film bonded strongly to the substrate surface and could not be removed by taping. This is drastically different from the typical CNT films directly grown by CVD which have very weak interface bonding. The desired morphology for the field emission cathodes is shown in Figure 3.4. This is the desired morphology because this arrangement optimizes the field enhancement and because the electrons emitted from the nanotube tips under the electrical field. The activation process is very important because it eliminates

the loose particles on the substrate. These loose particles are detrimental to device operation because they can cause arcing under high voltage. Adhesion of the CNTs to the substrate surface also plays a significant role in the emission stability, especially under high voltage. Removal of the CNTs under high voltage is a common cause of arcing as mentioned previously, which is detrimental to the performance and operation of vacuum electronic devices.
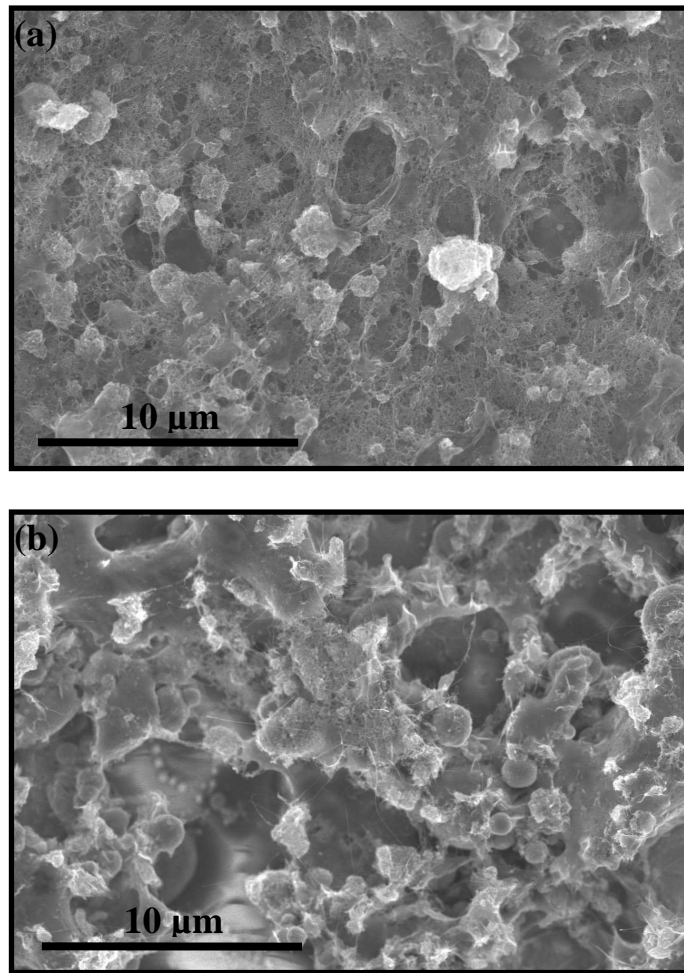
Figure 3.3: SEM images showing the top surface of the composite CNT film both (a) before and (b) after activation process.

As is well known, CNTs are excellent electron field emission emitters with low turn-on field and high emission current density due to their unique properties. However, the situation is different for macroscopic CNT cathodes. The desire morphology for these macroscopic CNT cathode depend on different parameters, such as the type of nanotubes, orientation, aspect ratio, and CNTs density, the interaction with the substrate surface and film uniformity.
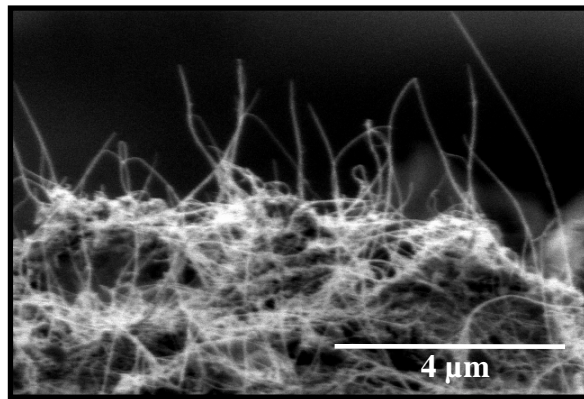
Figure 3.4: Cross-sectional SEM image of the CNT cathode after the activation process. The surface CNTs are now vertically aligned in direction perpendicular to the substrate surface. The protruding length of the CNTs is remarkably uniform considering the large length variation of the raw CNTs.

The orientation of the CNTs is an important parameter for these macroscopic cathodes due to the electrons are emitted from the tip and vertically aligned CNTs are better emitters than the random films as shown on Figure 3.5 [14]. The complication of the orientation of the CNTs is due to the effect of electrical screening. The ideal situation based on calculations is to have individual vertically aligned tubes spaced apart by twice their height to minimize the electrical screening and to optimize emitted current density (Figure 3.5c) [15]. This is the desired morphology for field enhancement. The protruding length of the CNTs is remarkably uniform considering the large length variation of the raw CNTs.
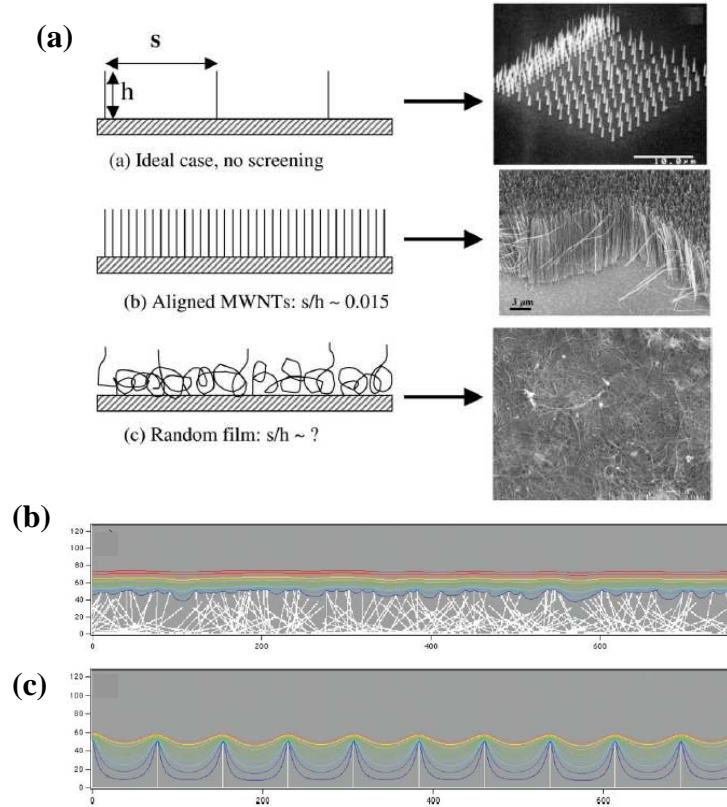
Figure 3.5: (a) Schematics illustrating the different geometries of macroscopic CNT field emission cathodes and images of the actual CNT structures fabricated [14]. (b) Schematic showing (b) dense CNTs where screening of the equipotential lines are observed, leading to electric field shielding and (c) CNTs spaced apart to minimize field shielding [15].

EPD, with the help of photolithography, has been shown be a convenient method to fabricate CNT cathodes with the required geometry. The optimization of several parameters such as SU-8 photoresist thickness, deposition time, deposition voltage, electrodes distance, CNT concentration in the EPD suspensions are parameters that plays an important role in the CNT cathode fabrication and is reflected in the CNT cathode performance. The optimal combination of these parameters results in a CNT cathode with the required properties for X-ray source applications. In the next sections, the surface morphology of CNT cathode film, the effect of the SU-8 thickness on the CNT film, and CNT cathode field emission performance will be discussed.

95

3.2   Surface Morphology of the CNT Cathode Film

The surface morphology of the CNT cathode film will be discussed in detail in this section. The CNT film morphology is important because it directly impacts on the performance of the CNT cathodes. The characterization of the surface morphology and the relation with the field emission properties of the cathodes will be explained. As previously discussed the ideal situation for field emission applications is to have CNTs on the cathode surface individual separated, vertically aligned, and spaced apart by twice their height in order to minimize the electrical screening and to optimize emitted current density. The variation of deposition voltage, deposition time and SU-8 thickness will be used in order to meet the required morphology for CNT cathode for X-ray source applications.

3.2.1   Surface Morphology and Field Emission Characterization

In order to study the effect of the CNT film thickness on the cathode a series of 2.35 x 0.50 mm (0.92 cm^2 area) cathodes were fabricated using a single EPD suspension deposited under different deposition conditions. The EPD conditions used for the glass suspension vary from 100 – 200 V applied voltage with a 2 second deposition time. However, the EPD conditions used for the CNT suspension varies from 100 – 400 V applied voltage with a 30 second deposition time. A Hitachi S-4700 Cold Cathode Field Emission Scanning Electron Microscope was used to image a typical 2.35 x 0.50 mm CNT cathode. The SEM images of a 2.35 x 0.50 mm CNT cathode at different magnifications are shown in Figure 3.6. The SEM images show a uniform CNT film from low magnification images to a high magnification level; at high magnifications the individual CNTs can be appreciated. A profilometer (Veeco DekTak 150) was used to

96

characterize the uniformity and cathode to cathode consistency of the film thickness. The parameters and/or conditions for the film thickness measurement used were a standard scan type, with a 12.5 µm stylus radius, a resolution of 0.500 µm/sample and a stylus force of 10.00 mg. The surface roughness of the film was measured using the profilometer. The average film thickness was found to depend on the deposition conditions used such as deposition time and applied voltage. For cathodes made under the same conditions, the average film thickness is consistent. For the 3 groups of samples made (4 cathodes in each group), the individual cathode thickness, the average thickness, the average surface roughness and the standard deviation are shown in Table 3.1. The results of the surface roughness for these 3 different groups show surface roughness in the same value range; this is attributed to the fact that the same EPD suspensions was used each time.

Group	Cathode	Film Thickness (µm)	Average Film Thickness ± Std. Dev. (µm)	Average Roughness ± Std. Dev. (µm)
1	1	10.23573	9 ± 1	3.1 ± 0.7
	2	8.36759		
	3	8.39800		
	4	7.72509		
2	1	15.47080	15.6 ± 0.5	3.6 ± 0.8
	2	15.04418		
	3	15.90705		
	4	16.04305		
3	1	20.91090	21.0 ± 0.4	3.0 ± 0.8
	2	20.69363		
	3	20.88222		
	4	21.52637		

Table 3.1: Summary of the CNT film thickness from 3 different groups of cathodes fabricated by EPD using different conditions.
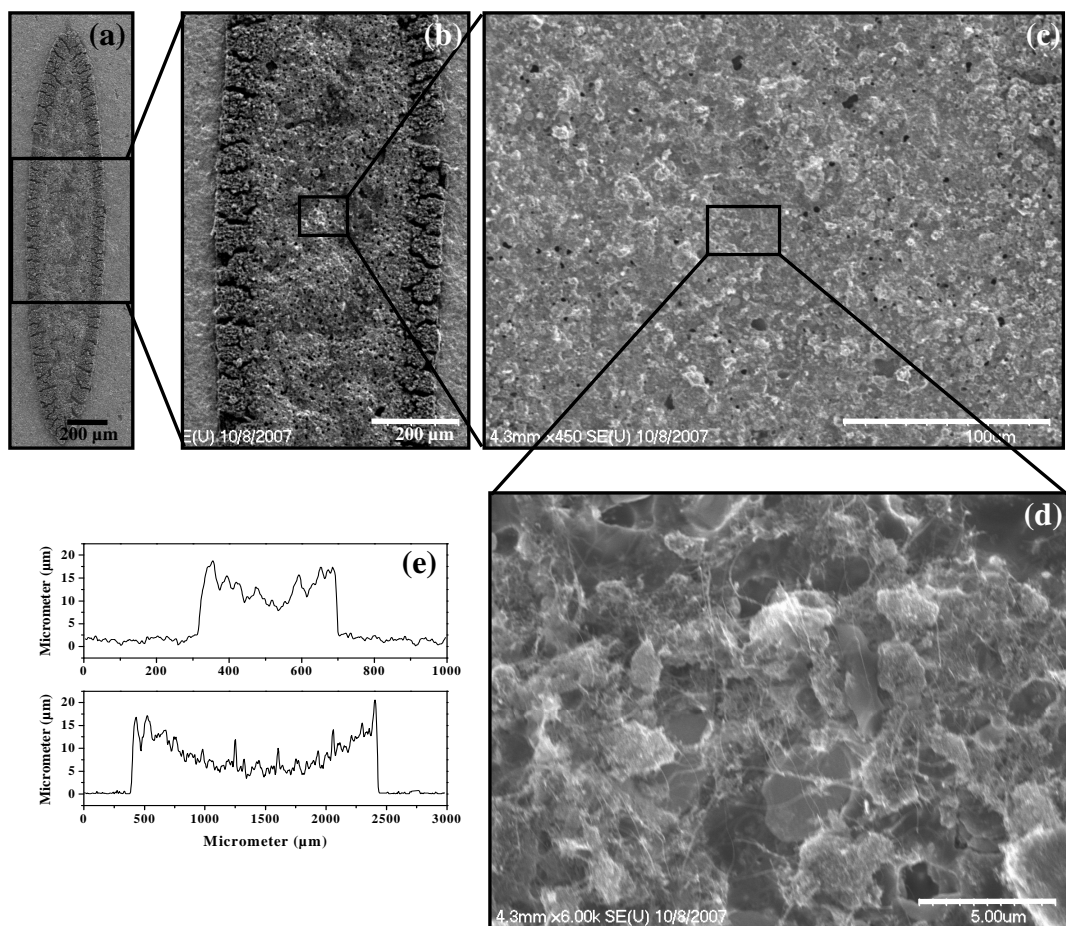
Figure 3.6: Top view SEM images of a 2.35 x 0.50 mm CNT cathode at different magnification (a) low magnification SEM image to (d) high magnification SEM image of the CNT film and (e) typical height profiles along the short and long axes measured by profilometer.

For a give cathode, the film is slightly thicker around the edge than in the center, as shown by the height profiles in Figure 3.6e. This variation depends on the thickness of the SU-8 photoresist used; this will be discussed in the next section. For 2.35 x 0.50 mm cathodes, the typical EPD conditions used for CNT micro-focus field emission X-ray source cathodes results in an average film thickness of 15μm and can be consistently fabricated with less than 10 % variation. The variation of the film thickness is about 5 - 10 μm over ~2000 μm distance. This is attributed to the electrical field concentration around the edge of the exposed silver contact line during EPD process which causes a high rate of CNT deposition. Figure 3.7 shows the 2-D scheme of electric field during

98

EPD process. The electric field at the edges is higher which causes a high rate of CNT deposition.
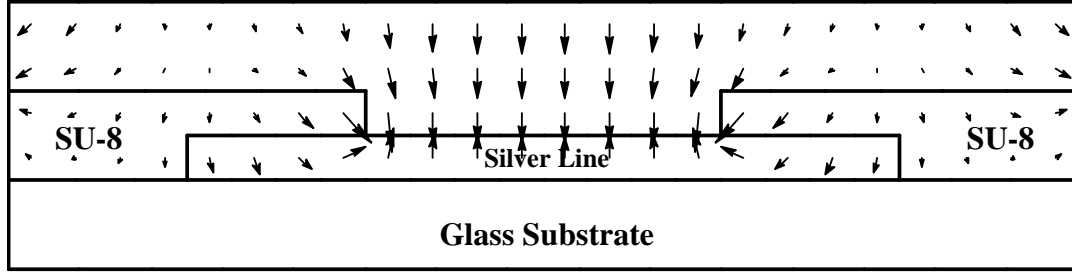
Figure 3.7: 2D scheme of electric field during EPD process (arrows represent the electric field). The electric field at the edges is higher, which causes a high deposition rate of CNTs. (Quick Field software)

The electron field emission properties of the cathodes were evaluated in diode mode. The field emission curve of a 2.35 x 0.50 mm CNT cathode in parallel plate geometry is shown in Figure 3.8a. The field emission current as a function of the applied electric field is shown in plotted. The voltage applied to the anode has a square waveform with 10 ms pulse width and 1 Hz repetition rate. The cathode to cathode consistency in the emission properties was evaluated for the CNT cathodes with different film thickness by measuring the electric fields required to obtain 1.0 mA (108 mA/cm^2) and 6 mA (650 mA/cm^2) from each cathode. The results obtained from 12 cathodes made under 3 different conditions are plotted in Figure 3.8b. The average electric field and the standard deviations to obtain 1.0 mA and 6.0 mA for each group were found to be: 5.9 ± 0.2 V/µm and 8.6 ± 0.2 V/µm, 5.9 ± 0.3 V/µm and 8.5 ± 0.5 V/µm, 6.2 ± 0.2 V/µm and 8.8 ± 0.3 V/µm for group 1, 2 and 3 respectively. These cathodes showed significantly improved emission current density and consistency compared to what we and others have reported in the literature in the past. Stable emission current density over 500 mA/cm^2 was readily obtained from these cathodes, with small cathode to cathode variation. It is interesting to note that despite the large variation in the film thickness for CNT cathodes

made under different conditions, the electrical fields are remarkably similar. This is attributed to two factors. SEM studies have shown that, after the mechanical activation step the cathodes have similar surface CNT density even through they have very different film thickness. This demonstrates that the CNT surface density is the predominant factor in determining the emission properties. Also it is important to note that EPD suspensions used in this study were the same, where the CNT concentration in the suspension was the same even though the EPD conditions were different. Second, the results were taken after each cathode was further conditioned electrically by running several current-voltage curves to relatively high currents. The purpose of this electrical conditioning process is to destroy the "hot spots" on the cathode which are typically CNTs with longer protrusion lengths compared to the average value. These "hot spots," in our experience, contribute to the variations in the cathode performances. During the conditioning process, the threshold electrical field increased initially before it stabilized as shown in Figure 3.9.
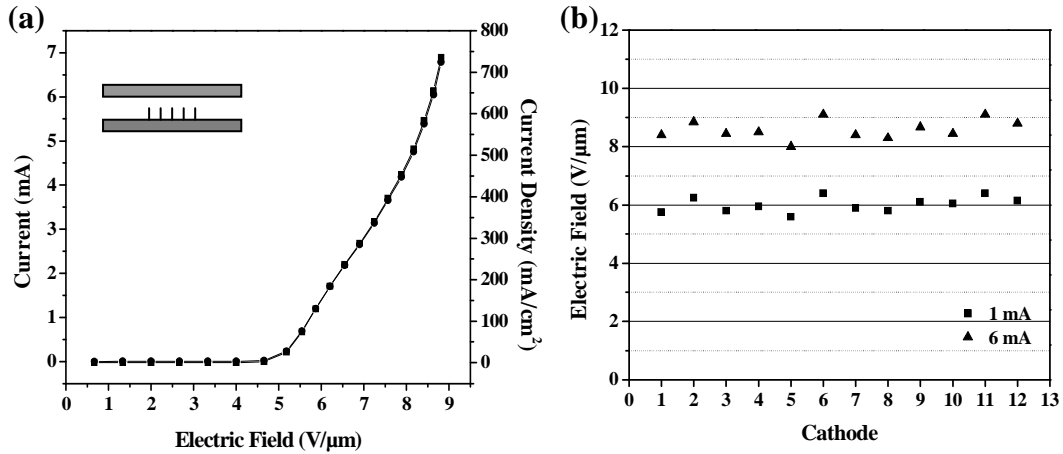
Figure 3.8: (a) Field emission curve of the CNT cathode (2.35 x 0.50 mm) in diode mode, emission current as a function of the applied electric field. (inset) Scheme of parallel plate geometry or diode mode geometry for field emission measurement. (b) Emission properties from 12 cathodes made under 3 different conditions measured in parallel plate geometry for 2.35 x 0.50 mm CNT cathodes. Electric field required to obtain a cathode current of 1.0 mA and 6.0 mA from each cathode. These values were taken after stabilization.
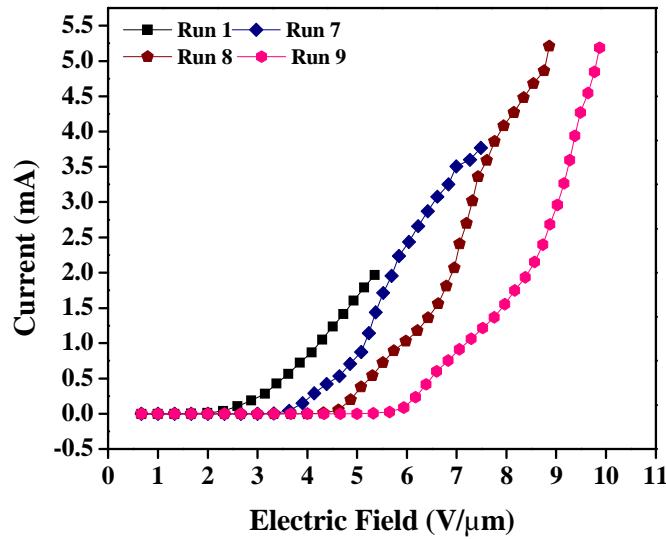
Figure 3.9: Field emission curve of 2.35 x 0.50 mm CNT cathode in diode mode, emission current as a function of the applied electric field for the same cathode after several runs.

The CNT cathodes fabricating using this EPD process have been shown to result in CNT films with high consistency capable of being used as CNT cathodes. The field emission properties of the CNT cathode depend predominantly on the CNT density on the cathode's surface and are independently of the CNT cathode film thickness. This was demonstrated by the consistency in the electric field that was required to obtain different levels of cathode currents. These cathodes fabricated by EPD showed the required field emission current density and consistency for field emission X-ray source applications. Also, these CNT cathodes showed superior field emission properties compared to CNT cathodes reported previously. The CNT cathodes can reach stable and high emission current densities, with small cathode to cathode variation.

3.2.2 Effect of the SU-8 Thickness on the CNT Film Variation and Field Emission Properties

As previously mentioned, the electric field at the edges is higher during the EPD process, reason why the study of the effects of the SU-8 thickness on the CNT film variation is valuable. The edge effect can be partially mitigated by increasing the thickness of the photoresist. A series of CNT cathodes with different SU-8 thicknesses were fabricated using a single set of EPD conditions. The glass suspensions conditions use were 100 V applied voltage over the course of 3 seconds. The conditions used for the CNT suspension were 100 V applied voltage over the course of 30 seconds. It is important to note that the distance between the electrodes for the EPD process was 1.0 and 0.5 cm. Figure 3.9 shows the height profile for a cathode after photolithography, the height profiles along the long axis of a 2.35 x 0.50 mm cathode using 10, 25 and 100 µm SU-8 photoresists respectively. Figure 3.9 shows the intended SU-8 thickness; thicker SU-8 photoresists allow us to reduce the electric field around the cathode edges because the SU-8 layer block or mitigate the electric field.
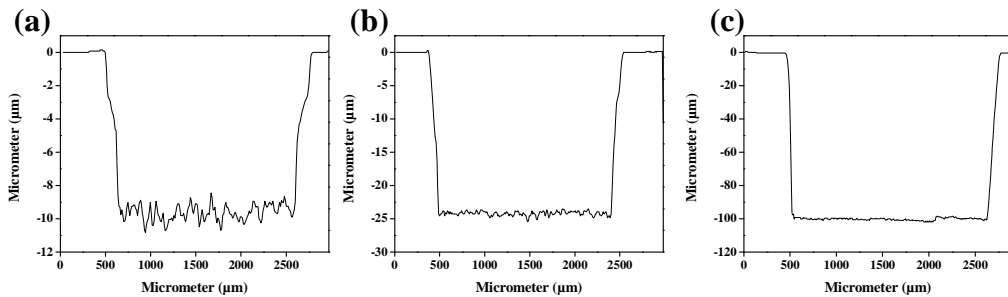
Figure 3.10: Profiler for a cathode after photolithography, the profiles along the long axis of a 2.35 x 0.50 mm cathode using (a) 10, (b) 25 and (c) 100 µm SU-8 photoresist.

For CNT cathodes made using the same deposition condition and 1.0 cm electrode distance, the average thicknesses and the standard deviations are: 6.4 ± 0.4, 7.4 ± 0.2 and 8.9 ± 0.7 µm for 10, 25 and 100 µm SU-8 thickness respectively. However, for an electrode distance of 0.5 cm, the average thicknesses and the standard deviations are: 6.6 ± 0.4, 8.2 ± 0.2 and 6.6 ± 0.4 µm for 1.0 cm electrode distance for 10, 25 and 100 µm SU-8 thickness, respectively. The thickness variation of the CNT film was reduced by 40 % when the thickness of the photoresist was increased from 10 µm to 100 µm. Figure 3.10 shows the height profiles along the long axis of a 2.35 x 0.50 mm cathode using 10, 25 and 100 µm SU-8 photoresists respectively at (a) 1.0 cm and (b) 0.5 cm electrode distance. It is important to note that the CNT film is not significantly affected when an electrode distance of 0.5 cm is used during the EPD process, with the exception of 100 µm SU-8 photoresist; when 100 µm SU-8 photoresist layers are used a more flat CNT film was observed relative to the same scenario using 1.0 cm electrode distance.
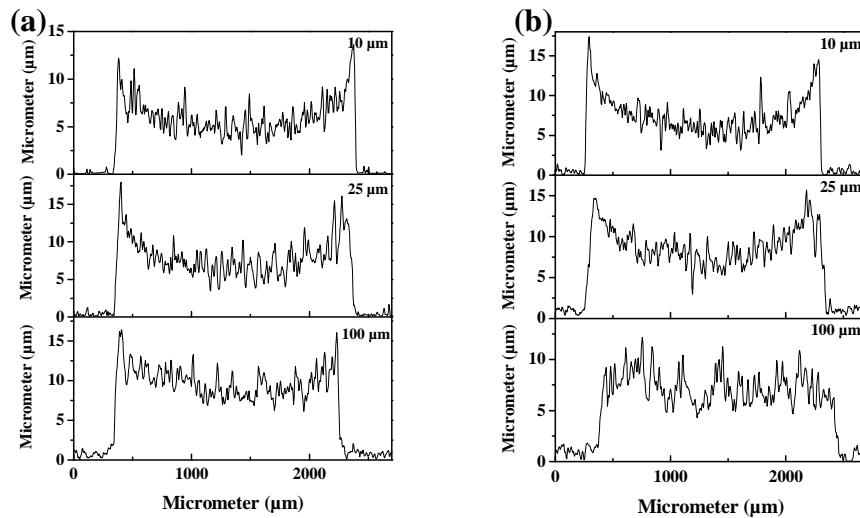
Figure 3.11: Height profiles for a CNT cathodes, the height profiles along the long axis of a 2.35 x 0.50 mm cathode using 10, 25 and 100 µm SU-8 photoresists respectively using (a) 1.0 cm and (b) 0.5 cm electrode distance.

The electron field emission properties of these cathodes were evaluated in diode mode. The average electric field and the standard deviations to obtain 1.0 mA (108 mA/cm^2) for each group (4 cathodes in each group) are shown in Table 3.2. The results show cathode to cathode consistency; the predominant factor in determining the emission properties are the CNT density on the film.

Group	SU-8 Thickness (µm)	Electrode Distance (cm)	Electric Field to obtain 1 mA ± Std. Dev. (V/µm)
1	10		5.42 ± 0.08
2	25	1.0	6.2 ± 0.5
3	100		6.6 ± 0.9
4	10		6.2 ± 0.5
5	25	0.5	6.1 ± 0.1
6	100		6.0 ± 0.2

Table 3.2: Summary of the electric field to obtain 1.0 mA and the standard deviation for 6 different groups where the SU-8 photoresist thickness and the electrode distance were change during the EPD process.

The reliable results for the CNT cathode fabrication by EPD have been demonstrated. The performance of the CNT cathode did not show any significant change when a different SU-8 photoresist thickness was used or when different electrode distances were used during the EPD process. The performance of the CNT cathodes did not change with the photoresist thickness and the electrode distances. It is noticeable the change of the CNT film morphology with the increment in the SU-8 photoresist thickness allowing the fabrication of more flat CNT films.

3.3 Performance and Film Morphology of CNT Cathodes with Different Sizes

The spatial resolution a micro-CT scanners depends strongly on the focal spot size and as a consequence on CNT cathode size (in the present CNT X-ray source design),

104

making the CNT cathode fabrication a crucial and essential part of the micro-CT construction. The fabrication process involves different parameters that can be change in order to fabricate CNT cathode with the require properties. The optimization parameters include the SU-8 thickness, the deposition time and the voltage applied during the EPD which was discussed in the previous sections. For small cathode size, 0.706 x 0.150 mm, the effective SU-8 thickness is 5-10 µm thick. If the SU-8 is too thick, the deposited material will be removed during lift-off. Similarly, the deposition time has to be shorter in comparison with large CNT cathode, 2.35 x 0.50 mm, because excess of the deposition material will cause a failure during the lift-off process. Figure 3.11 shows the typical height profiles along the long axis of an elliptical CNT cathode of 0.706 x 0.150 mm, 1.18 x 0.25 mm and 2.35 x 0.50 mm using the optimal EPD condition for each particular cathode size. In this figure it is evident that the edge effect diminishes as the cathode size decreases. This is attributed to more uniform electric field during deposition for the small cathode and can be appreciated in the film morphology.
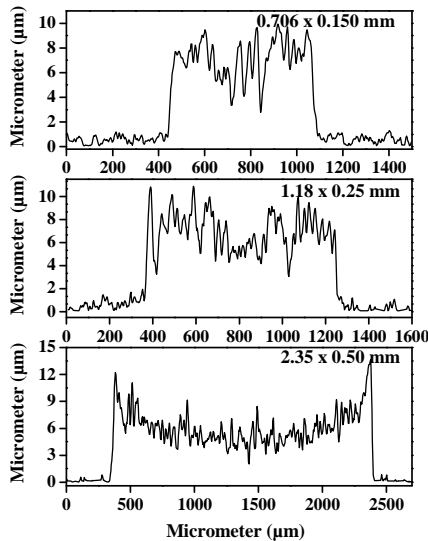
Figure 3.12: Typical height profiles along the long axis of an elliptical CNT cathode of 0.706 x 0.150 mm, 1.18 x 0.25 mm and 2.35 x 0.50 mm.

For cathodes fabricated with optimized surface CNT density a stable emission current density over 1500 mA/cm^2 was readily obtained. Figure 3.12 plots the experimentally measured emission current densities as a function of the applied electrical fields for 3 differently sized cathodes. At the same applied electrical field, the smaller the cathode area, the higher the current density achieved. For example, the smallest cathode (0.08 mm^2) reached a current density of over 1400 mA/cm^2 while the largest one (0.92 mm^2) generated ~ 400 mA/cm^2 density at the same applied field of 8.5 V/μm. This is attributed to the edge effect observed in the profilometer measurement. Cathodes with similar CNT surface density but different deposition time and film thicknesses have similar emission properties.
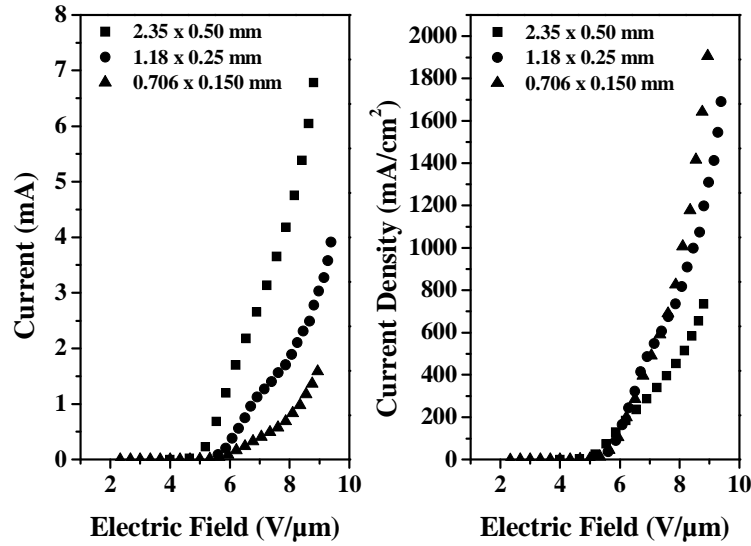
Figure 3.13: Field emission current as function of applied electrical field from 3 cathodes with different dimensions measured in the parallel plate geometry. Over 1500 mA/cm^2 density was readily achieved. The waveform of the anode voltage was 10 ms pulse width and 1 Hz and an external resistance of 100 KΩ was used and cathode to anode spacing of 150 μm. The cathode area from the smallest to largest cathode is 0.08, 0.23 and 0.92 mm^2.

EPD as a fabrication technique has shown to be an effective method for creating small CNT cathodes. The fabrication procedure illustrated in Figure 3.1 with some

variation in the SU-8 thickness and deposition time results in optimized CNT cathodes with the required properties for increasing the spatial resolution of the CNT X-ray source. The results revealed a linear relationship between current density and CNT cathode size with a significant increment in current density as the cathode area decrease.

3.4 CNT Cathode Characterization: Diode and Triode Mode

The electron field emission properties were evaluated in diode mode and triode mode as a routine inspection/characterization of the CNT cathodes fabricated by EPD. The typical conditions used for the diode field emission measurements included a high vacuum (10^{-7} Torr base pressure), a gap distance of 150 - 200 μm (cover glass) and a nickel plate as the anode. A labview program was used to control the anode voltage and to record the CNT cathode current as a function of applied voltage. In addition, a function generator is used to control the waveform of the anode voltage.

The field emission properties of different sizes of CNT cathodes made by EPD were evaluated in diode mode. The optimal EPD conditions for each cathode size were used. The measurements were performed in parallel plate geometry. The emission current from different cathode sizes exhibit a linear relationship with the cathode area. As previously mentioned, a significant increment in current density was observed as the cathode area decreased. Figure 3.13 shows the field emission current at 7.5 V/µm as a function of cathode area. The field emission current in Figure 3.13 is the stable current at this particular electric field, which does not represent the maximum stable current achieved for each CNT cathode size.
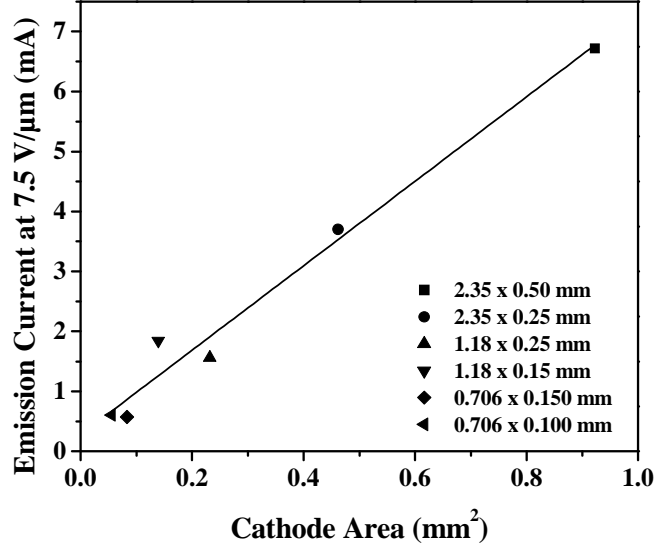
Figure 3.14: Field emission current at 7.5 V/µm as function of cathode area measured in the parallel pate geometry. The waveform of the anode was a 10 ms pulse width and 1 Hz for the CNT cathodes measured. The applied anode voltage was determined based on the external resistance used during the measurement. The equation of the linear fit is y = 7.0413x + 0.2795 (R^2 = 0.979).

Table 3.3 indicates summaries of the CNT cathode dimension, CNT cathode area, field emission current, and emission current density at 7.5 V/µm measured in the parallel plate geometry. For example, the smallest cathode (0.055 mm^2) reached a current density of 1095 mA/cm^2 while the largest cathode (0.92 mm^2) generated 728 mA/cm^2 current density at the same applied field of 7.5 V/µm. These results reveal the efficiency of the EPD process to fabricate CNT cathode of different sizes with the required field emission properties for an X-ray source.

CNT Cathode (mm)	CNT Cathode Area (mm^2)	Current (mA)	Current Density (mA/cm^2)
2.35 x 0.50	0.92	6.72	728
2.35 x 0.25	0.36	3.70	801
1.18 x 0.25	0.23	1.56	675
1.18 x 0.15	0.14	1.84	1327
0.706 x 0.150	0.083	0.57	690
0.706 x 0.100	0.055	0.61	1095

Table 3.3: Summary of the CNT cathode dimension, CNT cathode area, field emission current, and emission current density at 7.5 V/µm measured in the parallel plate geometry.

Figure 3.15 shows the histogram for 154 CNT cathodes (2.35 x 0.50 mm) fabricated by EPD. The histogram shows the distribution of the EPD process to fabricate CNT cathodes and it is possible to analyze the stability and reliability of the process. The constant examination of the EPD suspensions was an important part in the study of the fabrication process. In order to understand the impact of the EPD suspensions in the fabrication of CNT cathodes, UV-Vis spectroscopy and the conductivity of the suspensions were used to monitor the CNT and glass concentrations and the charger concentration, respectively. A series of standards were prepared in order to construct a calibration curve to monitor these concentrations. Figure 3.16 shows the CNT, glass and charger salt concentration for the EPD suspensions. CNT and charger concentration in the CNT suspensions does not vary significantly after the fabrication of 110 cathodes. On the other hand, the charger salt concentration decreases in 25 % in the glass suspensions without any serious impact on the performance of the CNT cathode. This examination demonstrates that EPD suspensions remain stable after the fabrication of hundred of CNT cathodes. Also can be concluded that the EPD process is very stable and this is reflected in the field emission properties.
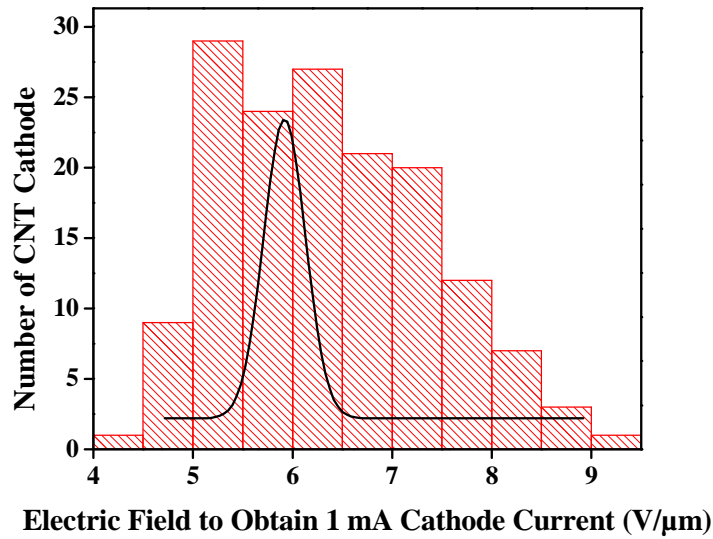
Figure 3.15: Histogram of the electric field to obtain 1 mA CNT cathode current for 2.35 x 0.50 mm CNT cthode fabricated by EPD.
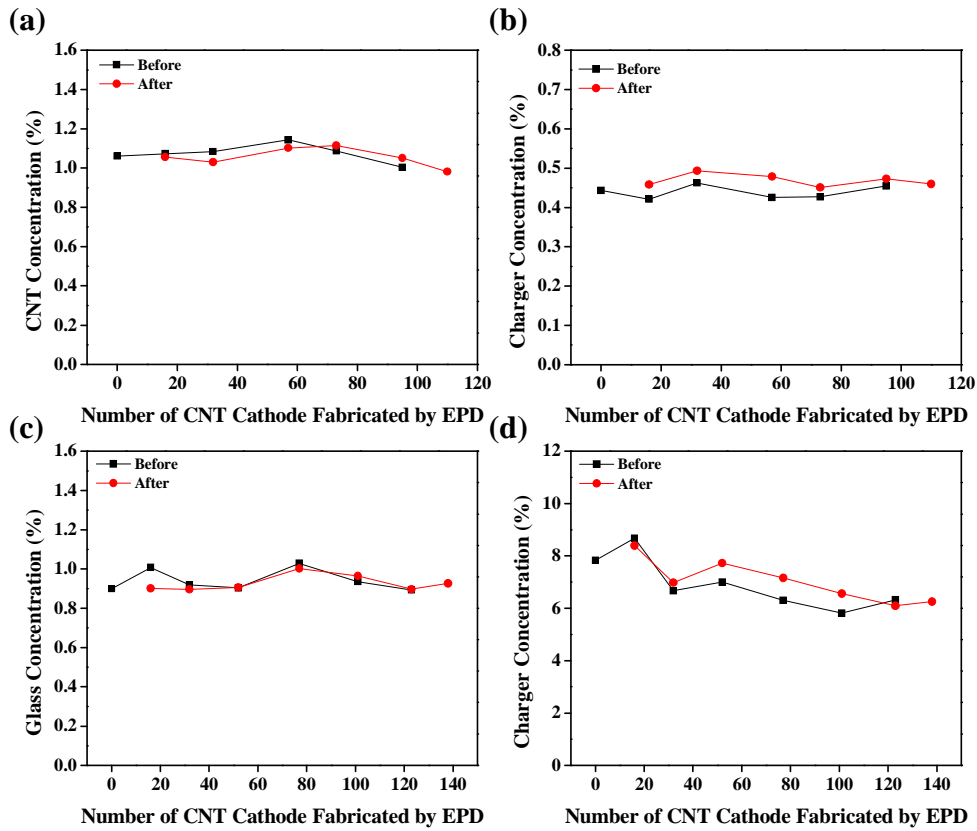
Figure 3.16: CNT suspension, (a) CNT concentration and (b) Charger concentration. Glass Suspension, (c) Glass concentration and (d) Charger concentration.

The emission lifetime measured in a constant current mode in parallel plate geometry from one large elliptical CNT cathode is shown in Figure 3.17. The voltage between the cathode and anode was adjusted automatically to maintain a constant emission current in this measurement. The total emission current was kept at 5mA (542mA/cm^2). The waveform of the anode voltage was chosen to mimic that used for micro-CT imaging which is 10ms in pulse width and 1Hz. Over the course of 30,000 second (30,000 pulses), the driving voltage increased by 720 volts. This driving voltage can be minimizing with a precondition of the vacuum chamber by increasing the baking temperature and increasing the baking time to remove water and/or absorbed gas molecules. The Charybdis micro-CT scanner typically takes 300 images per CT scan where each image uses one X-ray pulse of 10 – 100 ms pulse width. There the time period covered for this lifetime measurement covers the equivalent for 10 - 100 full CT scanners.
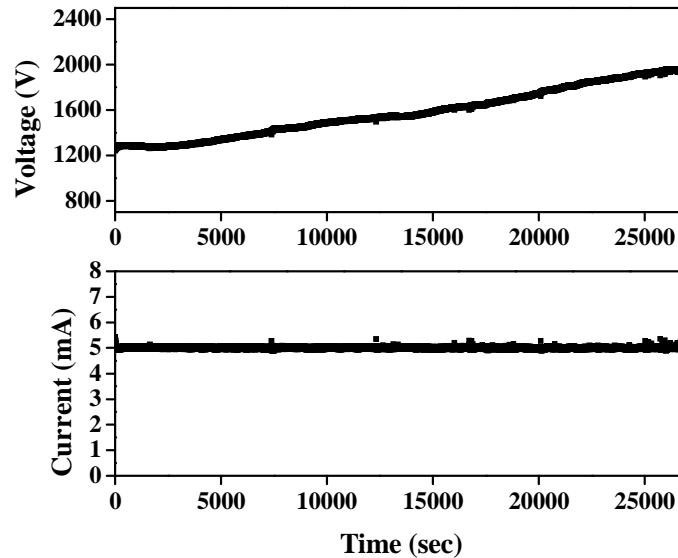
Figure 3.17: Emission lifetime measurement at constant current mode in the parallel plate geometry from one large elliptical CNT cathode. The measurement was performed under high vacuum at a peak emission current of 5 mA and an average peak emission current 4.99 ± 0.05 mA was obtained; the distance between anode and CNT cathode was 150 μm, the waveform of the anode voltage was 10 ms pulse width and 1 Hz and an external resistance of 100 KΩ was used.

111

The CNT characterization in triode mode at low anode voltage is fundamental because it mimics the micro focus X-ray source. A micro focused electron source was assembled using the CNT cathode fabricated by the EPD, as illustrated in Figure 3.18 (inset). The modified Einzel lens comprises two independently controlled focusing electrodes with the third electrode electrically connected to the gate electrode [16]; this will be discussed in detail in the next chapter. Figure 3.18 shows the relation between the emission current and the applied gate voltage while the anode voltage was kept at 4 KV constant, measured from a 2.35 x 0.50 mm cathode. This figure also shows the diode field emission for this cathode. The shift of the turn-on field in the triode mode measurement is attributed to the non-uniformity of the electrical field in the gate mesh.
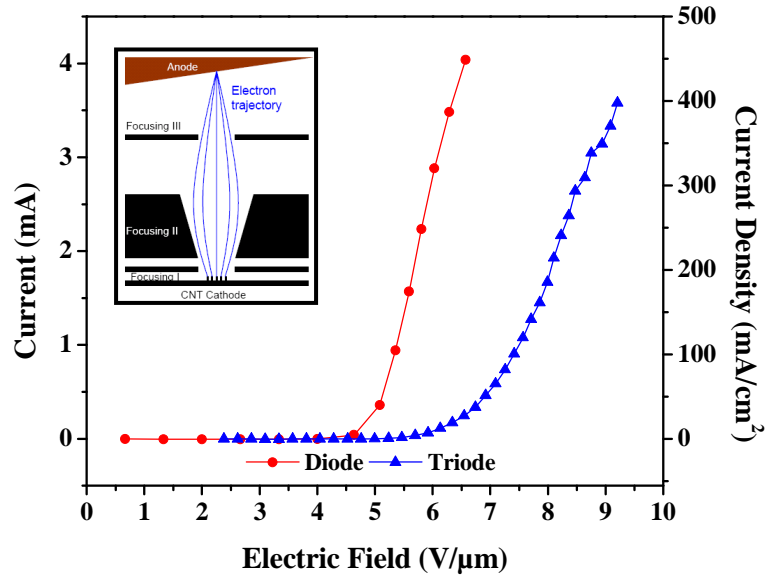
Figure 3.18: Field emission curve of the CNT cathode (2.35 x 0.50 mm) in triode mode, emission current as a function of the applied gate voltage. The gap distance between the gate and the cathode is 210 μm, the waveform of the anode voltage was a 10 ms pulse width operated at 1 Hz and an external resistance of 100 KΩ. The voltage on the middle focusing electrode was 300 V, top focusing electrode 2000 V and 4KV on anode. (inset) Scheme of triode mode geometry which consist of a gate, middle, top electrode and anode for field emission measurement.

The lifetime measurement of 2.35 x 0.50 mm CNT cathode was performed at low anode voltage. The former is required for the long term stability of the CNT cathode study. The condition used for the measurements were: 1200 V on middle electrode, 2000 V on top focusing electrode and 4 KV anode voltage. Three different CNT cathodes were tested at different conditions. For cathode current of 1.5 mA, the duty cycle used was 12.5 % (1 Hz and 125 ms pulse width); for a cathode current of 2.0 mA, the duty cycle used was 5.0 % (1 Hz and 50 ms pulse width); and for a cathode current of 3.0 mA, the duty cycle used was 2.0 % (1 Hz and 20 ms pulse width). About 70, 60 and 70 % of the cathode current pass through the gate electrode for 1.5, 2.0 and 3.0 mA, respectively. The lifetime was evaluated by measuring the variation of the applied gate voltage needed to maintain the constant current.

Figure 3.19 shows the applied gate voltage and the CNT cathode current as function of time. Also in this figure the average applied gate voltage as function of number of pulses for each current level is shown. The number of pulses and the duty cycle define the beam-on-time of the CNT cathode. The beam-on-time for the CNT cathode at a current level of 1.5, 2.0 and 3.0 mA is 7.5, 3 and 1.2 min/hr, respectively. For example, at 6.0×10^4 pulses the cathode with a current level of 1.5 and 2.0 mA showed an increment in the driving gate voltage. On the other hand, for the same number of pulses the cathode at a current level of 3.0 mA showed a decrement in the driving gate voltage. These results did not reveal a clear relationship among the CNT cathode current level and the duty cycle used. Similarly, the driving applied gate voltage for these three CNT cathodes show a decrement and an increment after a certain time or number of pulses. This fact can be explained as the measurement time increases the "hot spots" are

destroyed. These contribute with higher emission current in comparison with the average CNTs, contributing to maintaining the current level and reducing the driving voltage. Likewise, after the destruction of these "hot spots" or arcing events (Figure 3.19e after arcing event occurred at ~ 30th hour indicated by the spikes in the voltage current plots) the driving voltage increases gradually to keep the current level stable.
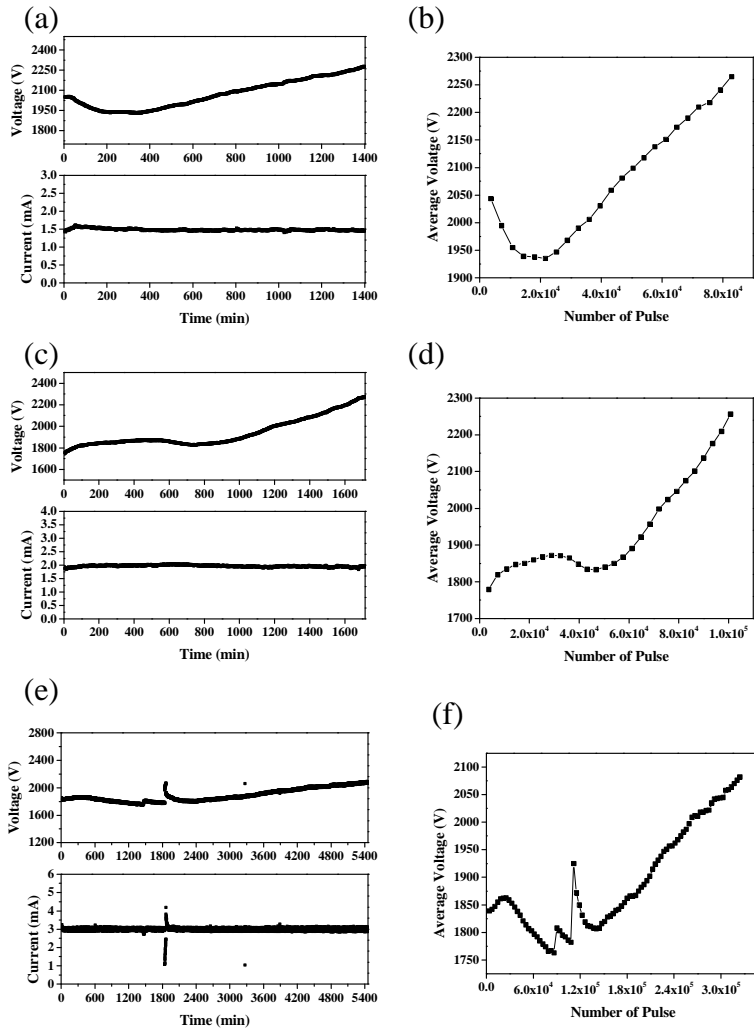
Figure 3.19: Emission lifetime measurement at constant current mode in the triode mode geometry from 2.35 x 0.50 mm CNT cathodes. The measurement was performed under high vacuum at a peak emission current of (a) 1.5 (c) 2.0 and (e) 3.0 mA and a average peak emission current 1.49 ± 0.03, 1.97 ± 0.03 and 3.0 ± 0.1 mA was obtained respectively. The average voltage as function of number of pulses for current level of (b) 1.5 (d) 2.0 and (f) 3.0 mA and the beam on time of 7.5, 3.0 and 1.2 min/hr respectively can be calculated from the duty cycle.

114

The CNT cathodes fabricated by EPD have been shown to have good field emission properties for field emission X-ray source. The effectiveness of this method can be appreciated in Figure 3.14 and 3.15, where cathodes of different sizes can be fabricated with the required geometry and properties. Also, the shift of the turn-on field in the triode mode measurement due to the non-uniformity of the electrical field in the gate mesh indicated that the CNT cathode required a turn-on field as low as possible in diode mode geometry to compensate this non-uniformity. In addition, the lifetime measurement did not reveal a relationship between the long term stability of the cathode and the current level or the pulse width.

Table 3.4 shows the summary of the field emission performance for CNT cathodes fabricated by screen printing, CVD, and EPD before and after the development of this fabrication process. The field emission properties of the CNT cathodes made by the fabrication method developed in this research study show superior or similar field emission properties in comparison with EPD method or other fabrication methods. The CNT cathodes in this study have the required properties for X-ray generation. In the next chapter, the high performance and long term stability for these CNT cathodes will be discussed.

Fabrication Method	Cathode Area (mm^2)	Geometry	Electric Field ($V/\mu m$)	Emission Current (mA)	Current Density (mA/cm^2)
CVD	0.25	Triode	-	0.30	120
EPD this Study	0.23	Triode	8.0	2.50	1200
EPD	0.12	Triode	12.0	0.12	100
EPD this study	0.14	Triode	11.0	2.00	1400
Screen Printing	100	Diode	8.35	100	100
EPD this study	12.57	Diode	9.0	52	414

Table 3.4: Summary of the field emission performance of CNT cathodes fabricated by Screen Printing, CVD, and EPD before and after this work.

3.5 *CNT Cathodes for Stationary Micro-CT Scanner: Multi Beam Field Emission X-Ray Source*

The CNT cathodes fabricated for a multi beam field emission X-ray source brings an additional challenge, the uniformity of the field emission properties. The stationary micro-CT scanner consists in a source array with 20 individually controlled X-ray beams. This system can generate a scanning X-ray beam to image an object from different viewing angles (coverage of 36°) without any rotation. The advantages of a stationary, multi beam micro-CT scanner over single beam system includes improvement in the temporal resolution and scanning speed due to the gantry rotation being no longer needed. In addition, the distributed source array technology makes multiplexing (simultaneous collection of multi-images at the time) a reality. Multiplexing can significantly increase the data collection speed. The fabrication procedure is described in Figure 3.1 with variation in the EPD conditions which were used for creating these CNT cathodes. The EPD conditions used for glass suspension are 100 V during 3 seconds and for CNT suspensions are 100 V during 1 minute. The CNT field emission cathode array

consists of 20 independent CNT cathodes in a circular arrangement with a diameter of 1mm with a pitch of 5mm between two adjacent cathodes.

Figure 3.20 show different stages of the fabrication process, optical microscope images of a 1.0 mm size cathode after (a) photolithography, (b) oxygen plasma treatment (c) lift-off with NMP, (d) vacuum annealing, (e) tape activation, and (f) SEM image of the vertically aligned CNTs. A Hitachi S-4700 Cold Cathode Field Emission Scanning Electron Microscope was used to image a typical 1.0 mm CNT cathode. The optical images show the intended geometry and a uniform CNT deposition.
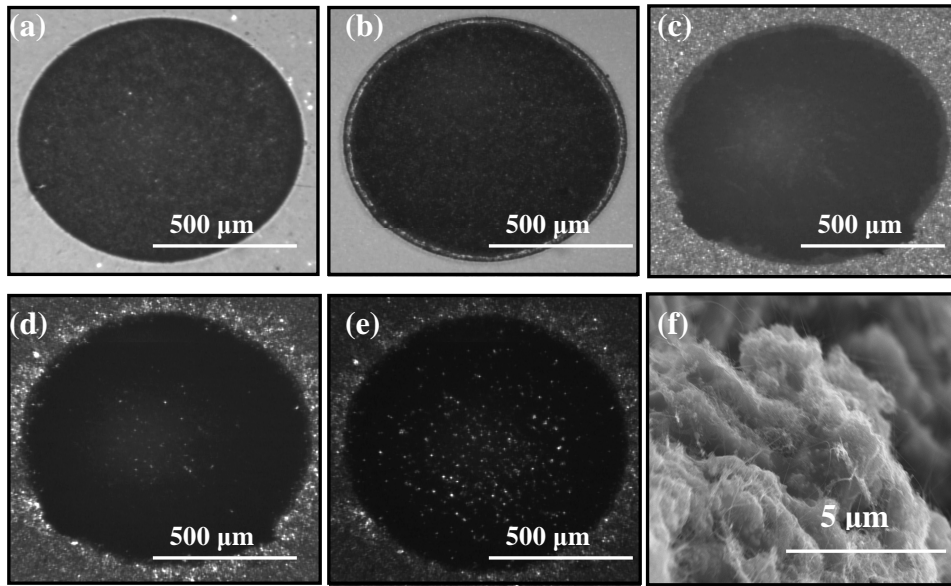
Figure 3.20: Optical microscope images of a 1.0 mm size cathode after; (a) photolithography, (b) oxygen plasma treatment (c) lift-off with NMP, (d) vacuum annealing, (e) tape activation and (f) SEM image of the vertically aligned CNTs.

A profilometer (Veeco DekTak 150) was used to characterize the uniformity and cathode to cathode consistency of the film thickness. The parameters and/or conditions for the film thickness measurement used were a standard scan type, with a 12.5 µm stylus

radius, a resolution of 0.333 µm/sample and a stylus force of 10.00 mg. The surface

roughness of the film was measured using the profilometer. Table 3.4 summarizes the

film thickness, average film thickness, surface roughness and average surface roughness

for CNT cathodes for a stationary micro-CT scanner. Figure 3.21 shows typical profiler

data for a cathode after photolithography using 10 µm SU-8 photoresists. In the same

figure are pictured the height profilers for 5 CNT cathodes on one glass piece. The film

thickness revealed the uniformity of the CNT film during the EPD deposition. The

average film thickness is 6.3 ± 0.4 µm with an average surface roughness of 0.4 ± 0.1

µm.
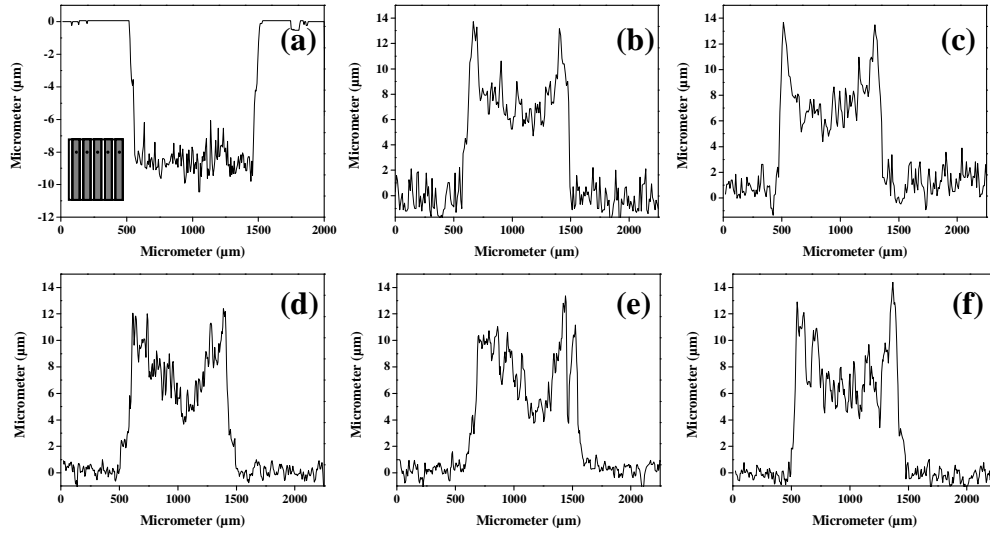
Figure 3.21: (a) Typical profiler for a cathode after photolithography using 10 µm SU-8 photoresists. (inset) Scheme of one of four of the glass pieces which consist of 5 CNT cathodes with a diameter of 1mm and a pitch of 5mm between two adjacent cathodes. (b-f) Height profilers for 5 CNT cathodes on one glass piece.

CNT Cathode	Film Thickness(µm)	Ave. Film Thickness ± Std. Dev. (µm)	Surface Roughness (µm)	Ave. Surface Roughness ± Std. Dev. (µm)
1	6.21979		0.45534	
2	5.86258		0.50279	
3	6.11882	6.3 ± 0.4	0.28202	0.4 ± 0.1
4	6.33147		0.33297	
5	6.84886		0.29327	

Table 3.5: Summary of the film thickness, average film thickness, surface roughness and average surface roughness for a stationary micro-CT scanner.

The field emission properties for the CNT cathodes in Figure 3.22 are show in Figure 3.23. The electric field to obtain 1.0 mA CNT cathode current is 8.06, 7.91, 7.82, 7.73 and 8.16 V/µm for CNT cathode 1, 2, 3, 4 and 5 respectively. The results show the uniformity of the field emission properties of the CNT cathodes on the same glass piece as well for the CNT film properties.
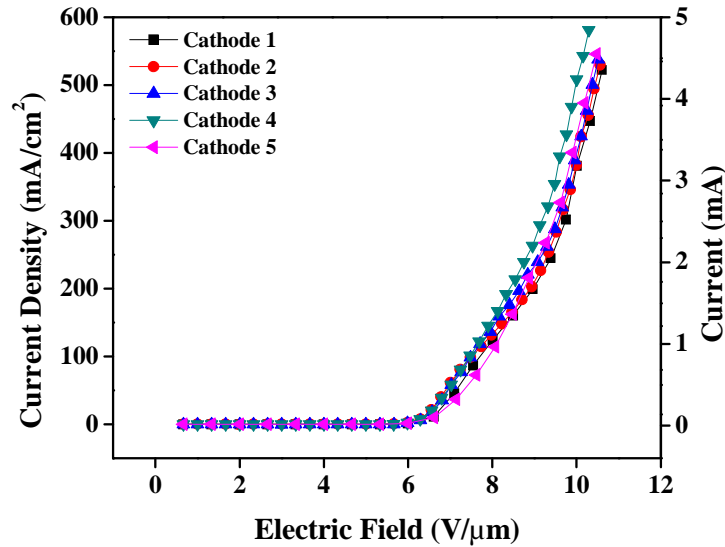
Figure 3.22: Field emission current as function of applied electrical field from 5 cathodes on one glass piece measured in the parallel plate geometry.

The analysis of the field emission properties for 20 individual CNT cathodes for a stationary micro-CT scanner is shown in Figure 3.23. Figure 3.23a shows similar field emission properties for 20 individual CNT cathodes on four different glass pieces measured in parallel plate geometry. The electric fields to obtain 1 mA CNT cathode current revealed the uniformity of these CNT cathode fabricated under the same EPD conditions. For 20 individual CNT cathode measured in parallel plate geometry the

average electric field needed to obtain 1 mA CNT cathode current is 7.5 ± 0.4 V/µm, which represent 5.33 % of variation in the electric field.
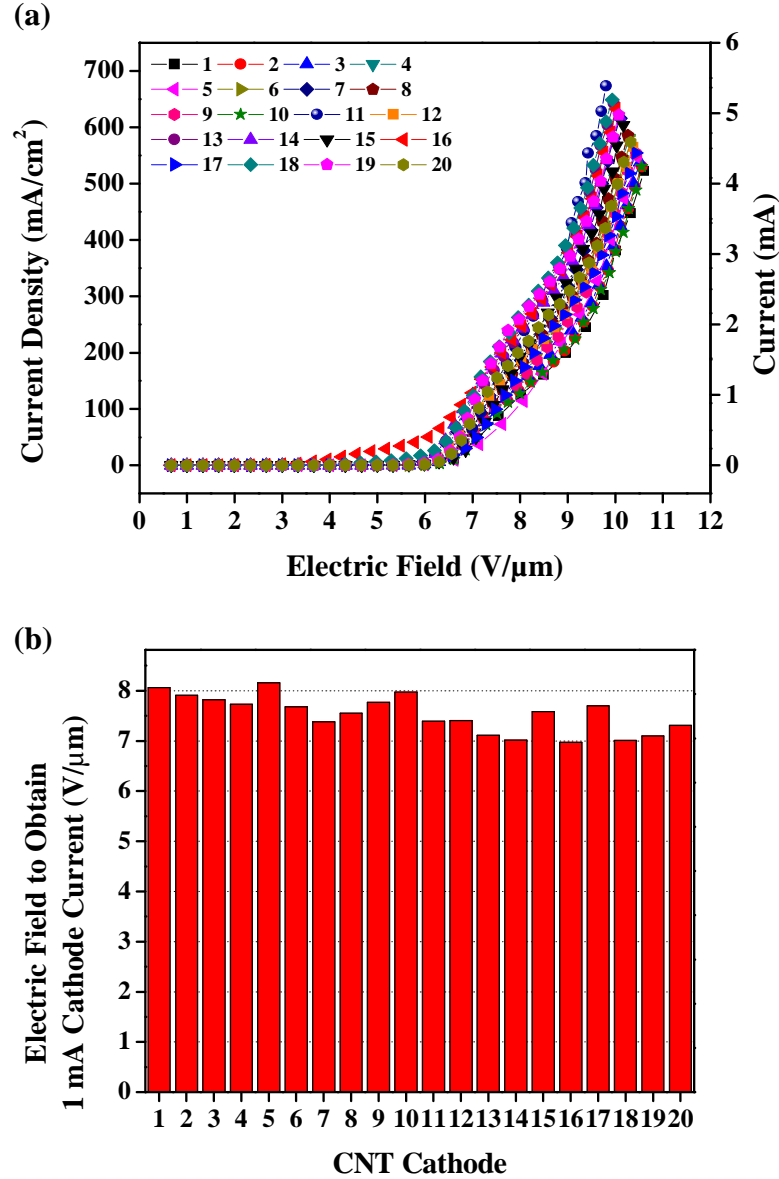
Figure 3.23: (a) Field emission current as function of applied electrical field from 20 CNT cathodes on four glass pieces measured in the parallel plate geometry. **(b)** Electric field needed to obtain 1 mA cathode current as function of CNT cathode number.

As previously mentioned, EPD has been show an efficient, reproducible and reliable method for the CNT cathodes fabrication. The results for CNT cathodes for a

stationary micro-CT scanner revealed high uniformity in the field emission properties as well in the CNT film thickness for CNT cathode fabricated under the same conditions.

3.6   CNT Cathodes for Stationary Digital Breast Tomosynthesis System

Digital breast tomosynthesis (DBT) is a three dimensional imaging technique. It a limited angle tomography technique that provides reconstruction planes in the breast using projection images from a limited angular range [17-18]. DBT's advantages over conventional mammography which project the 3D breast into a 2D image include: (1) acquisition of depth information, (2) increased efficiency with denser tissues common in younger and post menopausal women, and (3) its ability to help to avoid the false positive and false negative results often obtained due to tissue density, tissue overlap, or tumor depth issues [19]. The stationary digital breast tomosynthesis system consists of multiple X-ray beams which are positioned in a straight line parallel to the detector plane the source array containing 25 individually controlled X-ray beams. The Argus 2 system parameters include: imaging an object from different viewing angles without any rotation, a focal spot size around 500 µm, a total scan time of 3 seconds and a tube current of 80 mAs. The advantages of a stationary DBT system over conventional DBT systems (1) include less gantry vibration by eliminating the mechanical movement, (2) the increased efficiency for X-ray power and imaging time, and a total scan time which is the shortest among all systems under similar imaging conditions [19]. Argus 2 is a stationary DBT system with larger CNT cathodes (8 x 2 mm). These CNT cathode size provide high current and the benefits of this include: (1) better signal to noise ratios, (2) better image quality, and (3) decreased scan time [18].

The fabrication procedure is described in Figure 3.1 where variation in the EPD conditions for these CNT cathodes was used. The EPD conditions used for glass suspension were 15 seconds deposition time at 100 V and CNT suspensions are 30 seconds deposition time at 200 – 250 V. The typical SEM image for an individual 8 x 2 mm CNT cathode and the typical height profiles along the short and long axes measured by profilometer is shown in Figure 3.24. The average CNT film thickness for 5 CNT cathodes fabricated under the same EPD deposition condition is 4.3 ± 0.1 µm.
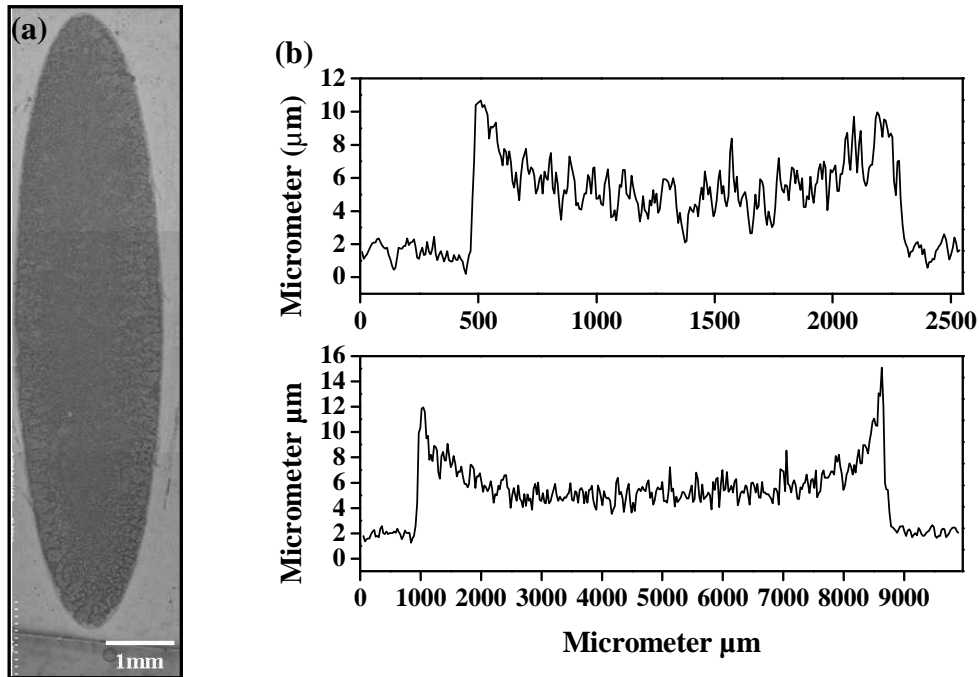
Figure 3.24: (a) Typical SEM image for an individual 8 x 2 mm CNT cathode and the typical height profiles along the short and long axes measured by profilometer.

The field emission properties of 8 x 2 mm CNT cathodes were evaluated in diode mode as shown in Figure 3.25. The results reveal good consistency in the field emission properties for CNT cathode individually fabricated. The target current for DBT applications is 52 mA current per 8 x 2 mm CNT cathode. Based on the result of the diode mode measurement the CNT cathodes can easily achieve the target current.
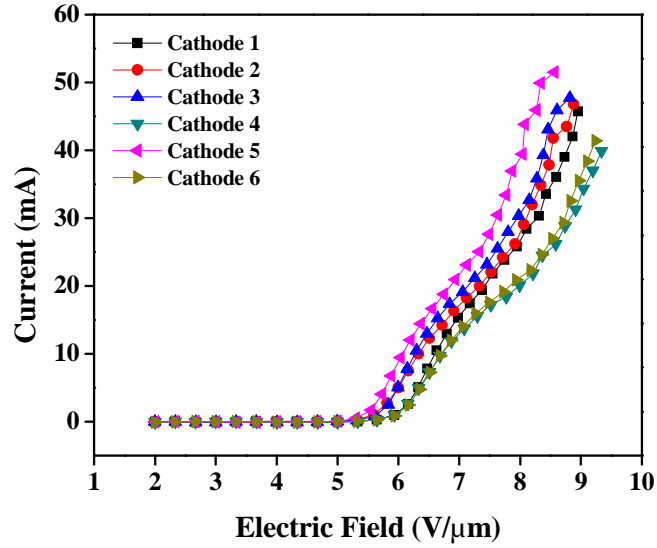
Figure 3.25: Field emission current as function of applied electrical field from 8 x 2 mm CNT cathodes in the parallel plate geometry. The waveform of the anode voltage was 10 ms pulse width and 1 Hz and an external resistance of 100 KΩ was used and cathode-to-anode spacing of 150 μm. The cathode area is 12.57 mm^2.

Figure 3.26 shows a CAD drawing of a single pixel X-ray source, which consists of a CNT cathode holder, gate electrode with a spot welded tungsten metal mesh, middle focusing electrode, top focusing electrode and a molybdenum anode at a tilt angle of 16°. In the same figure, the field emission current as function of electric field for an 8 x 2 mm CNT cathode is shown. The field emission measurements were performed using the single pixel set-up and the measurements parameters used were: 4.7 KV anode voltage, 1100 V for the top focusing electrode and 400 V for middle focusing electrode. The transmission rate or the percent of the CNT cathode current that passed through the gate is around 70 %. As previously mentioned, the shift in the turn-on field is attributed to the non uniformity of the electric field on the metal gate mesh.
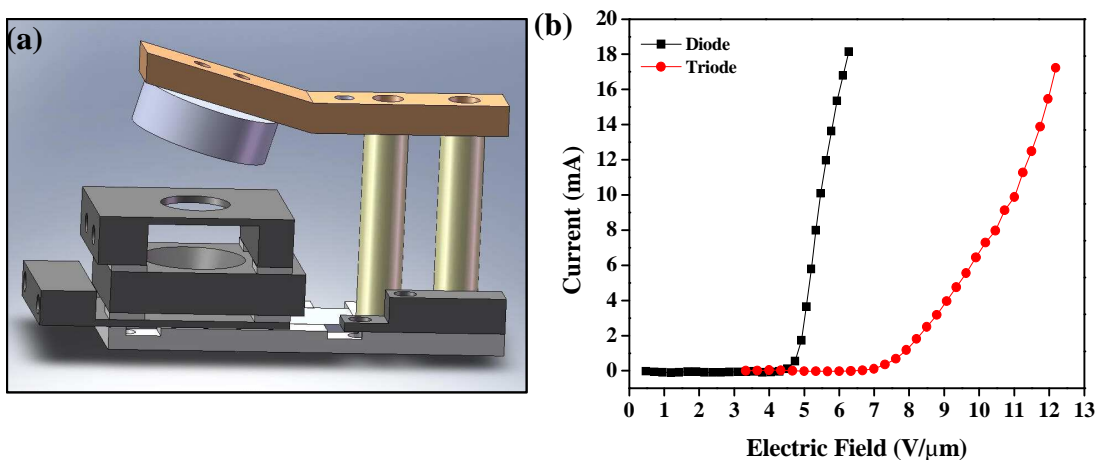
Figure 3.26: (a) CAD drawing of a single pixel X-ray source (image courtesy of Matthew McIntosh). (b) Field emission current as function of electric field for an 8 x 2 mm CNT cathode. The waveform of the anode voltage was 10 ms pulse width and 1 Hz and an external resistance of 100 KΩ was used.

The electron field emission properties of the 8 x 2 mm cathodes were investigated in triode mode under low anode voltage (4 KV). The anode and focusing electrodes potentials were the same for all the measurements. The potentials used during the measurements were 4.0 KV anode voltage, 1100 V for the top focusing electrode and 400 V for middle focusing electrode. The gate potential was adjusted to maintain a constant cathode current. The effect of pulse width or duty cycle on the CNT cathode was studied. For comparison purpose, four different 8 x 2 mm CNT cathodes were studied at different lifetime conditions: 1 Hz and 10 ms pulse width (1 % duty cycle), 1 Hz and 25 ms pulse width (2.5 % duty cycle), 1 Hz and 400 ms pulse width (40 % duty cycle) and 0.2 Hz and 1 sec pulse width (20 % duty cycle) at a current level of 5 mA. Figure 3.27 shows emission lifetime measurement at constant current mode in the triode mode geometry from 8 x 2 mm CNT cathodes. In the same figure the average voltage as function of beam-on-time is shown.

124
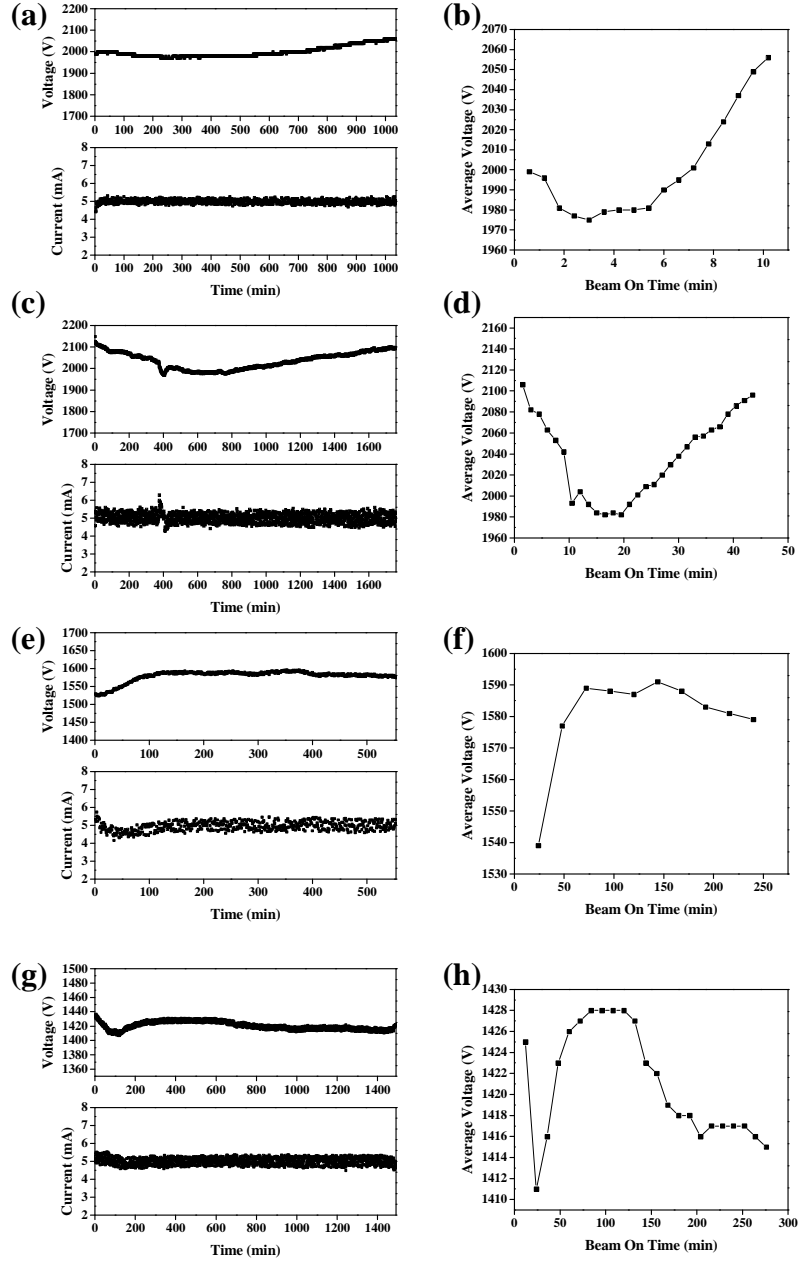
Figure 3.27: Emission lifetime measurement at constant current mode in the triode mode geometry from 8 x 2 mm CNT cathodes. The measurement was performed under high vacuum at a peak emission current of 5 mA and a average peak emission current (a) 5.0 ± 0.1, (c) 5.0 ± 0.3, (e) 5.0 ± 0.3 and (g) 5.0 ± 0.2 mA was obtained respectively. The average voltage as function of beam on time, (b) 0.6, (d) 1.5, (f) 24 and (h) 12 min/hr respectively.

The results reveal that as the pulse width increases, the driving voltage over time is more constant. Four different 8 x 2 mm CNT cathodes were studied at a CNT cathode current level of 10 mA, the lifetime conditions studied were: 1 Hz and 10 ms pulse width

(1 % duty cycle), 1 Hz and 25 ms pulse width (2.5 % duty cycle), 1 Hz and 150 ms pulse width (15 % duty cycle) and 0.150 Hz and 1 sec pulse width (15 % duty cycle). Figure 3.28 shows the emission lifetime measurement at a constant current of 10 mA and the average voltage as a function of beam-on-time. In general, the driving voltage decreases until a certain point and after that point start to increase as the measurement time increase. In Figure 3.28 it is clear that the driving voltage decreases at a beam-on-time of 8, 10, 50 minutes for 10, 25 and 150 ms pulse width respectively. On the other hand, when the same duty cycle is used (1 Hz and 150 ms pulse width and 0.150 Hz and 1 sec pulse width) the driving voltage is more stable as the pulse width increases.
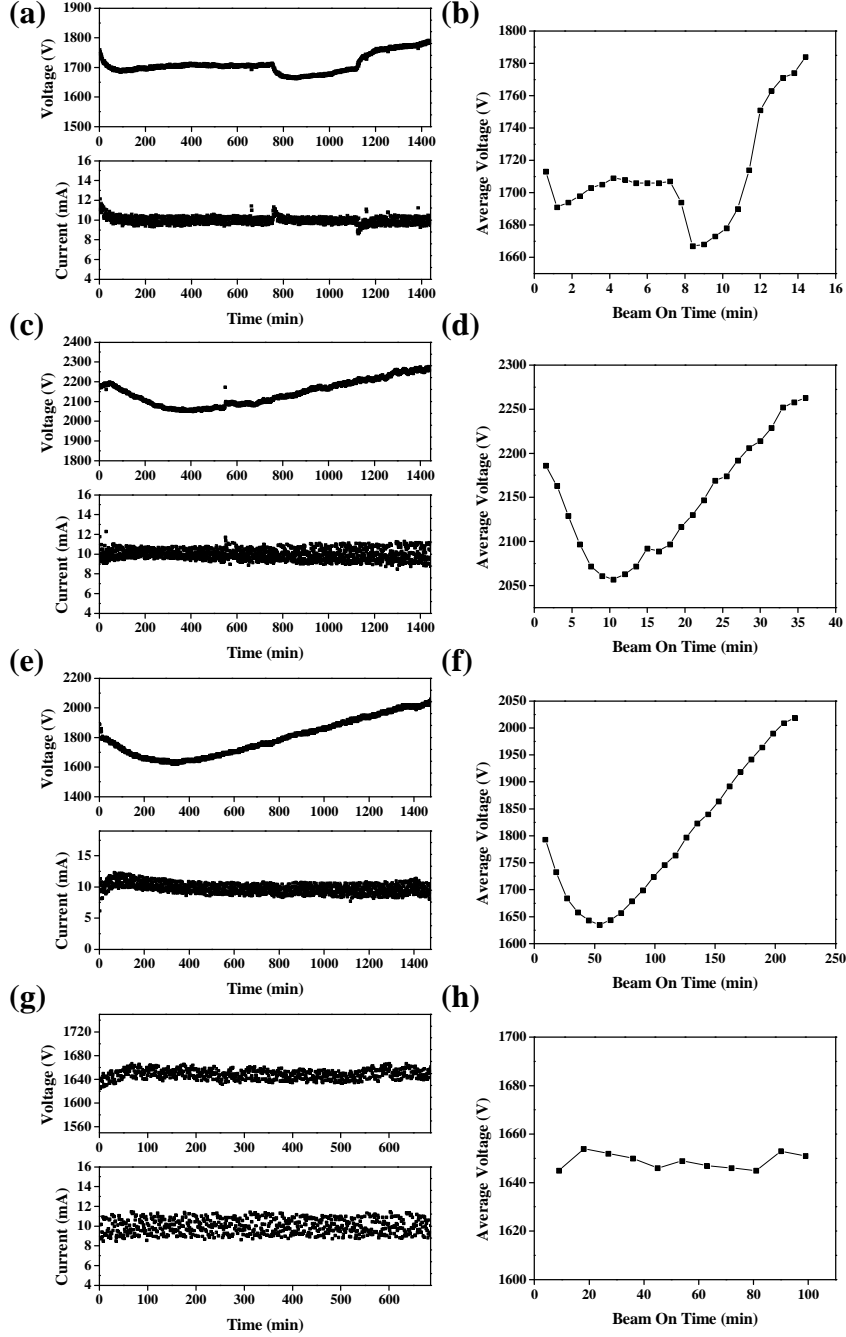
Figure 3.28: Emission lifetime measurement at constant current mode in the triode mode geometry from 8 x 2 mm CNT cathodes. The measurement was performed under high vacuum at a peak emission current of 10 mA and a average peak emission current (a) 10.0 ± 0.4, (c) 10.0 ± 0.7, (e) 9.8 ± 0.8 and (g) 10.0 ± 0.7 mA was obtained respectively. The average voltage as function of beam on time, (b) 0.6, (d) 1.5, (f) 9 and (h) 9 min/hr respectively. The Frequency and the pulse width used (a) 1 Hz and 10 ms, (c) 1 Hz and 25 ms, (e) 1Hz and 150 ms and (f) 0.150 Hz and 1 sec.

Figure 3.29 shows lifetime measurements performed on the same electron source with two 8 x 2 mm elliptical cathodes. During the measurement the gate voltage was automatically adjusted to maintain a constant emission current. For the first 3 measurements shown in Figure 3.29a, the current waveform was programmed to be a square waveform with 1 second pulse width. The respective duty cycles are 20 % at 5mA, 12.5 % at 8mA, and 15 % at 10mA with an average peak current of 5.0 ± 0.2, 8.0 ± 0.5 and 10.0 ± 0.7 mA respectively. In Figure 3.29b the current was kept at 15mA with an average peak current of 15 ± 1 mA using 10 ms pulse width and 1 % duty cycle. As shown, the cathode was found to be stable during the measurement period. The gate voltage remained essentially stable. These 4 different measurement conditions yielded a 5.0, 8.0, 10.0 and 0.15 mAs which are important to control the total tube current during the operation of the system. This results show the good stability of CNT cathode at different cathode current levels.
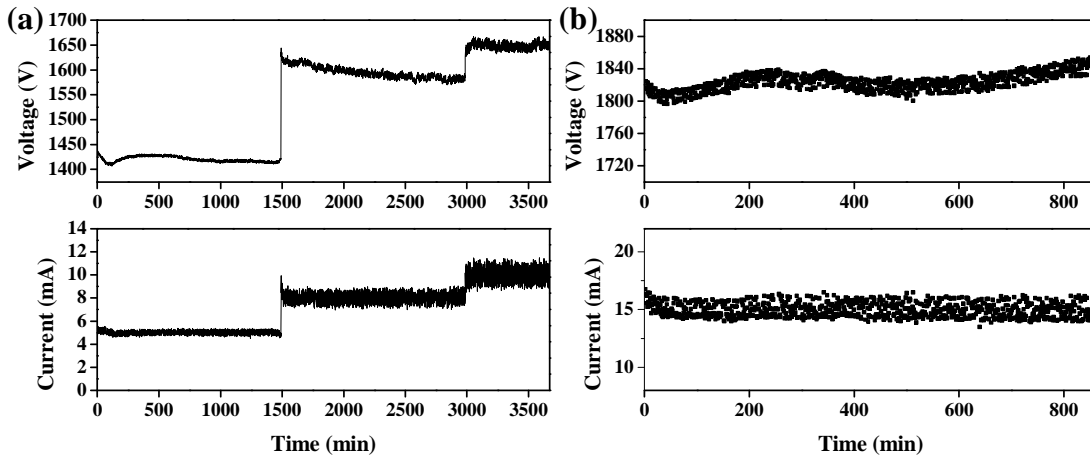
Figure 3.29: Electron field emission current from an 8 x 2 mm elliptical CNT cathode measured in the triode mode. The applied gate voltage was varied to hold the emission current constant. The measurement conditions are: (a) 1s pulse width, 0.2Hz, 0.125Hz and 0.15Hz at 5mA, 8mA, and 10mA, respectively. (b) 10ms pulse width, 1Hz.

For the 8 x 2 mm elliptical cathode a stable emission of 18mA was readily obtained at 1800V applied gate voltage. For an imaging protocol using 100 mAs per tomosynthesis scan with 25 X-ray beams, the exposure value from each X-ray beam is 4 mAs, which translates to 5.7 mAs per cathode using the measured transmission rate of 70 % (70% of the cathode current reached the anode). Assuming the tube is operating at the cathode current of 10 mA (the actual test was performed in multiple steps with the currents ranging from 5mA to 15mA), the required exposure time is 0.57 seconds per cathode. The 570 minutes electron beam-on time measured from one cathode in the stability test translates to an X-ray source array lifetime of at least 60,000 scans. For a busy mammography clinic with ~ 60 patients per day, the results means that MBFEX source can be operated for at least 1000 working days at this output level. During measurement the gate voltage essentially remained the same, indicating the CNT cathode can be operated for far longer time [18].

3.7 *Summary and Conclusions*

A successful, consistent, effective and reliable CNT cathode fabrication process has been developed. The fabrication process involved photolithography in combination with EPD, which makes this method cost effective. In addition, use of a glass substrate provides low-cost and scalability to the fabrication process. The advantage of the photolithography process is the control of several parameters, which allows the fabrication of a cathode with the intended geometries and the dimensions required with well designed boundaries. The optimal combination of parameters results in a CNT cathode with the required properties for X-ray generation. However, the fabrication process conditions depend strongly on the CNT cathode size. The fabrication procedure

illustrated in Figure 3.1 with some variation in the SU-8 thickness and deposition time resulted in an optimized CNT cathode with the required properties to increase the spatial resolution of the CNT field emission X-ray source. EPD has been demonstrated to be an effective method to fabricate CNT cathodes with different sizes.

The results revealed a linear relationship between current density and CNT cathode size with a significant increment in a current density as the cathode area decreased. The consistency on the field emission properties for the CNT cathodes fabricated using EPD depend predominately on the CNT density on the cathode's surface. In addition, the field emission properties are independent of the CNT cathode film thickness and this can be observed in the consistency in the electric field that was required to reach different levels of current. These cathodes fabricated by EPD showed the required field emission current density and consistency for X-ray generation. Also, these CNT cathodes compared to CNT cathodes reported previously using this fabrication method or other fabrication methods show significant improved field emission properties with small cathode to cathode variation. The CNT cathodes can reach stable and high emission current densities with long term stability.

Moreover, the variation from cathode to cathode and between the individual pixels within the cathode array is, in general, small. The long term stability of the CNT cathodes is not clear, the results revealed as the pulse width increases the driving voltage overtime is more constant.

References

1. W.R. Hendee and E.R. Ritenour, Medical Imaging Physics. 4 th ed. 2002, Ney York: Wiley-Liss.

2. Zhu, W., *Vacuum micro-electronics*. 2001: Wiley.

3. A. M. Fennimore, et al., *Enhancing lifetime of carbon nanotube field emitters through hydrocarbon exposure.* Applied Physics Letters, 2008. **92**.

4. W.I. Milne, et al., *Aligned carbon nanotubes/fibers for applications in vacuum microwave amplifiers.* J. Vac. Sci. Technol.B, 2006. **24**: p. 345.

5. Zhu, W., et al., *Very high current density from carbon nanotube field emitters.* Appl. Phys. Lett., 1999. **75**(6): p. 873-875.

6. D. Shiffler, et al., *A High Current, Large Area, Carbon Nanotube Cathode.* IEEE Trans Plasma Science, 2004. **32**(5): p. 2152.

7. Wei, Y., et al., *Stability of carbon nanotubes under electric field studied by scanning electron microscopy.* Appl. Phys. Lett., 2001. **79**(27): p. 4527-4529.

8. J. Zhang, et al., *Efficient fabrication of carbon nanotube point electron sources by dielectrophoresis.* Adv. Mat., 2004. **16**(14): p. 1219-1222.

9. Wang, Z.L., et al., *In-situ imaging of field emission from individual carbon nanotubes and their structural damage.* Appl. Phys. Lett., 2002. **80**(5): p. 856-858.

10. B. Gao, G.Z. Yue, Q. Qiu, Y. Cheng, H. Shimoda, L. Fleming, and O. Zhou, "Fabrication and electron field emission properties of carbon nanotube films by electrophoretic deposition," Adv. Mater. **13** (23), 1770-1774 (2001).

11. S.J. Oh, J. Zhang, Y. Cheng, H. Shimoda, and O. Zhou, "Liquid-phase fabrication of patterned carbon nanotube field emission cathodes," Appl. Phys. Lett. **87** (19), 3738 (2004).

12. C. Qian, et al., *Fabrication of small diameter few-walled carbon nanotubes with enhanced field emission property.* Journal of Nanoscience and Nanotechnology, 2006. **6**: p. 1346.

13. Soojin Oh and O. Zhou, *U.S. 7,455,757, Deposition method for nanostructured materials.* 2008.

14. Y.Cheng, O. Zhou, *Electron field emission from carbon nanotubes.* C.R. Physique 4, 2003. p. 1021-1033.

15. W.I. Milne, et al., *Carbon nanotubes as field emission sources*. Journal of Materials Chemistry, 2004, **14**: p. 933-943.

16. Zejian Liu, et al., *Carbon nanotube based microfocus field emission x-ray source for microcomputed tomography.* Appl. Phys. Lett., 2006. **89**: p. 103111.

17. Guang Yang, et al., "*Stationary digital breast tomosynthesis system with a multibeam field emission x-ray source array*", Physics of Medical Imaging, Proceedings of the SPIE, 2008. **6913**: p. 69131A-10.

18. Xin Qian, et al. "*Design and Characterization of a Spatially Distributed Multi-Beam Field Emission X-ray Source for Stationary Digital Breast Tomosynthesis*", Medical Physics 36 (10), October 2009.

19. Guang Yang, et al., "*Carbon nanotube based stationary X-ray tomosynthesis scanner for detection of breast cancer*", Chapel Hill, NC, University of North Carolina at Chapel Hill, 2008.

20. Rajaram R., "*A stationary digital breast tomosynthesis system: design simulation, characterization and image reconstruction*". (2009) Dissertation Thesis.

4 CNT Micro-Focus Field Emission X-Ray Source: Characterization and Evaluation

Micro computed tomography (micro-CT) is an important non-destructive tool to visualize the internal structure of an object [1]. This powerful imaging tool provides spatial resolution in the micron domain range and is used in medical imaging [2-5]. Our research group's main focus is the preclinical cancer studies of small animal models. Computed tomography technique enables the reconstruction of three dimensional objects from hundreds of two dimensional projection images [3]. A typical micro-CT scanner consists in a micro focus X-ray source, a sample stage and, an X-ray detector. The most important component of a micro-CT scanner is the micro focus X-ray source. The spatial resolution of the micro-CT scanner depends largely on the focal spot size of the X-ray source [6]. Reduction of the focal spot size is essential to achieve high resolution for an X-ray micro-CT scanner.

Commercial micro focus X-ray sources use thermionic cathodes to generate X-rays. This technology has several limitations such as low temporal resolution associated with the slow response time. In addition, the tube can not be easy miniaturized due to the high temperature of the cathode. Also, the high operating temperature reduces the lifetime of the X-ray source not making this technology cost effectively. Beside these

deficiencies, limited programmability and single pixel availability limits this technology. All these limitations affect the size, speed, flux, and overall performance of the commercial available micro-CT systems.

CNT based micro focus field emission X-ray sources are able to improve upon the deficiencies of the thermionic technology. CNT technology with an instantaneous response time, programmable wave form and high temporal and spatial resolution overcome all disadvantages of the thermionic sources. Furthermore, this technology offers reduction in the overall size of the X-ray source and multi-pixel availability. The performance of the CNT electron source under high emission current density and high anode voltage is one of the big challenges in developing this technology. These two factors affect the flux and the lifetime of the fist generation of the CNT micro focus X-ray source. In this chapter the studies of the CNT cathode performance under high voltage and long term stability will be presented. Also the studies of different parameters that affected the resolution (focal spot size) of a micro focus X-ray tube will be explained.

4.1 CNT Based Micro Focus X-Ray Electron Source

The first generation of CNT micro focus X-ray sources in "Zhougroup" [2-3, 7] consisted in a triode field emission X-ray tube with no focusing structure. It consists of a CNT cathode, a gate electrode with a gate mesh, and a stationary anode. Then this triode field emission X-ray tube was modified with the introduction of an electrostatic focusing unit, which includes a single focusing electrode. It consisted of a CNT cathode, a focusing electrode, a gate electrode with a gate mesh, and a Mo target. Figure 4.1 shows

the schematic of this first generation of CNT micro focus X-ray source. The first generation of CNT based micro focus X-ray electron source demonstrated the capability of generated pulsed X-ray radiation with temporal resolution in a nanosecond range [2]. Furthermore, the first generation demonstrated utility for small animal imaging [3]. In addition, the limitation of the design came out. Limitations of the first generation of the micro focus X-ray source include spherical aberration and inability to decrease the focal spot to small enough size. Also, another practical limitation of the first generation of micro focus X-ray sources is the distance between the metal electrodes being too small that introduces arcing and small apertures in thick focusing electrodes limits the flux of the source.
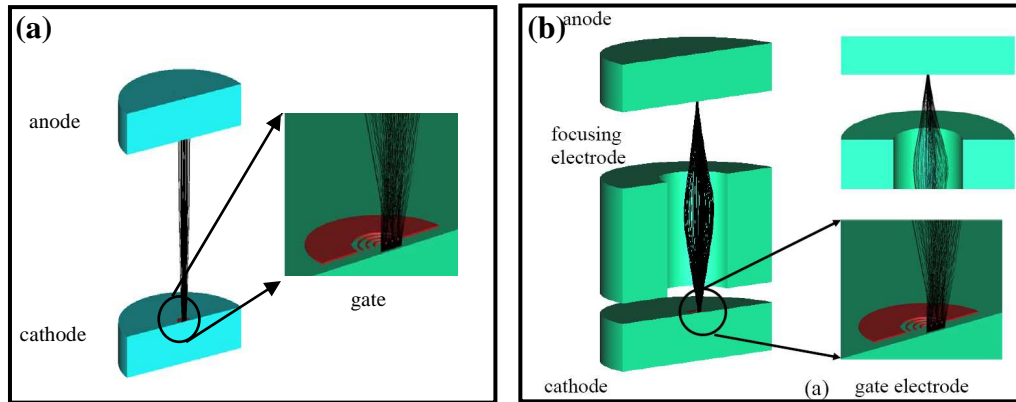
Figure 4.1: Schematic of the micro focus X-ray tube (a) no focusing structure and (b) single focusing electrode [2-3, 7].

The second generation of CNT micro focus X-ray source comprised of a modified asymmetrical Einzel type electrostatic focusing lens with three independently controlled electrodes [6]. Einzel type lenses are commonly used for three-electrode lenses, where the first and third electrodes are held at the same potential. The advantage of asymmetric designs with conical central electrodes is in reducing the spherical aberration [8] present

in the first generation. Gate and top focusing electrodes consist of planar metal and the middle focusing electrode is in the shape of a truncated cone. The stationary anode has a tilt angle of 12°. The micro focus X-ray source uses an elliptical CNT cathode. An isotropic focal spot can be achieved by using an elliptical CNT cathode, where the anode take-off angle (θ) matches the ratio of the major length (D) over the minor length (d) of the elliptical electron probe on the anode surface for generating an X-ray focal spot with a diameter (d) as illustrated on Figure 4.2.
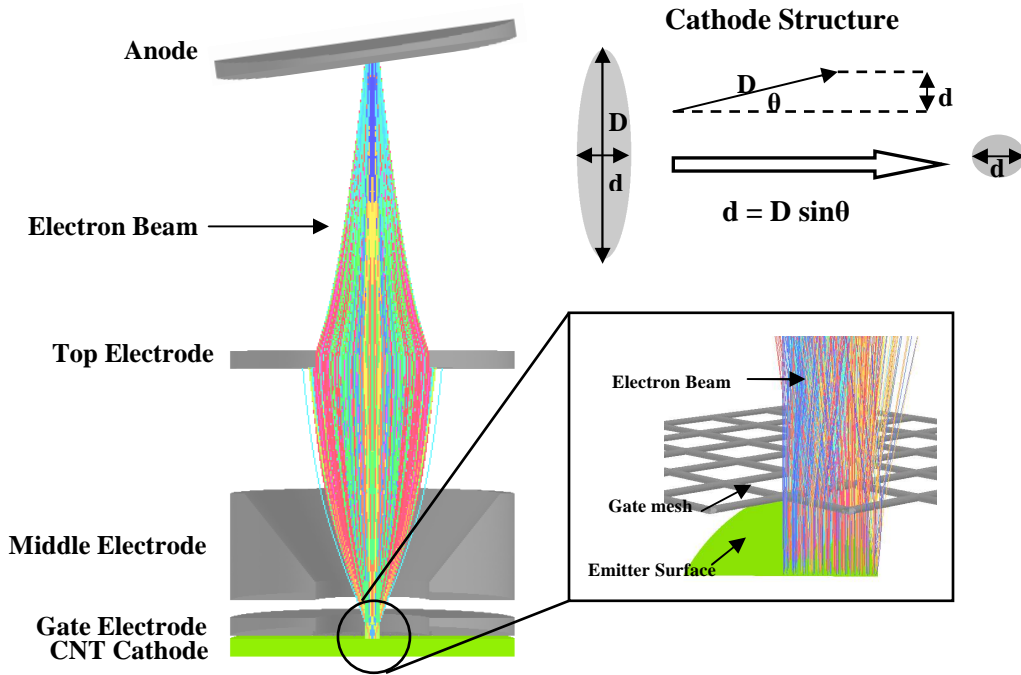
Figure 4.2: Schematic of a CNT based micro focus X-ray source which consists of CNT cathode, gate electrode, focusing electrode and a stationary anode and formation of an isotropic effective focal spot on the projected plane with the take-off angle of θ. (Images courtesy of Shabana Sultana; Vector Field Opera-3D Software).

The micro focus X-ray tube used in this study comprised of a CNT cathode, a gate electrode with a 1D or 2D mesh, two Einzel-type focusing electrodes and a stationary anode, as illustrated in Figure 4.2. The details for the modified Einzel electrostatic

136

focusing electrodes description and dimensions are illustrated in Figure 4.3. The cathode and anode assembly are placed inside a stainless steel vacuum chamber with a Be or Al window, mini ion pump, valve, a high voltage feedthrough for the anode, and a multi-pin feedthrough for the focusing and gate electrodes under high vacuum. A constant high voltage is applied to the anode. The electrons are extracted from the CNT cathode by applying a variable electric field to the gate electrode, usually in the order of 0-10 V/μm. Therefore the X-ray flux is maintained by automatically adjusting the extraction electric field. Two power supplies are used for the two focusing electrodes. In this particular design, up to three CNT cathodes can be installed either with same resolution or three different resolutions. Electron emission and the emission current from these cathodes can be independently programmed by varying the gate electric field. The detailed study and characterization of the field emission properties, emission stability, and focal spot size as a function of CNT cathode size and parameters that affect the focal spot size will be discussed using a CNT micro focus X-ray source.
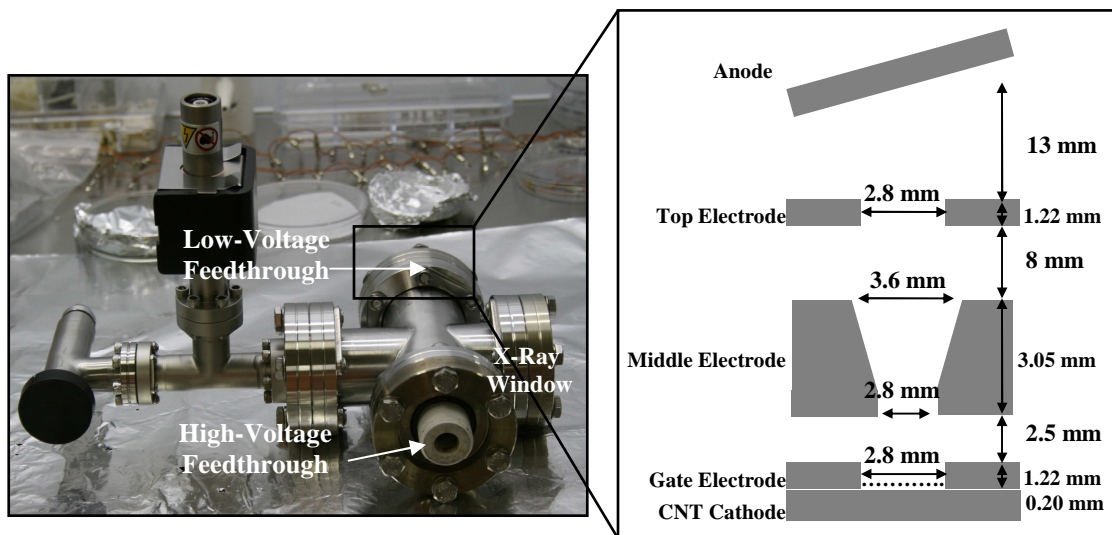
Figure 4.3: A compact CNT based micro focus X-ray source and cross sectional view of the focusing unit (designed by Shabana Sultana).

4.2 Field Emission Performance of the CNT Micro Focus X-Ray Source

To evaluate the field emission properties of the CNT cathodes fabricated by EPD, the micro focus X-ray tube was assembled with different CNT cathode sizes. The micro focus X-ray tube was baked at high temperature to remove moisture or any adsorbed gas molecules. The initial operation procedure includes the performance of an initial conditioning process. This initial conditioning process consists of high voltage conditioning where the anode voltage was slowly brought up to 55 KV. The field emission measurement was performed in triode mode geometry. The anode voltage was set at 10 KV, 2000 V for top focusing voltage and 300 V for middle focusing. A *labview* program was used to control the applied gate voltage. The voltage applied to the gate electrode with one dimensional mesh has a square waveform with 10 ms pulse width and 1 Hz repetition rate. Figure 4.4 shows plots of the experimentally measured emission current densities versus the applied electrical fields for six different cathode sizes. The results indicated high current densities for micro-CT imaging of small animal models. For a CNT cathode with an area of 0.92 mm^2, the current density at 8.7 V/µm is 385 mA/cm^2. On the other hand, at the same electric field the current density for a CNT cathode with area of 0.06 mm^2 is 2080 mA/cm^2. The field emission results showed excellent current densities levels required to generate enough X-ray flux for medical imaging. In addition, the large variation of the electric field at the gate mesh can be appreciated in the field emission of these different CNT cathode sizes. For example, in a diode mode geometry a metal plate is used as the anode where the electric field is uniform. Instead in triode mode geometry the alignment of the CNT cathode with the gate mesh is different for every cathode which results in the larger variation of the field

emission properties. Optical images of the CNT cathodes with the intended geometries and dimensions required with well defined boundaries are illustrated in Figure 4.4.
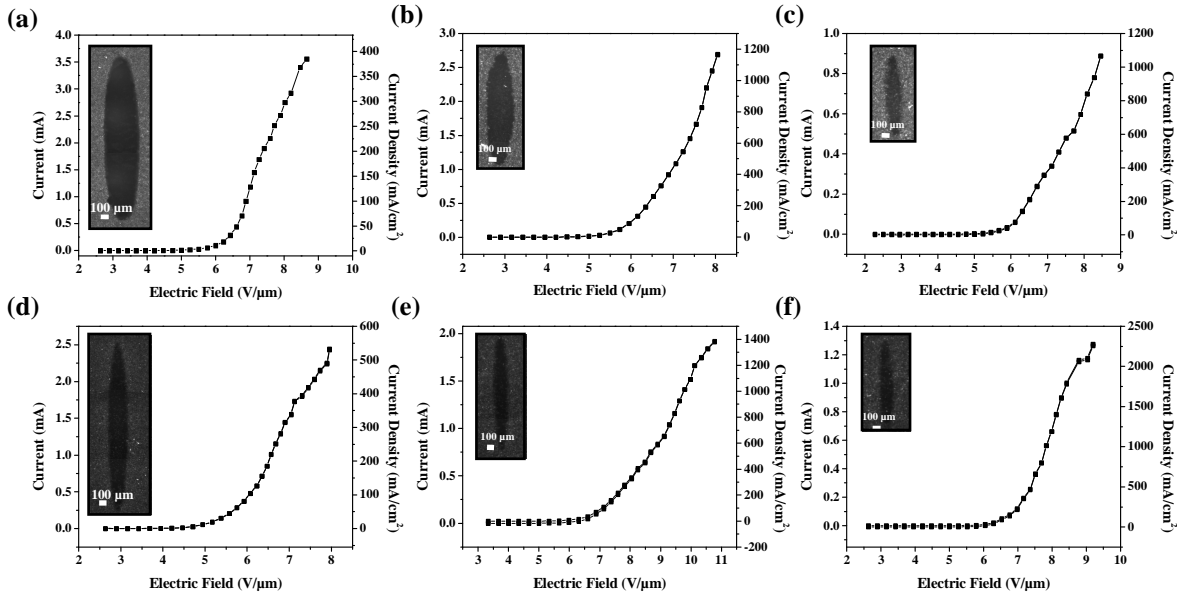
Figure 4.4: Field emission current as function of applied electrical field from 6 cathodes with different dimensions measured into the micro focus X-ray tube. The CNT cathode dimensions measured are (a) 2.35 x 0.50 mm, (b) 1.18 x 0.25 mm, (c) 0.706 x 0.150 mm, (d) 2.35 x 0.25 mm, (e) 1.18 x 0.15 mm, and (f) 0.706 x 0.100 mm. The measurement conditions used were 10 KV at anode, 2000 V at top focusing electrode and 300 V at middle focusing electrode. The voltage applied to the gate electrode with one dimensional mesh has a square waveform with 10 ms pulse width and 1 Hz repetition rate. Optical images of the CNT cathodes with the intended geometries are shown.

4.3 Long Term Stability of CNT Micro Focus Field Emission X-Ray Source at High Current Densities

The cathodes were further evaluated under high anode voltage using a micro focus X-ray tube. The stability measurements were performed after an initial conditioning process where the anode was conditioned for several hours with the desire CNT cathode current. The CNT cathode and field emission X-rays were operated stably at the anode voltage of 40 KV for a period of 3 days at a constant cathode current. The long-term emission stability was evaluated by measuring the variation of the applied gate voltage needed to maintain a constant cathode current. A stable cathode current of 3 mA (325

mA/cm^2) was readily obtained at gate voltage (V_g) of ~ 1650 V from a 2.35 x 0.50 mm elliptical CNT cathode. About 67 % of the cathode current reached X-ray anode. The rest leaked through the gate and focusing electrodes. The cathode current reached 3 mA, which is close to the maximum current allowed under the present stationary anode conditions. As shown in Figure 4.5a, after 72 hours Vg essentially stayed the same, indicating no measurable cathode degradation. The long-term emission stability was evaluated by measuring the variation of the applied V_g needed to maintain a constant 3 mA cathode current, which is close to the maximum current allowed under the present conditions. The maximum X-ray tube current that can be achieved, therefore the maximum X-ray flux, is primarily determined by two factors: the maximum emission current from the cathode and the anode heat load. Due to limitations of the anode heat dissipation the maximum power P_{max} (in watts) of a fixed anode micro-focus X-ray tube can be estimated as $P_{max} \approx 1.4(X_{f,FWHM})^{0.88}$ [9], where $X_{f,FWHM}$ is the focal spot size in microns. For the 2.35 x 0.50 mm elliptical cathode with an effective focal spot size of ~100x100μm P_{max} is ~80W or ~3mA cathode current (with ~ 67 % transmission rate) at 40 KV anode voltage.

A second 2.35 x 0.50 mm elliptical CNT cathode was evaluated at a stable cathode current of 2.0 mA (217 mA/cm^2) obtained at the gate voltage (V_g) of ~ 1850 V during 5 days without cathode degradation. About 62 % of the cathode current reached X-ray anode and a gate transmission rate of 76 %. High performance CNT cathodes were fabricated and demonstrated high current densities and long term stability was achieved.
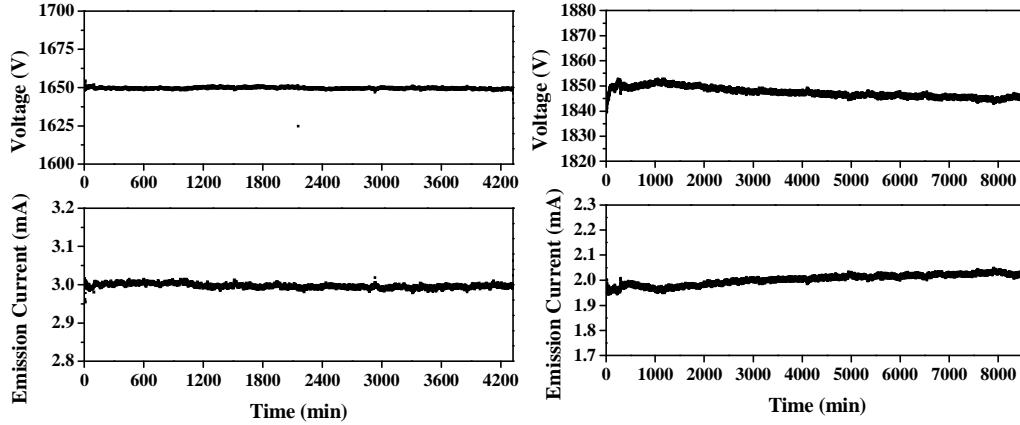
Figure 4.5: Emission lifetime measurement of two different 2.35 x 0.50 mm CNT cathode at constant current mode into the micro focus X-ray tube. The measurement conditions used were 40 KV at anode, 1400 V at top focusing electrode and 1300 V at middle focusing electrode. (a) The peak emission current in the pulsed mode was fixed at 3 mA and an averaged peak current of 3.00 ± 0.01 mA was obtained. The average voltage to keep the constant current of 1649.7 ± 0.7 V was applied and corresponds to an average electric field of 8.683 ± 0.004 V/μm. The gate transmission rate (percentage of the current passed through the gate electrode) was 74 %. The waveform of the gate voltage was 10 ms pulse width and 1 Hz. (b) The peak emission current in the pulsed mode was fixed at 3 mA and an averaged peak current of 2.00 ± 0.02 mA was obtained. The average voltage to keep the constant current of 1848 ± 2 V was applied and corresponds to an average electric field of 9.72 ± 0.01 V/μm. The gate transmission rate (percentage of the current passed through the gate electrode) was 76 %. The waveform of the gate voltage was 20 ms pulse width and 1 Hz. The distance between gate and CNT cathode was 190 μm. An external resistance of 100 KΩ was used.

The most important performance characteristics of an X-ray source are flux, resolution, and stability. The flux and stability of the micro focus field emission X-ray tube has been achieved with excellent performance and the maximum current and power allowed for a fixed anode. These results proves that at least for this micro focus X-ray tube, the flux from the CNT cathode can be at least as high as that afforded by a conventional thermionic X-ray tube operating at the same focal spot size.

4.4 *Variable Focal Spot Size of CNT Micro Focus Field Emission X-Ray Source*

The resolution of the micro-CT scanner is an important parameter to achieve, the study of the focal spot size as function of different parameters were used to fully characterize the micro focus field emission X-ray tube. Because the system resolution

depends strongly on the CNT cathode size, Table 4.1 summarizes the CNT cathode size used to experimentally measure the focal spot size (or the focal area). The cathode consists of an elliptically patterned CNT composite film which when is projected at a small anode target angle, generates isotropic focal spot. The focal spot size was measured following the European Standard (EN 12543-5) [10]. This measurement determines the spatial resolution. In this method the focal spot size is measured indirectly by measuring the geometric unsharpness. The experimental set-up is illustrated in Figure 4.6a, where the crosswire phantom is placed as close as possible to the X-ray source and the detector is placed to meet the standard magnification specification. The crosswire phantom consists of tungsten wires with diameters of 1.0 mm. The wires cross each other at an angle of 90˚. The exposure window of the detector and X-ray on time of the X-ray source are synchronized to acquire the projection image. The X-ray image sensor used was a flat panel sensor with 50 x 50 μm^2 pixel size (Hamamatsu C7921CA-02). The resolution in two orthogonal directions is obtained based on the line profiles of the transmitted X-ray intensity of tungsten cross-wire phantom. Figure 4.6b show the projection image of the cross wire phantom and the region of interest used to obtain the line profile in the vertical 4.6c and horizontal 4.6d direction.

Cathode Size (mm)		Cathode Area (mm^2)
Long Axis	Short Axis	
2.35	0.50	0.923
2.35	0.25	0.461
1.18	0.25	0.231
1.18	0.15	0.139
0.706	0.15	0.083
0.706	0.10	0.055

Table 4.1: Summary of the cathode size and area for CNT cathode experimentally used for the focal spot size measurement. The elliptical geometry of the cathode is based on the final focal spot. The initial elliptical geometry and the anode inclination in the system result in an isotropic focal spot.
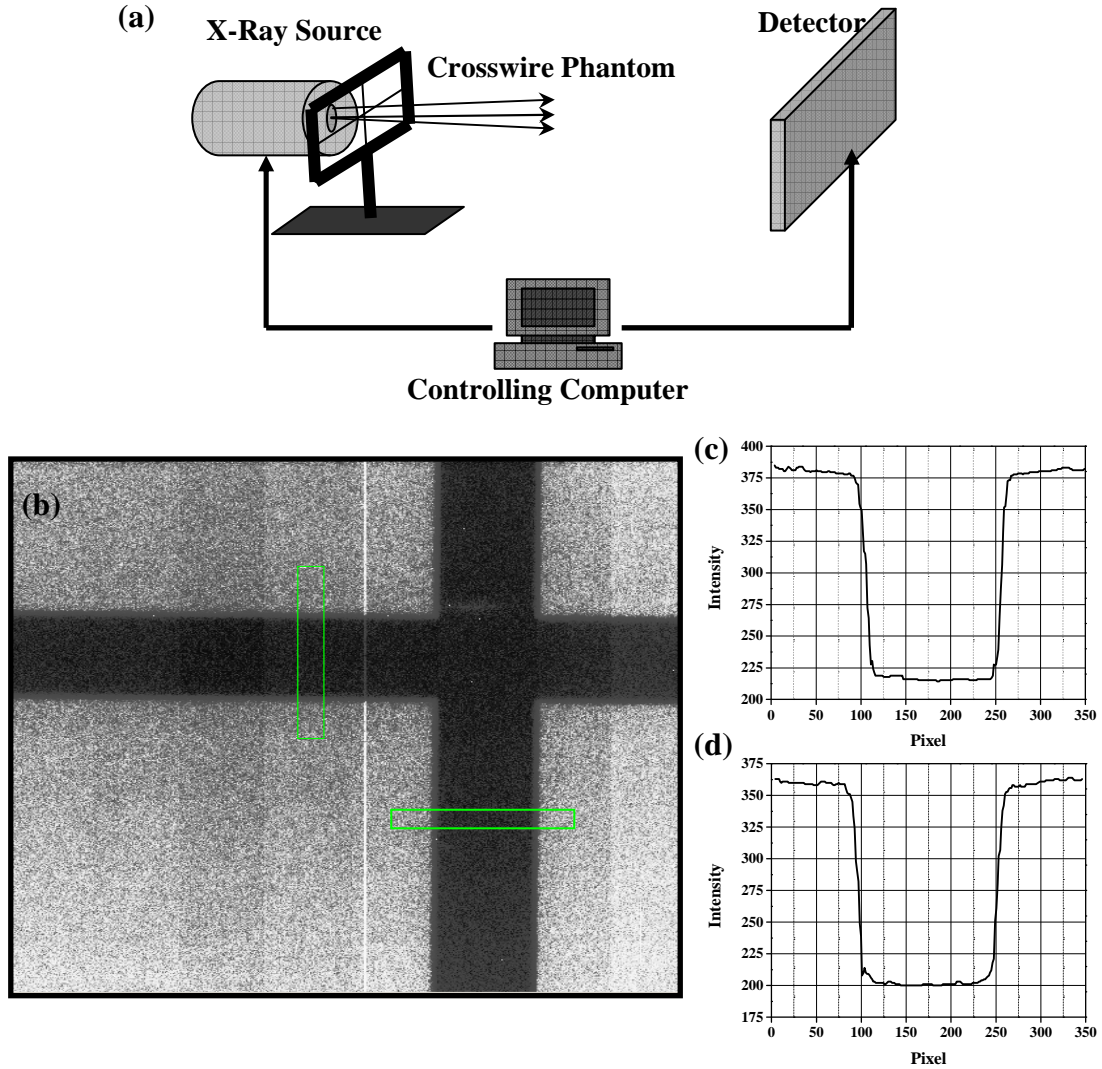
Figure 4.6: (a) Schematic of the experimental set-up for the focal spot size measurement. (b) Projection image of the cross wire phantom and the region of interest used to obtain the line profile in the vertical (c) and horizontal (d) direction using a 1.18 x 0.25 mm CNT cathode.

4.4.1 *Effect of Gate Mesh and Gate and Focusing Electrodes Potentials on the Focal Spot Size*

The function of the metal gate mesh on the gate electrode is to extract the electrons from the CNT cathode when an electric field is applied to the gate electrode. The difference in the extraction field between diode and triode geometry is higher extraction field to reach the same current level in triode geometry. This is due to the non-uniformity of the electric field at the gate mesh. In addition, the gate mesh can affect the

focal spot size and the transmission rate at the gate electrode and consequently the current that reaches the anode. In order to study the effect of the gate mesh on the focal spot size and the gate transmission rate, two different 2D gate mesh and one 1D meshes were used. The 2D meshes used in this study include (1) 100 mesh woven tungsten gauze with 89 % open area and (2) 400 mesh circular molybdenum grid with 55 % open area. The 1D mesh or 75 etched mesh consist in 25 µm horizontal bars with 75 µm spaced made of tungsten with an opening area of 75 %. Figure 4.7 show the optical images for the gate meshes studied.
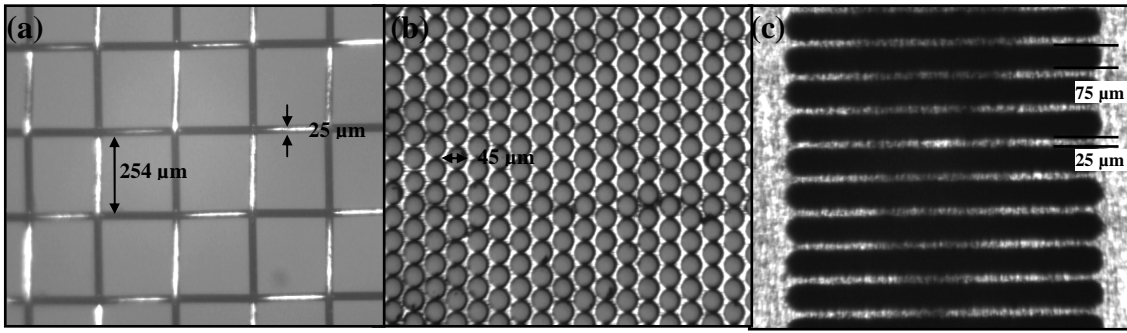
Figure 4.7: Gate Meshes: (a) 100 mesh woven tungsten gauze, (b) 400 mesh circular molybdenum grid, and (c) tungsten 75 etched mesh.

The CNT micro focus X-ray source was assembled with a 2.35 x 0.50 mm CNT cathode, different gate meshes were used under the same experimental conditions. The focal spot size measurements were performed using a frequency of 0.2 Hz and a pulse width of 2.5 second (50 % duty cycle) and same CNT cathode current. The focusing electrodes potential was adjusted to obtain the effective focal spot size at an anode voltage of 40 KV.

144

Mesh	Effective Focal Spot Size (μm)	Effective Focal Area (μm^2)	Transmission Rate at Gate (%)
100 mesh	68 x 131	6996	78
400 mesh	65 x 130	6637	40
75 etched mesh	87 x 97	6628	67

Table 4.2: Summary of the effective focal spot size, effective focal area, and transmission rate at gate electrode for different gate meshes.

Table 4.2 summarize the results for the effective focal spot size, effective focal area, and transmission rate at gate electrode for three different gate meshes. The results reveal more isotropic focal spot size when a 75 etched mesh is used. This is attributed to the divergence of the electron beam. When 1D mesh is used the electron beam diverges in one direction making easer to focus the beam back in comparison with 2D meshes. In the case of the 2D mesh, the divergence of the electron beam is in all directions and is reflected in the size of the focal spot. The transmission rate is an important factor in the overall current that reaches the anode. The transmission rate at the gate electrode changes accordantly with the opening area of the mesh. As the results reveal the transmission rate at gate electrode is higher when 100 mesh is used. In addition, the results demonstrate that the 1D mesh (75 etched mesh) is more effective in terms of effective focal spot size and transmission rate at gate. It is possible to conclude that 75 etched mesh and 400 mesh gives smaller focal spot size compared to the 100 mesh. Also, the focal spot sizes for 75 etched mesh and 400 mesh are comparable, however 75 etched mesh show better transmission rate at the gate and consequently the overall transmission rate.

An important factor in the performance of the CNT micro focus X-ray source is the stability of the CNT cathode under high current densities and high anode voltage which has been demonstrated. During normal operation of the micro focus X-ray source causes

that the gate potential has to be adjusted so as to maintain a constant CNT cathode operational current level due to CNT cathode degradation. One important factor to study is the effect of the gate potential on the focal spot size. The ideal situation is to be able to adjust the gate potential without affecting the effective focal spot size. The focal spot size measurement was performed at an anode voltage of 40 KV, top focusing electrode voltage of 1300 V, middle focusing electrode of 1400 V, and at same CNT cathode current. Table 4.3 summarizes the focal spot size and focal area as a function of the gate potential. The results show that similar focal spot size is maintained even when gate potential is increased over time to maintain the same CNT cathode current.

Gate Potential (V)	Focal Spot Size (µm)	Focal Area (µm^2)
1100	78 x 124	7596
1190	80 x 113	7100
1630	63 x 123	6086

Table 4.3: Summary of the focal spot size and focal area as function of the gate potential. The experimental conditions used an anode voltage of 40 KV, top focusing electrode was set at 1300 V and middle focusing electrode was set at 1400 V.

The effect of the CNT cathode current on the focal spot size has been investigated. A 2.35 x 0.50 mm CNT cathode was used to determine the focal spot size at two different CNT cathode current levels, 0.30 and 1.00 mA. The experimental conditions were the same for these two currents. A duty cycle of 50 % (0.2 f/s and 2.5 sec pulse width), anode voltage of 40 KV and the gate voltage for a 0.30 and 1.00 mA is 1160 and 1400 V, respectively. The experimental results show similar focal spot size with very small variation as is illustrated in Table 4.4 and Table 4.5. These results are very important because the CNT micro focus tube can be operated at different current levels without affecting the focal spot size.

Middle/Top Electrode (V)	1400	1500	1600	1700	1800	1900
1400	80 x 163	100 x 117	107 x 137	107 x 130	100 x 162	113 x 188
1500	80 x 155	87 x 97	107 x 130	114 x 136	107 x 162	107 x 194
1600	93 x 163	87 x 111	87 x 111	100 x 144	113 x 176	107 x 214
1700	87 x 163	86 x 117	87 x 110	87 x 130	107 x 183	107 x 208
1800	93 x 169	94 x 124	93 x 104	87 x 130	100 x 162	114 x 220
1900	93 x 160	86 x 124	90 x 110	87 x 123	93 x170	114 x 214
2000	93 x 170	86 x 124	94 x 111	87 x 137	93 x 162	107 x 216

Table 4.4: Summary of the typical variation of the focal spot size as function of the applied potential for the middle and top focusing electrodes for a 2.35 x 0.50 mm CNT cathode at a current of 0.30 mA. The unit for the vertical and horizontal direction is micrometer.

Middle/Top Electrode (V)	1400	1500	1600	1700	1800	1900
1400	94 x 183	100 x 136	120 x 130	120 x 130	114 x 150	114 x 181
1500	94 x 196	94 x 124	107 x 124	120 x 144	120 x 155	114 x 196
1600	93 x 195	94 x 123	87 x 111	114 x 123	106 x 170	127 x 201
1700	100 x 201	93 x 137	94 x 104	87 x 124	100 x 176	120 x 208
1800	107 x 201	87 x 137	87 x 117	87 x 124	93 x 156	114 x 215
1900	100 x 215	87 x 144	86 x 117	86 x 124	87 x 163	120 x 207
2000	107 x 203	94 x 136	86 x 110	87 x 130	94 x 156	100 x 202

Table 4.5: Summary of the typical variation of the focal spot size as function of the applied potential for the middle and top focusing electrodes for a 2.35 x 0.50 mm CNT cathode at a current of 1.00 mA. The unit for the vertical and horizontal direction is micrometer.

The effects of the two focusing electrodes potential on the focal spot size is illustrated in Figure 4.8. The main function of the middle focusing electrode is harnessing the divergence of electrons coming out of the gating mesh and thereby prefocusing the electrons into a more parallel shape before they reach the top focusing electrode [6]. In addition, the middle focusing electrode expands or shrinks the electron beam. On the other hand, the primary function of the top focusing electrode is moves the axial focal position closer or farther to the anode. In order to study the effect of the focusing electrodes potential, the micro focus X-ray source was assembled with a 2.35 x 0.50 mm CNT cathode.
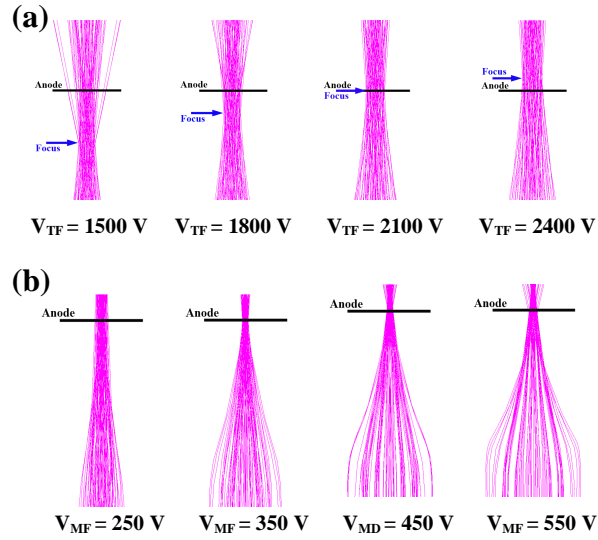
Figure 4.8: (a) Axial focal position moves resulting if the focal spot size change. (b) Axial focal position fixed, electron envelop expands/shrinks [6].

The potential of the two focusing electrodes were adjusted to study the variation of the focal spot size. Typical variations of the focal spot size as a function of the applied potential on the middle and top focusing electrodes for a 2.35 x 0.50 mm CNT cathode are illustrated in Table 4.6. However, several combinations of voltages result in an optimal region where the focal spot size can be maintained around the target focal spot of 100 µm x 100 µm (7854 µm^2).

Middle/Top Electrode (V)	1400	1500	1600	1700	1800	1900
1400	80 x 163	100 x 117	107 x 137	107 x 130	100 x 162	113 x 188
1500	80 x 155	87 x 97	107 x 130	114 x 136	107 x 162	107 x 194
1600	93 x 163	87 x 111	87 x 111	100 x 144	113 x 176	107 x 214
1700	87 x 163	86 x 117	87 x 110	87 x130	107 x 183	107 x 208
1800	93 x 169	94 x 124	93 x 104	87 x 130	100 x 162	114 x 220
1900	93 x 160	86 x 124	90 x 110	87 x 123	93 x 170	114 x 214
2000	93 x 170	86 x 124	94 x 111	87 x137	93 x 162	107 x 216
2100	100 x 169	94 x 124	100 x 110	100 x 130	100 x 177	107 x 222

Table 4.6: Summary of the typical variation of the focal spot size as function of the applied potential for the middle and top focusing electrodes for a 2.35 x 0.50 mm CNT cathode. The unit for the vertical and horizontal direction is micrometer.

(a) **(b)**
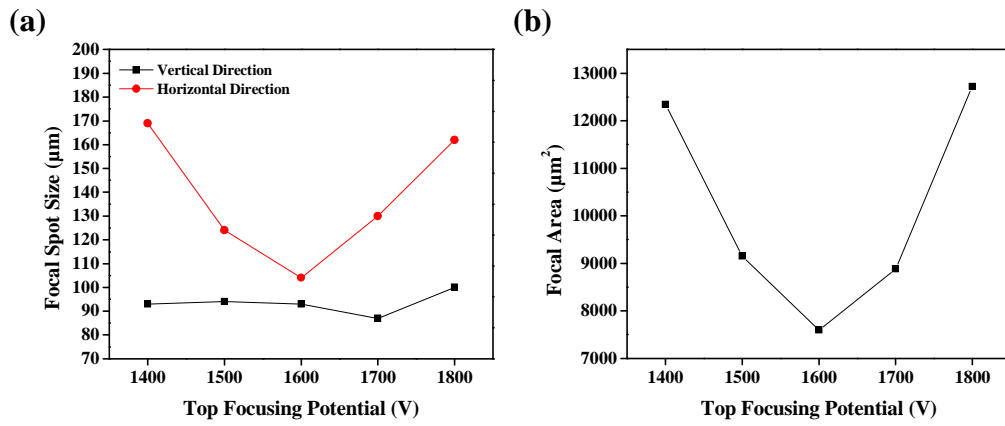
Figure 4.9: (a) Focal spot size as function of the variation of top focusing potential with a fixed middle focusing potential of 1800 V. (b) Focal area as function of the variation of the top focusing potential with a fixed middle focusing potential.

Figure 4.9a show the focal spot size as function of the variation of the top focusing potential with a fixed middle focusing potential. The behavior of the focal spot in the vertical and horizontal directions reveals that the focal spot size depends highly on the top focusing voltage. Figure 4.9b show the focal area as function of the variation of the top focusing potential with a fixed middle focusing potential. An optimal region can be appreciated when the focal area is at the minimum.
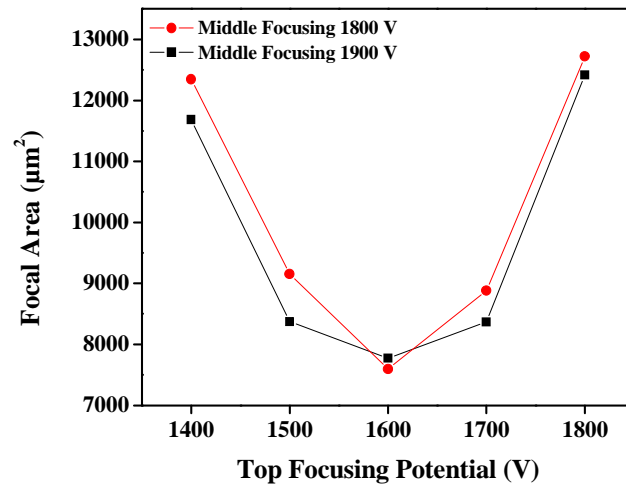

Figure 4.10: Focal spot area as function of top focusing potential at two different middle focusing electrode potential.

The focal spot size (area) is insensitive to the middle focusing voltage as shown in Figure 4.10. This is because the middle focusing voltage primary pre-focuses and/or expands or shrinks the electron beam making it more parallel. The focal spot size gets affected by different parameters such as cathode size, anode voltage and top and middle focusing potential. The focal spot size dependence on the CNT cathode size will be discussed in the next section. On the other hand, experiments and simulations showed that as the anode voltage increases, the focal spot size decreases. In addition, the focal spot size is insensitive to the gate voltage as experimental results showed. Also the middle focusing voltage is not significantly sensitive to the focal spot size. However, the focal spot size is highly dependant on the top focusing voltage. All these parameters affect the focal spot size in different ways, but in order to increase the resolution of the CNT micro focus X-ray source, different CNT cathode sizes will need to be analyzed and characterized.

4.4.2 *Focal Spot Size of CNT Micro Focus Field Emission X-Ray Source*

A micro focus field emission X-ray source with a variable focal spot size has been fully characterized using different CNT cathode sizes. The experimental effective focal area is shown in Table 4.7 for each CNT cathode size at 40 and 50 KV anode voltages. The effective focal area decreases as the CNT cathode size decreases as expected. The focusing power decreases as the CNT cathode size decreases as shown in Table 4.7. The demagnification factor can be defined as the ratio of the CNT cathode size divide by the experimental focal spot size on the anode. For example, the demagnification factor for 2.35 x 0.50 mm CNT cathode is about 6 in the vertical direction and about 5 in the

horizontal direction. For the 0.706 x 0.100 mm CNT cathode, the demagnification factor is about 4 in the vertical direction and about 1 in the horizontal direction. Figure 4.11 shows the effective focal area as function of CNT cathode area and a linear relationship can be appreciated at 40 KV anode voltage. It is important to mention that simulation results reveal a linear behavior of the focal spot size up to a certain range and then reaches a limit with a variation in the cathode diameter. For smaller size cathodes, the electrostatic electrodes become ineffective for focal spot size less than 50μm with the present design. The focusing power also depends on the anode voltage applied. A slightly smaller focal spot size can be achieved when the anode voltage increases from 40 KV to 50 KV as is shown in Table 4.7.

Cathode Area (mm^2)	Effective Focal Area (µm^2)	
	40 KV Anode Voltage	50 KV Anode Voltage
0.923	7596	6951
0.461	5150	4773
0.231	3117	3117
0.139	4536	4334
0.083	2565	2706
0.055	3205	2757

Table 4.7: Effective focal area at 40 and 50 KV anode voltages. The measurements were performed at a magnification of 8 using a tungsten cross-wire phantom and following the European Standard (EN 12543-5).
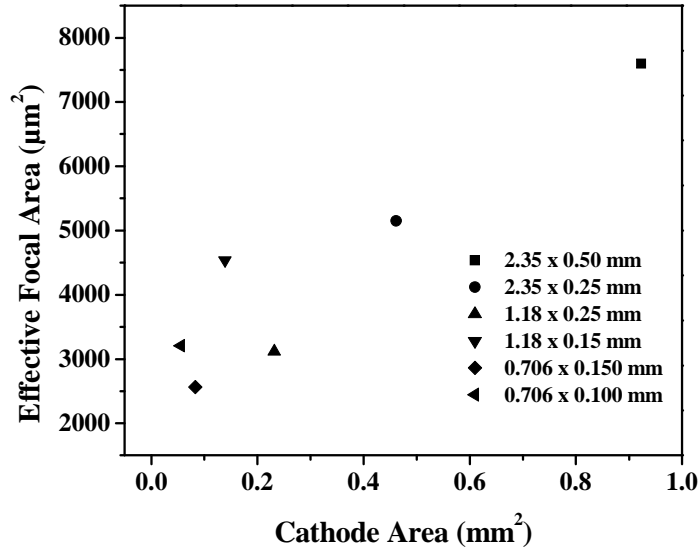
Figure 4.11: Effective focal area as function of CNT cathode area at 40 KV anode voltage.
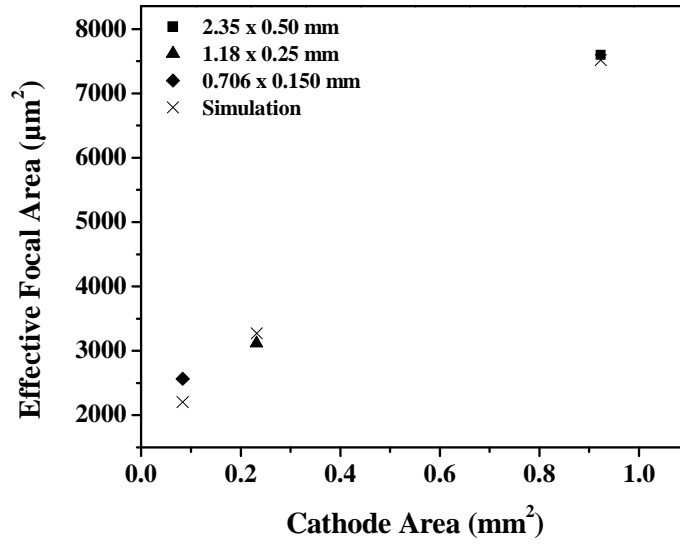

Figure 4.12: Experimental and simulated focal area as function of CNT cathode area at 40 KV anode voltage.

Using commercial Vector Field Opera-3D software, simulations that mimic the experimental conditions were carried out. The simulated and experimental results show high degree of agreement. A CNT micro focus X-ray source has been fully characterized

and evaluated. Moreover, the parameters that affect the focal spot size have been detailed studied.

4.5 *X-Ray Imaging Application*

To demonstrate the applications of the high performance of the CNT micro focus field emission X-ray source, a high resolution dynamic micro-CT scanner developed at UNC called Charybdis [4-5]. The system provides high spatial ($\leq100\mu$m) and temporal (10-20msec) resolutions, stationary and horizontal mouse bed configurations, and *prospective free-breath* gating capability. The cone-beam micro-CT scanner consists of a rotating source and detector pair and a stationary sample stage, as shown in Figure 4.13. In a typical CT scan, 400 projections are acquired over a circular orbit of 199.5° with a stepping angle of 0.5∘.
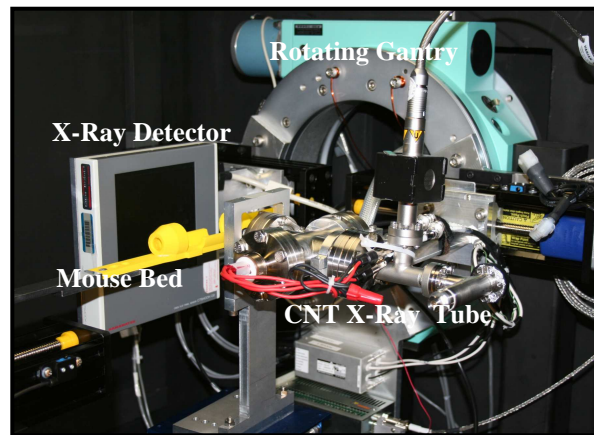
Figure 4.13: Photo of the Charybdis scanner using a compact CNT micro-focus x-ray source. It consists of a compact CNT X-ray tube, a flat-panel X-ray detector, a mouse bed, and (d) a rotating gantry.

A reconstructed cardiac gated micro-computed tomography image of an anesthetized free breathing mouse is shown in Figure 4.14. The high resolution image was collected using a 20 ms X-ray pulse and 100 µm system resolution that is made

possible by the high current density achieved from the CNT cathodes fabricated by EPD [11].
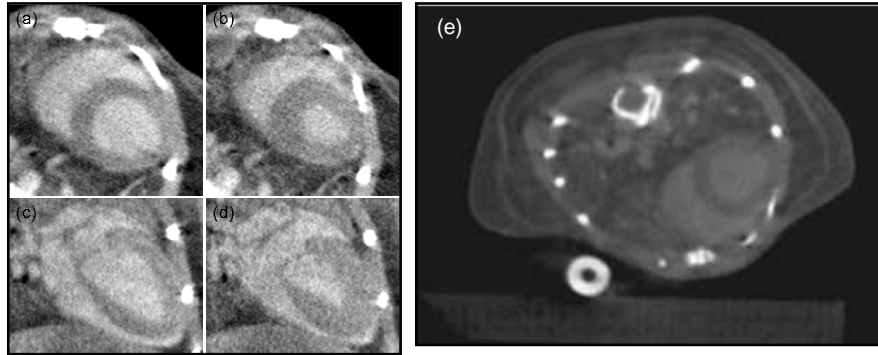
Figure 4.14: A physiologically gated micro-computed tomography image of anesthetized mouse using the CNT based micro-focused X-ray source. The image was collected using a 20 msec x-ray pulse and 100 μm system resolution. The reconstructed slice images of mouse heart show clear difference between systole (a) and (c), and diastole (b) and (d) in the axial and coronal views, respectively. (e) Reconstructed slice of cardiac gated micro-CT image [11-12].

Figure 4.15 shows the evolution of small animal *in vivo* studies in Zhou's Research Laboratories. The evolutions of small animal in vivo studies started from the grainy original micro-CT image to Mouse models of brain tumors, lung tumors with respiratory gating, and even contrast enhanced cardiac and respiratory gated imaging. This big evolution was the results of the CNT cathodes performance improvement; in 2006 a CNT cathode with 2.5 mm in diameter delivered an emission current of 0.600 mA (60 mA/cm^2) to a CNT cathode of 2.35 x 0.50 mm capable to deliver 3.00 mA (385 mA/cm^2) in 2009.
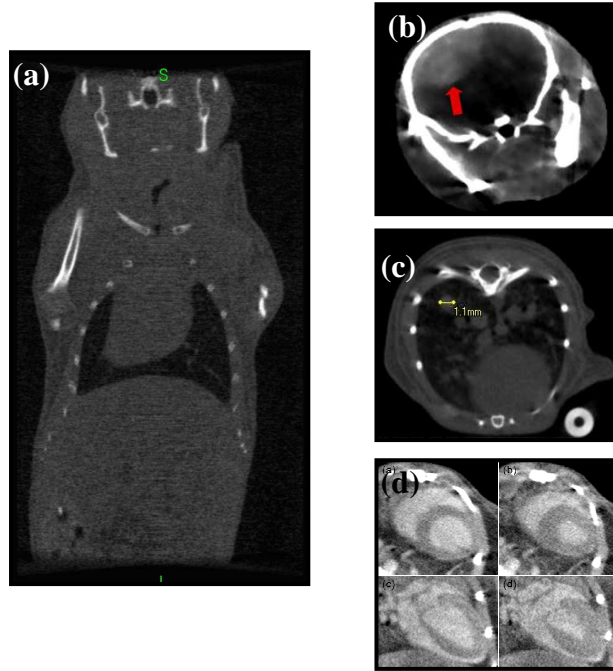
Figure 4.15: Evolution of small animal *in vivo* studies in Zhou's Research Laboratories; (a) Grainy original micro-CT image, Mouse models of brain tumors (b), lung tumors with respiratory gating (c), and even contrast enhanced cardiac and respiratory gated imaging (d).

4.6 Summary and Conclusions

In summary, a CNT micro focus field emission X-ray source with a variable focal spot size has been fully characterized. The most important performance characteristics of an X-ray source are flux, resolution, and stability. The flux and stability of the CNT micro focus field emission X-ray tube has been achieved with excellent performance. Current density of 2080 mA/cm^2 was achieved for a CNT cathode with 0.06 mm^2. Also current densities were demonstrated with enough intensity to generate X-ray flux for medical imaging.

In addition, results reveal that 1D mesh (75 etched mesh) is more effective in terms of effective focal spot size and transmission rate at gate. The results show that similar focal spot size is maintained even when gate potential is increased over time to

maintain the same CNT cathode current. Also, similar focal spot size is maintained when a different CNT cathode current is used. On the other hand, the focal spot size gets affected by different parameters such as cathode size, anode voltage and top and middle focusing potential. As the cathode size change, at first a linear behavior of the focal spot size is observed up to certain range; but then reaches a limit. Moreover, as the anode voltage increases, the focal spot size decreases. In addition, the focal spot size is insensitive to the gate voltage and middle focusing potential. However, the focal spot size is highly dependant on the top focusing voltage.

The effective focal area decreases as the CNT cathode size decreases making it possible to achieve different resolutions. The focusing power decreases as the CNT cathode size decreases when the same electrostatic optics are used. The simulated and experimental results show high degree of agreement. Also, the applications of the high performance of the CNT micro focus field emission X-ray source in medical X-ray imaging are demonstrated.

References

1. Methods in Molecular Biology, Vol. 455: Osteoporosis: Methods and Protocols. Micro-Computed Tomography: A Method for the Non-Destructive Evaluation of the Three-Dimensional Structure of Biological Specimens.

2. Y. Cheng, et al., *"Dynamic radiography using a carbon nanotube-based field emission x-ray source"*. Rev. Sci. Inst., 2004.Vol.75 No.10 p. 3246.

3. J. Zhang, et al., *"A nanotube-based field emission x-ray source for microcomputed tomography"*. Rev. Sci. Inst., 2005, **76**, 094301.

4. G. Cao et al., *"Respiratory-gated micro-CT of free-breathing mice using a carbon nanotube based micro-focus field emission x-ray source"*, SPIE Medical Imaging conference proceeding 2008, submitted.

5. G. Cao, et al., "A dynamic micro-CT scanner based on a carbon nanotube field emission x-ray source," Phys. Med. Biol., 2009 **54**, 2323-2340.

6. Z. Liu, et al., *"Carbon Nanotube Based Micro-Focus Field Emission X-ray Source for Micro-Computed Tomography"* Applied Physics Letters, 2006, 89, 103111.

7. Z. Liu, et al., *"Development of a carbon nanotube based microfocus x-ray tube with single focusing electrode"*, Rev. Sci. Instrum. 2006, **77**, 054302.

8. G. H. N. Riddle, *"Electrostatic eizenl lenses with reduced spherical aberration for use in field-emission guns"*, J.Vac. Sci. Technol. 1978, 15 (3), 857-860.

9. M.J. Flynn, et al., *Microfocus x ray sources for 3-D microtomography.* Nucl. Instr. Meth A, 1994. **353**: p. 312-315.

10. European Standard DIN EN 12543-5, 1999.

11. G. Cao et al., *"A dynamic micro-CT scanner using a compact carbon nanotube field emission micro-focus x-ray source"*. SPIE Medical Imaging, February 2009.

12. Xiomara Calderón-Colón, et al., *Carbon nanotube field emission cathode with high current density and long-term stability.* Nanotechnology Vol. 20 No.32, 325707 (2009).

5 Conclusions and Future Directions

In this research study, three main topics related with CNTs research and applications have been further investigated. Here, the studies of aspects such as chemistry, material science and application of CNTs for X-ray imaging have been developed. The development of CNT alcohol-based suspensions have been successfully accomplished with the use of different dispersants. These suspensions were developed in context of the EPD method requirements. But they can be used in any application where a stable CNT suspension is required. CNT alcohol-based suspensions with long term stability and well dispersed CNTs were been prepared.

On the other hand, a successful, consistent, effective and reliable CNT cathode fabrication process has been developed. The fabrication of CNT cathodes with the intended geometries and the required dimensions with well designed boundaries have been obtained by EPD. This method allowed the CNT cathode fabrication with the required properties for X-ray generation. Stable and reasonably high emission current, current density, and long term stability have been achieved by these CNT cathodes.

Extensive hard work enables us to fully characterize a CNT micro focus field emission X-ray source with a variable focal spot size. High flux and long term stability of the CNT micro focus field emission X-ray tube has been achieved. The results proves that at least for this micro focus X-ray tube, the X-ray flux from the CNT cathode can be as high as that afforded by a conventional thermionic X-ray tube operating at the same focal spot size. The X-ray medical imaging application has been demonstrated using the CNT micro focus X-ray tube into a dynamic micro-CT scanner developed at UNC for dynamic micro-computed tomography imaging of small animal models.

There are still however plenty of challenges and opportunities remaining. As mentioned previously, the lens becomes ineffective for focal spot size less than 50 µm with the present design. The present design limitations on the focal spot size bring out new ideas to achieve smaller focal spot size. Simulation studies have been done with different anode structure. The new anode tip shape structure will be able to reduce the focal spot size to 10 µm in the vertical direction and 20 µm in the horizontal direction. In this new design the electrostatic focusing electrodes remain the same as the one used in this dissertation work. Other approach to reduce the focal spot is to modify the electrostatic focusing electrode opening shape from circular to elliptical. Again, simulation studies have been done and results reveal more isotropic focal spot size and reduction of the focal spot size. For 0.706 x 0.150 mm CNT cathode the focal spot size will be reduce to 30 µm x 50 µm, which represent 54 % reduction in the focal spot size. On the other hand, for 0.235 x 0.050 mm CNT the focal spot size will be reduced to 25 µm x 20 µm, which represents 83 % reduction in the focal spot size. These new designs

can increase the focusing power for the next generation of the CNT micro focus X-ray source as well the X-ray flux.